NASA Contractor Report 198537

An Experimental Study of Ignition Effects and Flame Growth Over a Thin Solid Fuel in Low-Speed Concurrent Flow Using Drop-Tower Facilities

Richard Dale Pettegrew
Case Western Reserve University
Cleveland, Ohio

October 1996

Prepared for
Lewis Research Center
Under Grant NAG3–1046

National Aeronautics and
Space Administration

AN EXPERIMENTAL STUDY OF IGNITION EFFECTS AND FLAME GROWTH OVER A THIN SOLID FUEL IN LOW-SPEED CONCURRENT FLOW USING DROP-TOWER FACILITIES

by

RICHARD DALE PETTEGREW

Submitted in partial fulfillment of the requirements

for the degree of Master of Science

Thesis Advisor: Dr. James T'ien

Department of Mechanical and Aerospace Engineering

Case Western Reserve University

May, 1995

AN EXPERIMENTAL STUDY OF IGNITION EFFECTS AND FLAME GROWTH OVER A THIN SOLID FUEL IN LOW-SPEED CONCURRENT FLOW USING DROP-TOWER FACILITIES

Abstract

by

Richard Dale Pettegrew

An experimental study of ignition and flame growth over a thin solid fuel in oxidizer flow speeds from 0 to 10 cm/sec concurrent flow was performed. This study examined the differences between ignition using a resistively heated wire (woven in a sawtooth pattern over the leading edge of the fuel), and a straight, resistively heated wire augmented by a chemical ignitor doped onto the leading edge of the fuel. Results showed that the chemical system yielded non-uniform ignition bursts, while the system using only the hotwire gave more uniform ignition. At speeds up to 2.5 cm/sec, the chemical system yielded non-uniform pyrolysis fronts, while the hotwire system gave more uniform pyrolysis fronts. At speeds of 5 cm/sec or greater, both systems gave uniform pyrolysis fronts. The chemically-ignited flames tended to become too dim to see faster than the hotwire-ignited flames, and the flame lengths were observed to be shorter (after the initial ignition burst subsided) for the chemical system for all speeds. Flame and pyrolysis element velocities were measured. Temperature profiles for several tests were developed using thermocouples at the fuel surface and in the gas phase.

Comparisons between the flame element velocities and peak temperatures recorded in these tests with calculated spread rates and peak temperatures from a steady-state model are presented. Agreement was found to be within 20% for most flame elements for nominal velocities of 5 cm/sec and 7.5 cm/sec.

Acknowledgements

The author wishes to thank thesis advisor Professor James T'ien for his guidance and help with this project. Also thanks to Kurt Sacksteder, Ray Sotos, Dennis Thompson, Paul Ferkul and the support staff at the NASA Lewis Zero-G facility, without whom this work would not have been possible.

Table of Contents

Section		Page
Abstract		ii
Acknowledgements		iv
List of Figures		viii
List of Tables		xi
I.	Introduction	1
II.	Hardware Fuel Ignition Assembly	9
	Fuel Translation Device	11
	Imaging Equipment	13
	Thermocouples	14
	Test Chamber Test Facilities	16
	Image Analysis Equipment/Software	17
III.	Procedures Sample/Test Preparation	19
	Thermocouple Installation Test Atmosphere	20
	Test Procedure	21
	Data Reduction	22

IV. Results 30

Results by Velocity 32

Quiescent Flow 34

1 cm/sec Flow 37

2.5 cm/sec Flow 42

5 cm/sec Flow 49

7.5 cm/sec Flow 53

10 cm/sec Flow 55

Ashless Filter Paper 61

Thermocouple Data 64

V. Discussion 76
Hotwire Ignition vs. Chemical Ignition

Temperature Profiles 80

VI. Comparison with Steady-State Model 84
Flame Spread Rates

Flame Length 86

Peak Temperature 88

VII. Conclusions 89

VIII. Recommendations 91

IX. References 92

Appendix I Error Analysis 94
Experimental Errors
Test Environment

	Ignition System	95
	Thermocouples	
	Flow Velocity	
	Data Acquisition	97
	Flame Element Data	
	Pyrolysis Data	100
	Data Analysis	101
	Data Plotting	
	Flame & Pyrolysis Velocities	102
Appendix II	Buoyant Flow Approximation	106
Appendix III	Thermocouple Heat Loss Approximation	109
	Thermal Inertia	
	Conduction	110
	Radiation	111
	Heat Release Rate	
Appendix IV	Effect of Threshold Value	113
Appendix V	Calibration of Fuel Translation Device	115

List of Figures

Figure	Description	Page
1	Opposed & Concurrent Flow	1
2	Sawtooth Hotwire Ignitor Assembly	10
3	Chemical Ignitor Assembly	11
4	Fuel Translation Device	12
5	Front and Edge View of Flame (Test G-2-31)	14
6	Thermocouple Placement	15
7	Visible Flame & Pyrolysis Elements	18
8	Tracking Image (With Closeup)	23
9	Non-uniform Pyrolysis Zone	27
10	Area Measurement (Pyrolysis Zone)	28
11	Flame/Pyrolysis Elements (G-2-12)	35
12	Flame/Pyrolysis Elements (G-2-13)	36
13	Flame/Pyrolysis Elements (G-2-14)	36
14	Flame/Pyrolysis Elements (G-2-20)	38
15	Flame/Pyrolysis Elements (G-2-11)	39
16	Partially Burned Sample	40
17	Flame Elements (1 cm/sec tests)	41
18	Flame/Pyrolysis Elements (G-2-15)	43
19	Flame/Pyrolysis Elements (G-2-16)	43
20	Flame/Pyrolysis Elements (G-2-17)	44

21	Pyrolysis Lengths (2.5 cm/sec HW tests)	46
22	Partially Burned Sample	47
23	Flame/Pyrolysis Elements (G-2-8)	48
24	Flame Elements (2.5 cm/sec tests)	49
25	Flame/Pyrolysis Elements (G-2-7)	50
26	Flame/Pyrolysis Elements (G-2-23)	51
27	Flame Elements (5 cm/sec tests)	52
28	Pyrolysis Lengths (5 cm/sec tests)	53
29	Flame/Pyrolysis Elements (G-2-18)	54
30	Flame/Pyrolysis Elements (G-2-31)	56
31	Flame/Pyrolysis Elements (G-2-19)	57
32	Flame Elements (10 cm/sec tests)	58
33	Partially Burned Sample	59
34	Pyrolysis Lengths (10 cm/sec tests)	60
35	Flame/Pyrolysis Elements (G-2-21)	61
36	Flame/Pyrolysis Elements (G-2-22)	63
37	Partially Burned Sample	64
38	Temperature Trace (G-2-26)	66
39	Temperature Trace (G-2-27)	68
40	Flame/Pyrolysis Elements (G-2-27)	69
41	Temperature Trace (G-2-28)	70
42	Flame Propagation Past Thermocouple Junctions	71

43	Flame/Pyrolysis Elements (G-2-28)	72
44	Partially Burned Sample	73
45	Ignition Burst from Hotwire System	76
46	Ignition Burst from Chemical System	77
47	Flame Images from Test G-2-28	82
48	Experimental & Model Flame Element Velocity Data	84
49	Fuel Consumption Rate Contours: S.- S. Model	87
50	Fuel Consumption Rate Contours: S.- S. Model	88
51	Pyrolysis Front Velocity Error	102
52	Effect of Threshold Value on Flame Length	114
53	Calibration Plot: 10 cm/sec	119
54	Calibration Plot: 5 cm/sec	120
55	Calibration Plot: 2 cm/sec	121
56	Calibration Plot: 1 cm/sec	122
57	Calibration Plot: 0.5 cm/sec	123

List of Tables

Table	Description	Page
1	Test Matrix	30
2	Results by Velocity	32
3	Element Error & Correlation Coefficient	104
4	Mean-Element Spread & Growth Rate Error (%)	105
5	Buoyant Velocity Estimate	107

I. Introduction

The study of combustion and flame spreading is of vital interest to the manned space exploration program with regard to the issue of fire safety. Knowledge of the conditions under which a fire will initiate and propagate will aid in the design of safer spacecraft for future missions (Friedman and Sacksteder, 1988).

Most fire safety issues involve diffusion flames. These are flames in which the fuel and the oxidizer are initially unmixed; the combustion reaction

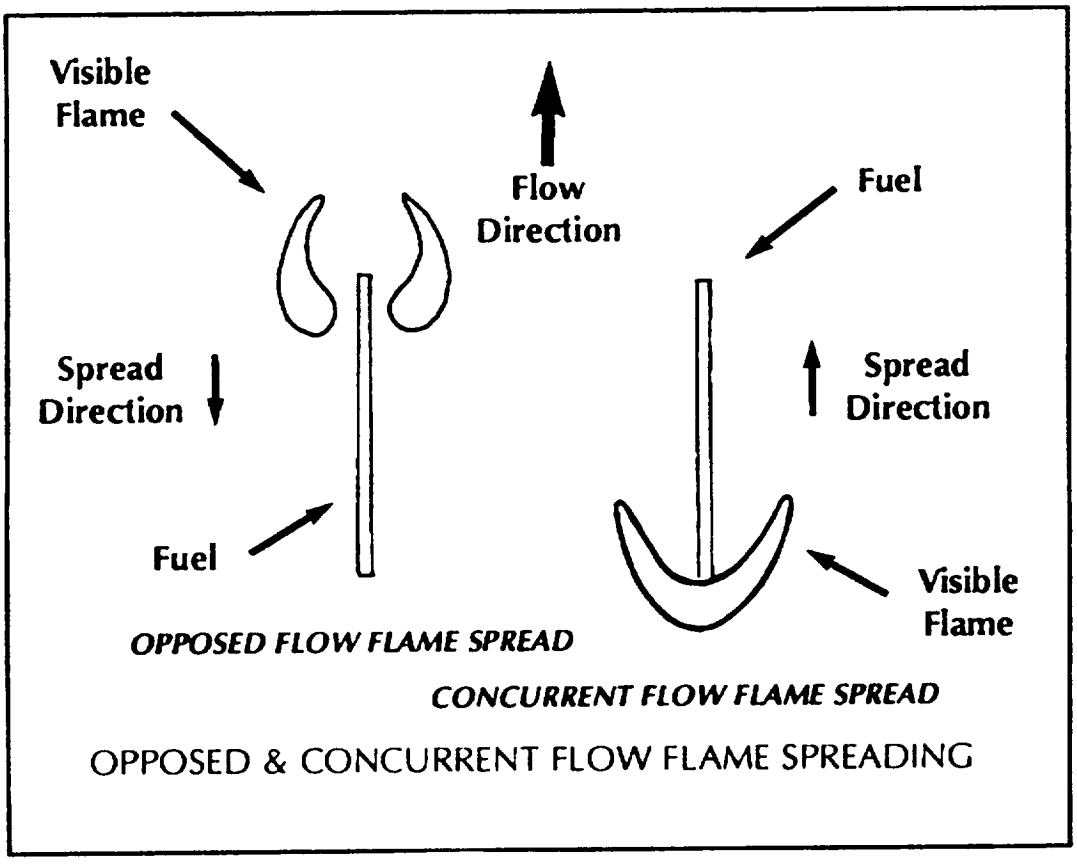

Figure 1 Opposed & Concurrent Flow

occurs in the region where they meet. When a solid fuel burns, heat is transferred in the direction of flame propagation to a region of unburned fuel. This heat gassifies the fuel in a process known as pyrolysis; it then diffuses into the reaction region where it is mixed with the incoming oxidizer. The arrangement where the incoming oxidizer flow is in the same direction as the flame propagation is referred to as concurrent flow; when the oxidizer flow is in the opposite direction, it is known as opposed flow. This is illustrated in Figure 1.

Concurrent flow provides greater heat transfer through convection; this typically leads to faster flame propagation, which is the most dangerous situation from a fire safety standpoint (DeRis, 1969).

These oxidizer flows can be generated in several ways. In the presence of a gravitational field, hot gases rise, causing natural buoyant flows. In normal earth gravity, these flows are on the order of 20 cm/sec or greater. Flows may also be induced artificially, such as in the ventilation system on a spacecraft. These flows can have velocities as low as several cm/sec.

While buoyancy is always present in normal gravity applications, there may also be a forced component of the flow. However, in conditions of zero (relative) gravity, all flows must be of the forced type.

The problem of studying low speed forced oxidizer flows then requires that the effects of gravity be suppressed. This can be accomplished using ground based facilities such as NASA's 2.2 Second Drop Tower or 5.18

Second Zero-Gravity facility. For experiments requiring a greater duration of reduced gravity time, flight facilities such as NASA's KC-135 aircraft or Shuttle missions are needed (Lekan et al, 1992).

In addition to the flow direction and velocity, other important parameters in the study of combustion include the fuel type and thickness. Two examples of commonly studied solid fuel are cellulosic fuels such as KimWipes or filter paper, and polymethyl methacrylate (PMMA) (Olson et al, 1988).

The fuel thickness is usually considered in terms of "thermal thickness". If a given fuel slab is thin enough that the temperature profile in the depth of the fuel is uniform, ie., uniform temperature across the fuel thickness, then it is considered to be thermally thin. In this case, gas phase conduction is the primary mode of heat transfer to the fuel ahead of the flame. If a non-zero temperature gradient exists into the depth of the fuel, then solid phase conduction plays a role in the heat transfer process, and this condition is referred to as thermally thick (DiBlasi, 1994).

Diffusion flames spreading in a quiescent atmosphere over a thin fuel were studied using drop tower facilities (Olson, 1987). In this work, a thin (0.076 mm) cellulosic paper sample was ignited at an edge, with the resulting flames spreading in an opposed flow fashion. The fuel samples were ignited by resistively heating a Nichrome wire which had been woven in a sawtooth shaped pattern over the edge of the fuel. The oxygen concentrations of the test

atmosphere were varied, and a flammability limit of 21% O_2 (with a diluent of N_2) was found. The opposed flow velocity for this result was found to be 0.54 cm/sec, which was the flame spread rate.

Later, opposed flow flame spread in micro-gravity over the same fuel was studied at higher flow velocities (Ferkul, 1989). These tests were also carried out using drop tower facilities. A device was constructed to carry the fuel sample through a quiescent atmosphere at speeds up to approximately 7 cm/sec. The fuel was ignited using a resistively heated Nichrome wire, as in the previous work. The results of this work showed that the flame spread rate increased with increasing flow velocity, as well as increasing oxygen concentration.

Recently, concurrent flow diffusion flame spread over the same fuel in micro-gravity was studied numerically by Ferkul (Ferkul, 1993), Jiang (Jiang, 1995) and experimentally by Grayson (Grayson, 1991). In Ferkul's model (which examines the steady-state propagation), the region near the base of the flame is modeled elliptically with one step finite rate gas phase chemical kinetics. The downstream region was modeled parabolically to save computational time. The solid fuel was modeled to pyrolyze according to a one step Arrhenius law, and a solid phase radiation loss term was included. Jiang's model was an extension of this work, with the addition of a gas phase radiation term and improvements in the calculation of certain material properties.

The results of Ferkul's calculations show that flame length, flame spread rate, and pyrolysis length all increase approximately linearly when either the flow velocity or the oxygen concentration is increased. Additionally, the model gives the flame temperature distribution, and shows that at low velocities, radiative losses lead to quenching.

Jiang's calculations show that gas phase radiation produce additional heat loss from the system and lead to lower flame temperatures, shorter flames and a narrower flammable region (in the low velocity regime). However, gas radiative feedback to the solid can either enhance or reduce the flame spread rate, depending on the flow conditions. Furthermore, the dependence of spread rate on flow velocity is greater than linear dependence when radiative feedback is important.

In Grayson's work, conducted at NASA's 5.18 second drop tower, flows up to approximately 5 cm/sec were induced with the device used by Ferkul in his opposed flow work. The fuel samples and ignition technique were similar to that used by Olson and Ferkul. Data was acquired using a 16 mm motion picture camera to image both the front and edge views of the flame, with the aid of a mirror. The edge view was then analyzed, and flame element position data was generated.

Grayson's work shows that flames spreading in concurrent flow are longer, wider, and spread faster than those in opposed flow, due to convective heat transfer. However, the constraint of the available reduced gravity time

prevented steady-state propagation from being reached, though in some cases the flames appeared to be near steady-state.

Several limitations hindered Grayson's work. One of the most significant was the control of the carriage velocity of the fuel translation device. The speed of the DC motor used to drive this device was controlled by means of an analog potentiometer. The repeatability of the flow speed was then influenced by the repeatability of the potentiometer setting. Additionally, the temperature of the device was also found to affect the carriage velocity. This led to velocity variations ranging from 7 percent at the highest selected velocities up to 35 percent at lower speeds.

Other problems with this work involved the optical arrangements used to acquire data. Flames were imaged using a stationary movie camera, so to keep the entire distance that the carriage traveled in the field of view, it was necessary to mount the camera a significant distance from the carriage. This led to flame images which typically used only a small portion of the field of view, leading to larger errors in flame position data.

A mirror was used to image the front of the test sample. This view was used only to determine whether or not the flame was approximately two dimensional. Because of the low light conditions used to optimize the edge view of the flames, the pyrolysis and burnout fronts were not visible.

All flame element data for this test was acquired using the edge view of the flames. When the data was reduced, the edge of the flame element was

determined by placing a cursor over the visible edge of the flame and recording the screen coordinates. The boundaries of some flames were indistinct, making determination of that edge a matter of operator judgement.

The objective of this project is to characterize the transient effects and subsequent flame-growth period produced by two different ignition techniques, with the intent of minimizing the time required to reach steady-state flame propagation. Other improvements over the previous work were made by using a new fuel translation device to improve the repeatability of the flow system. Improved imaging techniques were also used, including mounting a video camera on the carriage with the fuel sample. This simplified the data reduction by putting the fuel sample in fixed co-ordinates in the images. It also served to increase the size of the flame images relative to the field of view. Additional information was gathered from these tests by the use of a flashing light, which illuminated the pyrolysis and burnout front images in the front view.

The process of data reduction was improved by the use of a computerized digital processing technique to aid in the determination of the boundaries of the flame elements.

The majority of the tests in this work used the same fuel employed by Grayson, Ferkul, and Olson. For these tests, the oxidizer content of the atmosphere was held constant at 18% O_2 (by mole fraction), with a diluent of N_2. The induced flow velocities were varied from 1 cm/sec to 10 cm/sec.

Two different ignition techniques were used and compared. Flame and pyrolysis element spread rates were determined. Thermocouples were also employed in different locations for several trials with this fuel to develop a temperature profile of the combustion process. This data was then compared to the numerical results obtained by Jiang.

Two tests were also conducted using a thicker fuel specimen. Both of these tests employed the same ignition technique and induced flow velocity, while the oxidizer content of the test atmosphere was varied.

II. Hardware

Fuel

Two fuels were used in this study. The first was a thin cellulosic tissue paper known as KimWipes. This paper, manufactured by the Kimberly-Clark Company, consists of 99% cellulose, 1% polyamide resin. This fuel has an area density of 1.00 mg/cm^2, based on half-thickness of the fuel (Grayson et al., 1994). This fuel was selected because it is thin enough to allow significant flame propagation in a short time. Additionally, this fuel has been used extensively in previous micro-gravity studies, allowing direct comparison of results (Ferkul, 1989, Grayson, 1991, Olson , 1991, Sacksteder & T'ien, 1987).

The second fuel used was grade 1 ashless filter paper, made by Whatman. This paper consists of 100% cellulose, and has an area density of 4.35 mg/cm^2, also based on the half-thickness.

All fuel samples used were 5 cm wide, and 10 cm long. Samples were fixed to the metal sample holder by means of adhesive tape; the metal of the sample holder was a sufficient heat sink to quench the flame at the interface between the sample and the holder, thereby preventing the tape from interfering with the combustion.

Ignition Assembly

Two methods of ignition were used and compared. One method, similar to that used by Grayson, was a 0.0254 cm diameter Kanthal wire, configured in a sawtooth shape which was woven over the leading edge of the fuel sample.

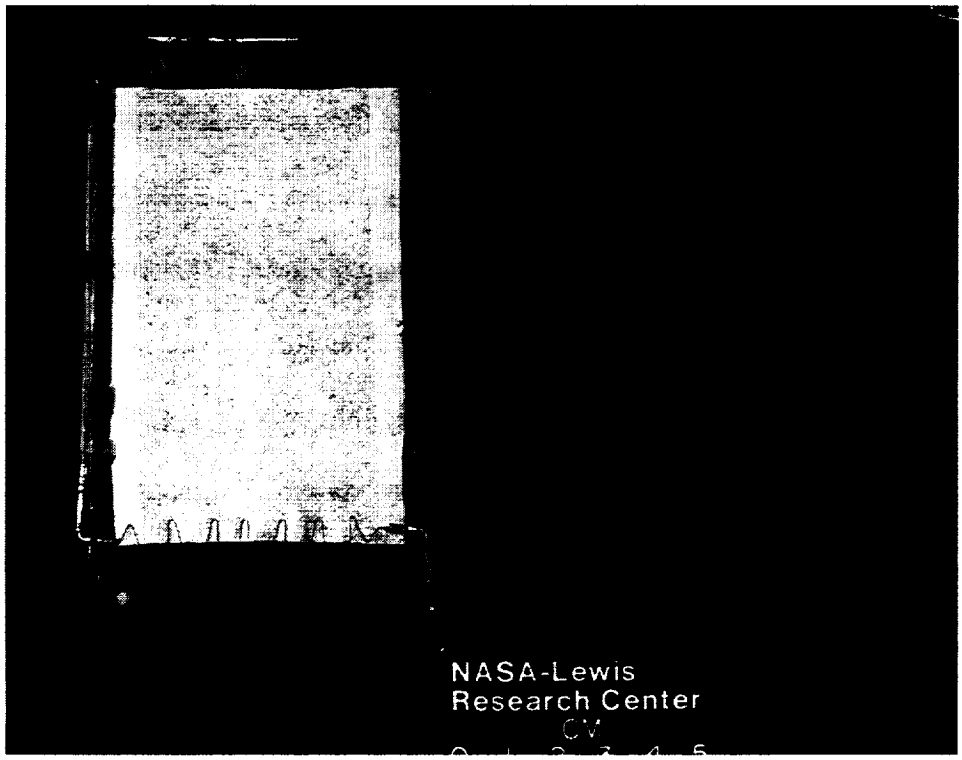

Figure 2 Sawtooth Hotwire Ignitor Assembly

Each of the 13 teeth in the pattern was approximately 0.4 cm wide. The pattern spanned the width of the paper. Figure 2 shows a KimWipe sample with this ignition system installed. The wire has a resistance of 3.57 ohms. A potential of 28 volts was applied across the wire for 0.2 seconds. This causes the wire to heat up quickly, which in turn ignites the surrounding paper. The energy released by this system is approximately 44 Joules.

The other ignition technique used a straight Kanthal wire placed touching the paper, parallel to and approximately 0.25 cm from the leading edge. This wire has a resistance of 1.99 ohms. A potential of 24 volts was applied across the wire for 0.1 seconds, releasing about 29 Joules. This in turn

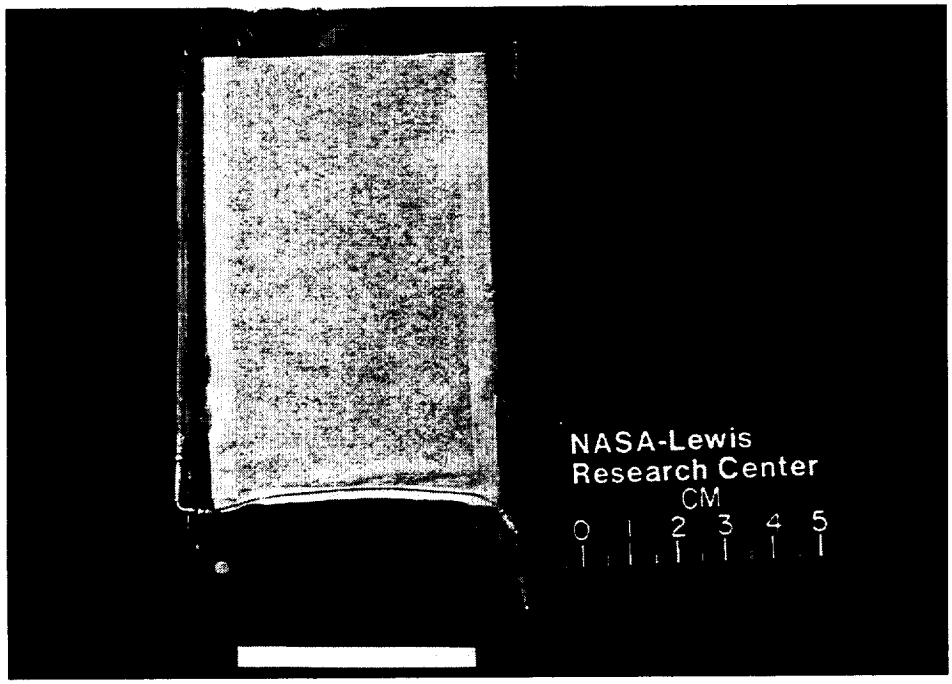

Figure 3 Chemical Ignitor Assembly

ignited a chemical ignitor consisting of a 10 milligram nitrocellulose strip. This strip was approximately 0.4 cm wide, and spanned the width of the paper. Figure 3 shows this configuration. The ignition of this strip quickly released about 25 Joules in the region of the sample's leading edge (Sacksteder, 1993). The total energy released by this system was approximately 54 Joules.

Fuel Translation Device

The new fuel translation device used a rectangular aluminum carriage measuring 2.54 cm x 5.08 cm x 13.41 cm to carry the fuel sample, ignition and thermocouple leads. The carriage also carries a video camera and mirror to acquire images of both the front and edge views of the flame (Figure 4).

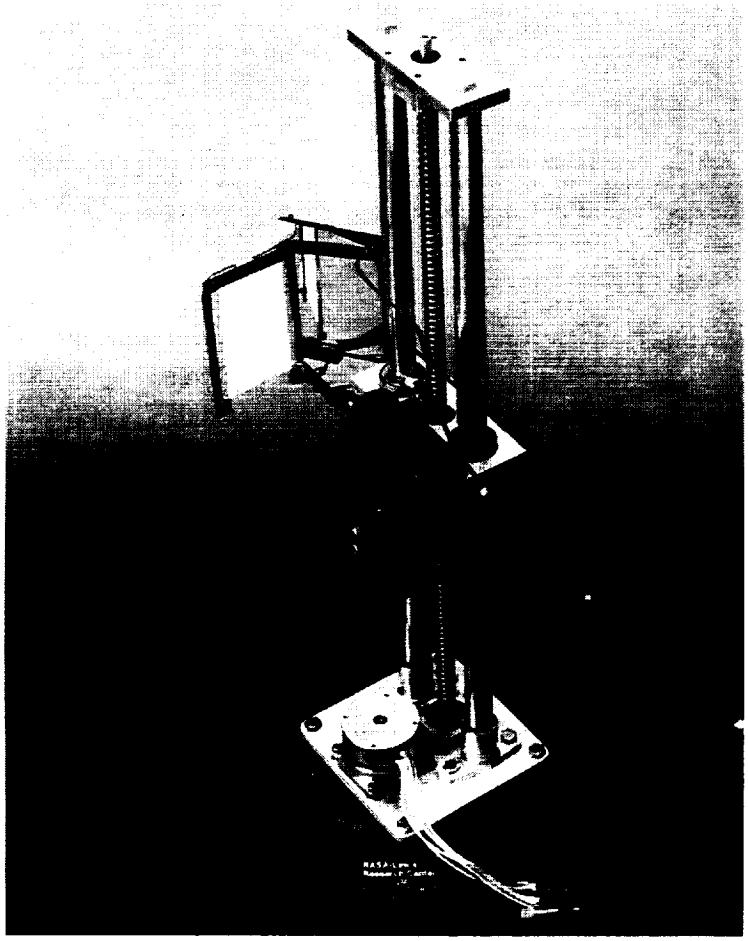

Figure 4 Fuel Translation Device

The carriage used Thomson linear bearings to ride on two parallel 1.41 cm bearing shafts. These shafts are 55.25 cm long and are secured to an aluminum base plate by means of a press fit into custom made shaft holders. These shaft holders are then bolted directly to the base plate. The shafts are constrained at the other end by an aluminum yoke, which is attached perpendicular to the axis of the shafts. The maximum travel distance for the carriage between the yoke and the shaft holders is 42 cm.

The carriage is moved using a precision ball screw mounted parallel with and between the two bearing shafts. The screw is coupled to the carriage with a threaded nut. The motion of the screw is constrained on both ends through the use of tapered roller bearings, eliminating the need for thrust bearings.

The ball screw is driven by a 4.6 volt Cygnus HB type stepper motor. The motor is mounted with the shaft axis parallel to the ball screw, and is coupled to it through two cast aluminum gears at a ratio of 8:1. The motor is activated and controlled through a Kollmorgen SMC-500 external, programmable controller. The controller is programmed through an interface with an external computer (Pettegrew, 1993).

Imaging Equipment

The video camera used in this work was a Cohu camera, Model 6810. The video head, measuring approximately 6 cm x 4.5 cm x 4 cm, was mounted on the carriage. Initially, a 5mm lens was used. For later tests, a 6.5mm lens was used. The camera body was mounted separately, and the signal was recorded on an 8mm "Super 8" video recorder.

The camera was positioned to view the front surface of the sample. The edge view was obtained using a front surface mirror mounted at a 45 degree angle next to the sample holder. This allowed both views of the flame to be imaged by one camera (Figure 5, Test G-2-31), and minimized the chance of the mirror interfering with the flame.

Figure 5 Front and Edge View of Flame (Test G-2-31)
18% O_2, Freestream Velocity = 10.07 cm/sec

Initially, a 4.8 watt light was mounted on the carriage. This allowed the pyrolysis front and burnout front to be imaged in the front view. Because the light interferes with the images of the flame in the edge view, the light was flashed on for 0.1 seconds at a rate of 2 Hz. This allows for discrete data points on the relatively slow moving pyrolysis/burnout fronts, and more continuous data acquisition on the faster responding flame element data. Later runs employed two 1.1 watt lights, in an effort to improve the imaging.

Thermocouples

Three of the later runs in the test matrix included the use of

thermocouples. The thermocouples used were Type K, and were 0.00762 cm in diameter. These were configured in a diamond shape with sides 1 cm long, and the bead at one corner. This was done to minimize the disturbance to the flame at the bead, while also minimizing the heat conduction path. Because of the difficulty in handling wires of this size, the 0.00762 cm diameter wire was spliced to 0.0254 cm diameter wire approximately 1 cm down from the diamond shape.

For each of these runs, one thermocouple was placed on the fuel surface and another was suspended in the gas phase (Figure 6). The exact placement

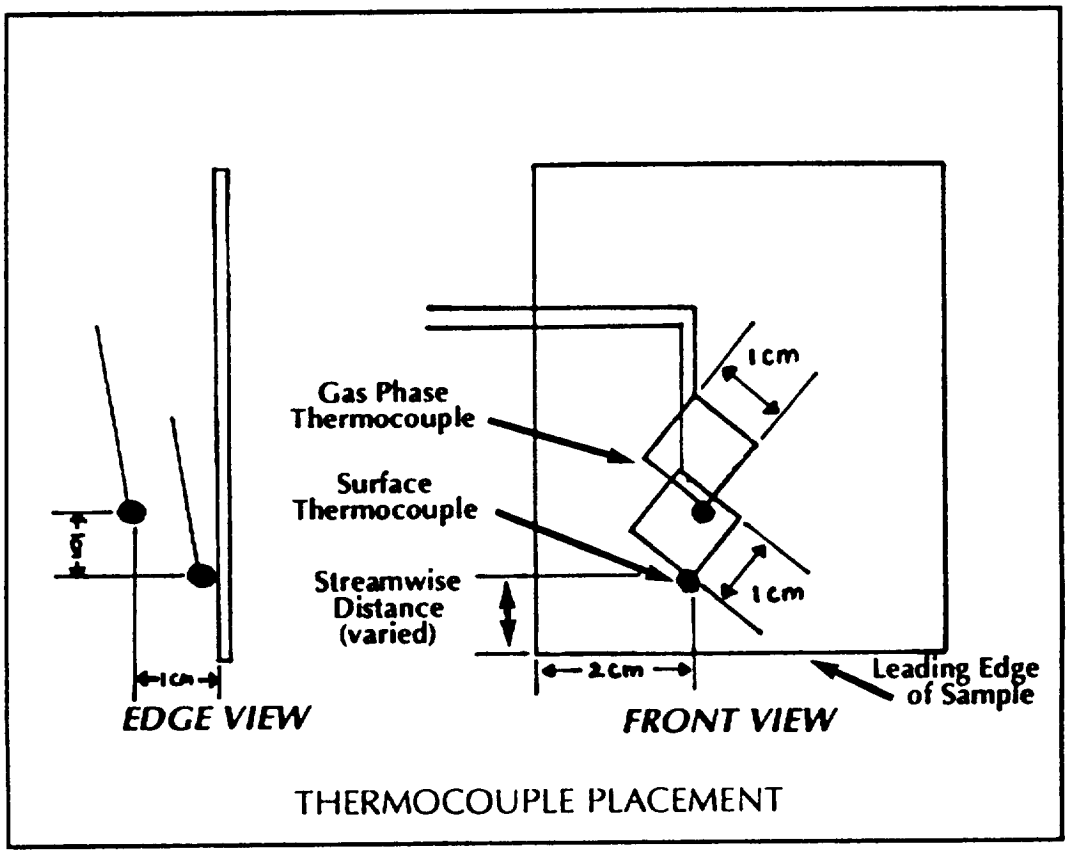

Figure 6

of the thermocouples varied with each run, and will be discussed in the results section. The output signal from the thermocouples was recorded by an onboard computer.

Test Chamber/Vehicle

The translation device was mounted in a combustion chamber with an internal volume of 0.087 m^3. Previous studies have shown that oxygen depletion is not a significant factor for similar conditions in a chamber of this size (Grayson, 1991).

To minimize reflections from the chamber wall, the portion of the wall in the field of view was covered with black paper. An anodized aluminum scale was mounted in the field of view to measure both the image magnification factor and the carriage speed for each run.

The chamber is mounted on a standard drop vehicle used by NASA's Zero Gravity facility. All on board equipment is operated by a Toshiba EX-40 PLC computer, also mounted on the test vehicle.

Test Facilities

The Zero Gravity facility consists of a 155 meter vertical shaft, containing a 145 meter long, 6.1 meter diameter steel vacuum chamber. Air is evacuated to a pressure of 10^{-2} torr, which reduces the aerodynamic drag to less than 10^{-5}g. After a free-fall of 5.18 seconds, the package is decelerated in a cylindrical container filled with expanded polystyrene pellets. The average deceleration rate is 35 g's, with peak loads reaching 65 g's for several

milliseconds (Lekan et al., 1992).

Image Analysis Equipment/Software

Analysis of the video images was aided by transferring the video images onto a laser disc, then using a digital object tracking software package developed by NASA (Klimek & Paulik, 1992). This system can track an object such as a flame element from frame to frame by digitizing a designated target area in the field of view, and turning the pixels in this area on or off based on whether the light or color intensity of each pixel falls above or below a user designated value. The elements tracked were the flame tip, flame base and burnout front. Due to the non-uniformity of the pyrolysis front in some cases, this element was found (in all cases) by determining the area of the pyrolysis zone, and dividing that area by the sample width. Figure 7 illustrates the flame and pyrolysis elements.

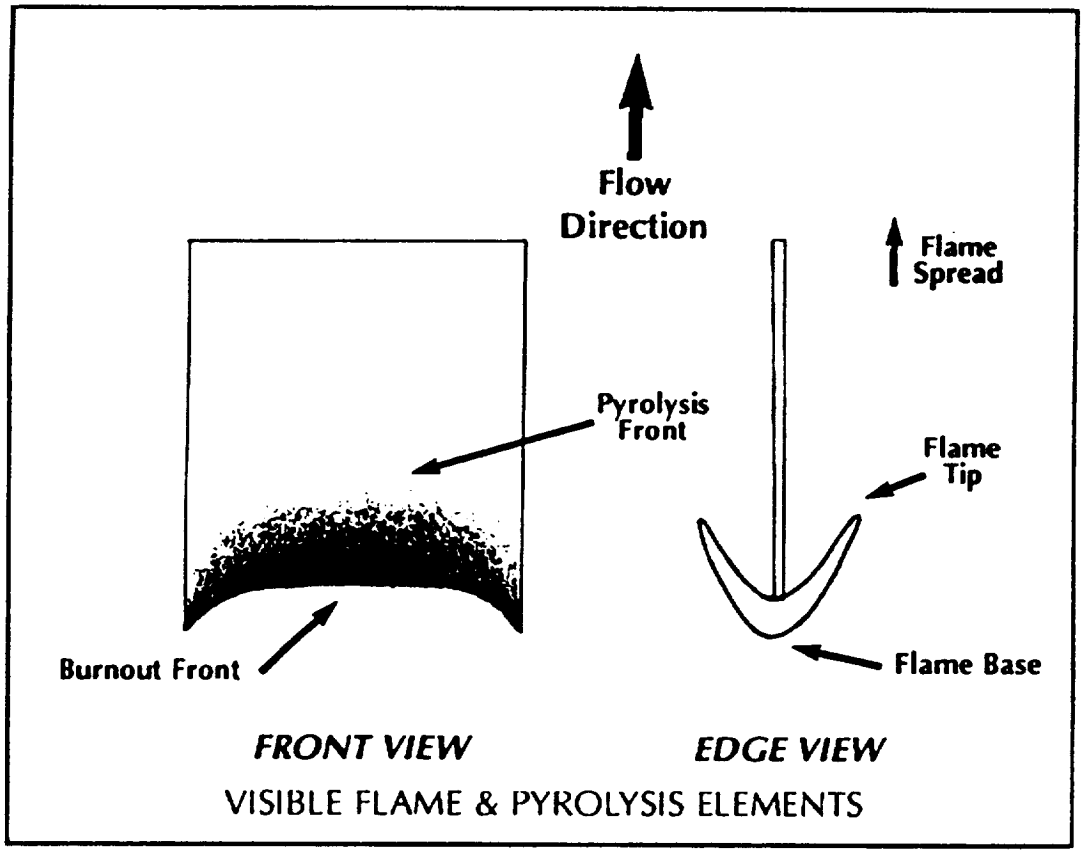

Figure 7

The pyrolysis zone area was determined using Sigma Scan, a commercial image analysis package which allows the user to trace the outline of an object, then counts the number of pixels enclosed in the shape.

III. Procedures

This chapter describes the experimental procedures used in this study, as well as a description of the data reduction techniques used. The description and results of the calibration for the fuel translation device can be found in Appendix V.

Sample/Test Preparation

All KimWipe fuel samples in this study were taken from one box, to eliminate any variation that may occur between different boxes. All samples were taken from portions of sheets which show no visible defects, folds or creases. Similarly, the ashless filter paper samples were both taken from a single sheet, and screened for defects.

After the sample was cut and taped to the metal sample holder, the ignitor was installed. For the sawtooth shaped hotwire, the wire was first bent into the proper shape on jig consisting of nails driven into a piece of wood at appropriate intervals. To insure good thermal contact between the wire and the paper, the wire was placed on the leading edge of the fuel sample with alternating bends on each side of the paper.

For the tests using chemical ignition, strips of nitrocellulose were cut to span the width of the fuel sample, and were weighed and trimmed to be within +/- 2% of 10 milligrams. Installation consisted of placing the chemical strip between the wire and the paper. Drops of acetone were then placed on the chemical strip, dissolving it into the paper. The acetone would then evaporate,

At the moment of release, the digital time stamp (imprinted on each frame of the video tape) was started. Movement of the fuel translation device began 0.1 seconds after release.

The ignitor circuit was energized 0.2 seconds into the drop. For the case of the sawtooth shaped hotwire, the circuit remained on for 0.2 seconds. For the chemical ignition case, the circuit was on for 0.1 seconds.

The flashing light was turned on for 0.1 seconds at a rate of 2 Hz. This was started at the package release, and continued until approximately 2 seconds after the drop.

Data Reduction

After the drop package was retrieved, the partially burned sample and video tape were recovered. The thermocouple data (when applicable) was downloaded and plotted using AXUM, a commercial data plotting software package. The samples were preserved for later examination. The images on the 8mm video tape were recorded onto a laser disc, allowing repeated viewing without the signal degradation that would occur through many viewings of video tape. This also facilitated the use of the digital object tracking software.

This software can track an object such as a flame element from frame to frame by digitizing a designated target area in the field of view, and turning the pixels in this area on or off based on whether the light or color intensity of each pixel falls above or below a user designated value (Figure 8). Other user inputs allow enhancement of the image through different electronic filters, as

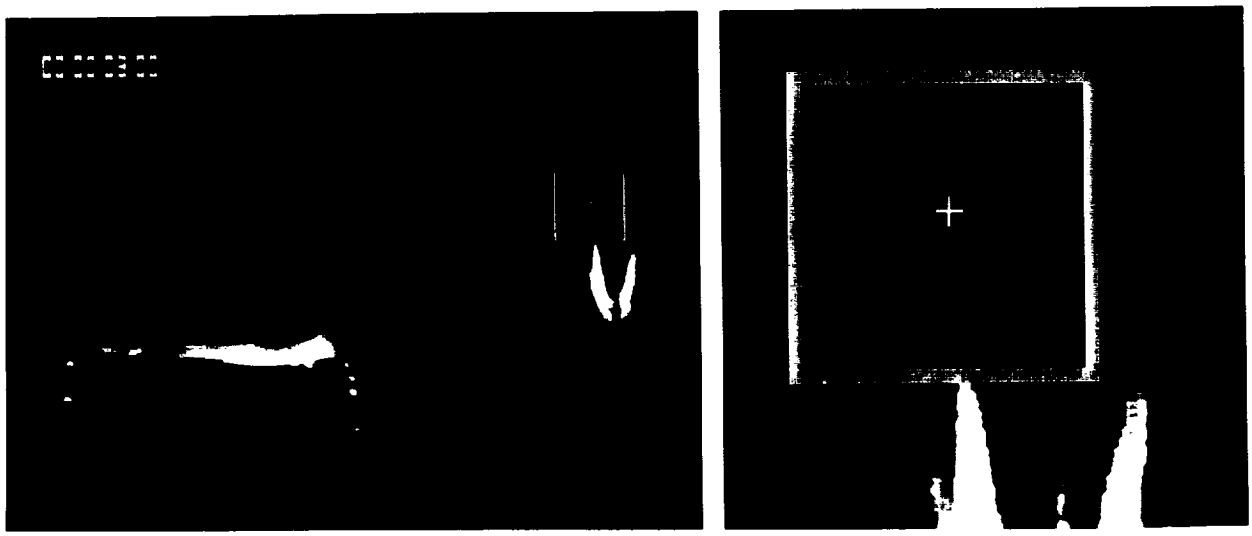

Figure 8 Tracking Image (With Closeup)

well as designation of the direction of motion of the object. Selection of the proper light or color intensity level is determined using a supporting program which shows the light or color intensity profile along a line which can be moved to any portion of the screen using the mouse. An additional program allowed the measurement in pixels of the length of an object in the field of view. Provided that the actual length of the object was known, an image magnification or scale factor could then be calculated. The scale factor was verified for each test, and was always found to be within +/- 0.6% of the average of the values (for each view).

To maintain consistency in the comparison of one test to another, all flame elements were tracked using a constant color intensity level. However, one test was also analyzed using a different intensity level, and compared to the results obtained using the constant level. For the details of this

comparison, see Appendix IV.

The interface of the regions where the pixels have been turned on or off can then be tracked from frame to frame, either automatically or manually. In the automatic mode, the co-ordinates of the farthest illuminated pixel in the designated direction is recorded and used as the center of the target area for the next frame. In the manual mode, selection of this point is left to the operator, using a mouse-driven cursor. In either mode, the screen co-ordinates of the selected point were written to an ASCII file, and could then be downloaded to a commercial plotting package.

All tracking with this software package was done using the manual mode. The dramatically varying light levels inherent with the flashing light caused several problems. The first problem was that the light was needed to track the progress of the pyrolysis and burnout fronts, but it overwhelmed the intensity values needed to track the flame elements. This caused the software to illuminate all of the pixels in the target box when the light flashed. When the automatic tracking mode was used, the program then looked for the farthest illuminated pixel in the designated direction of propagation. The target box then moved past the area where the flame actually was, and was unable to re-acquire it even after the light flashed off. By using the manual mode, the operator was able to, when the light was on, place the cursor in an obviously incorrect coordinate such as a corner of the screen. When the light would turn off, the cursor was returned to the general area of the flame element. The

proper coordinates were then re-acquired within one frame. After tracking, the output file was examined, and data points corresponding to the corner of the field of view were discarded.

The second problem caused by the light involved the response time of the Automatic Gain Control of the video camera. The Automatic Gain Control (AGC) selects the optimal light sensitivity of the camera. When the lighting conditions change, the AGC responds by appropriately resetting the sensitivity of the camera. The response time of the AGC was quoted by the manufacturers to be approximately 0.25 seconds. Since the camera was imaging at 30 Hz., approximately 7-8 frames would have incorrect gain settings after the light turned off. This was evident in the images by the apparent shortening of the flame immediately after the light went out, followed by its apparent growth back to its previous length. This problem was resolved by discarding 7-8 data points immediately after the light would go out. Although the gain setting would then also be incorrect at the moment the light flashed on, this was not relevant because the flame elements were not tracked during those times for the previously mentioned reasons. While the oversensitivity of the camera during the period when the light was on affected the images of the pyrolysis front, the problem was not as severe as it was for the flame element tracking. This is because the pyrolysis and burnout front data were acquired using a different technique.

These elements were tracked by manually scanning the frames until a

frame was found which clearly showed both the pyrolysis and burnout. The time, as recorded by the digital time stamp on each frame, was then noted and the pixel coordinate of the burnout front was found using the scale factor program. This program allows the user to draw a line with the cursor, and position this line on the screen. The program then gives the pixel coordinates of the beginning and end of the line. The technique was to draw a horizontal line, and place the line at the edge of the burnout front. The y-coordinate of the line was then recorded, and compared to the previously recorded y-coordinate of the initial leading edge of the fuel sample. This was repeated each time the light would flash on.

Because of the non-uniformities of the pyrolysis zones for some of the tests, both the pyrolysis front and the pyrolysis length were found (for all tests) by first calculating the pyrolysis area. Figure 9 shows an example of such a non-uniform pyrolysis zone (Test G-2-14). The "mean-area" pyrolysis length was found by dividing this area by the sample width. The mean-area position of the pyrolysis front was then found by adding the mean-area pyrolysis length to the position of the burnout front.

The pyrolysis zone area was calculated using a commercial software package known as Sigma Scan. This program allowed a shape to be drawn on the image (around the visible pyrolysis zone), using a mouse-driven cursor (Figure 10). The software would then count the number of pixels enclosed by the shape, and multiplication by the scale factor would give the surface area

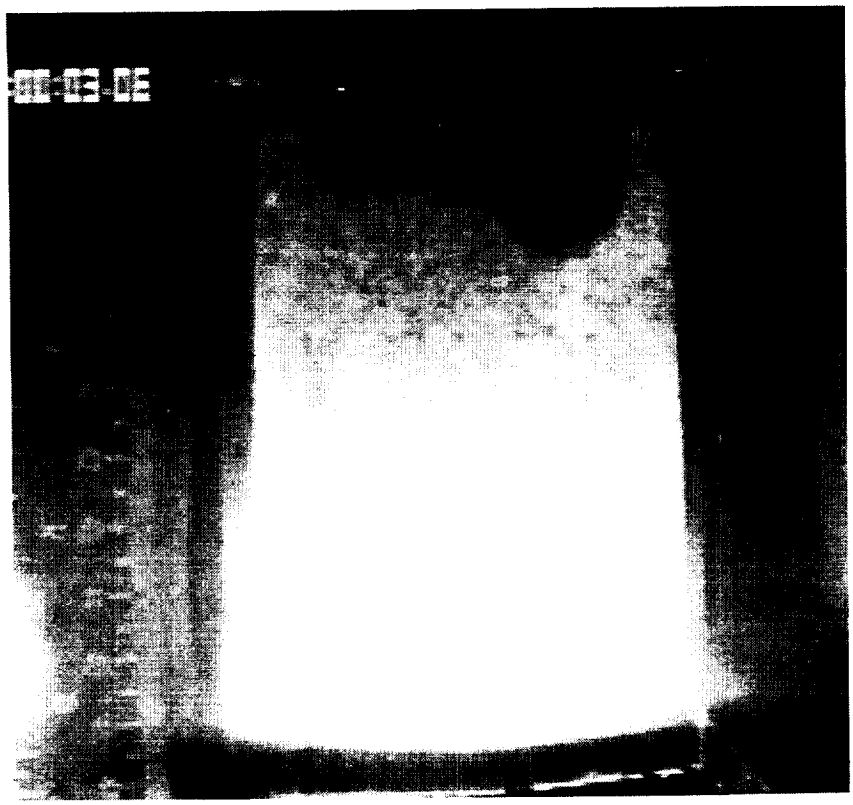

Figure 9 Non-uniform Pyrolysis Zone

represented by the shape.

The flow velocity for each run was verified using a technique similar to that used to find the burnout front position. A frame with the light on near the beginning of the drop would be selected. The scale program was run, and a horizontal line drawn. This line was then placed to intersect the visible aluminum scale. The time of this frame was noted, as well as the pixel coordinate and the value on the scale where the line crossed. The video was then advanced to an illuminated frame near the end of the run, and the scale program was then run again. The line was placed at the same pixel coordinates as in the previous measurement, and the new time value and scale measurement

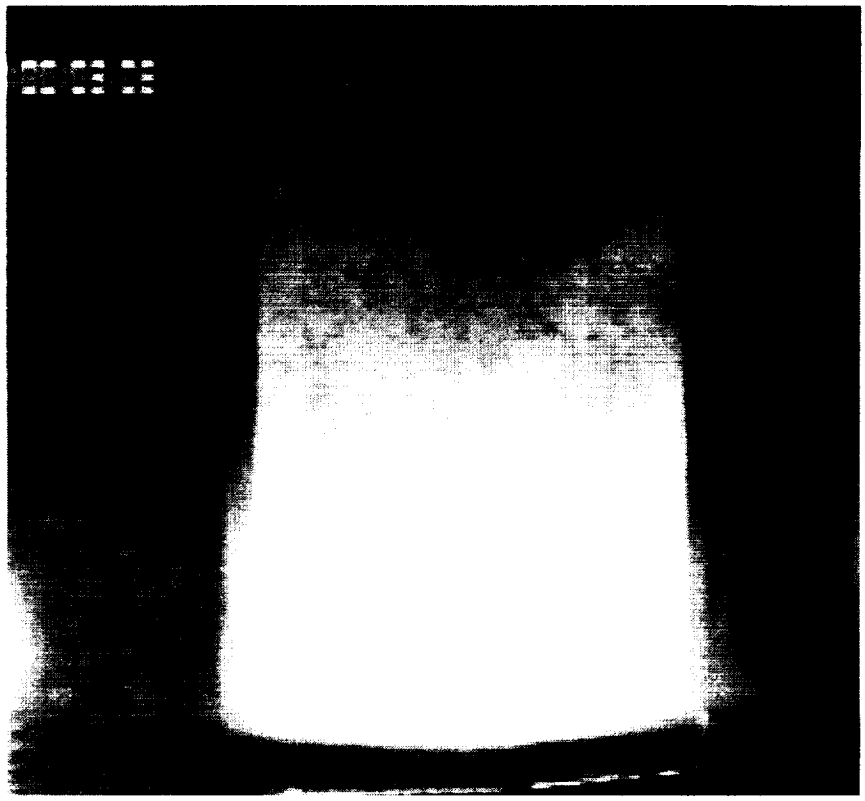

Figure 10 Area Measurement of Non-uniform Pyrolysis Zone, using Sigma Scan

were noted. The change in distance and change in time could then be calculated for these two points, giving an average velocity for the given time period. This technique does not account for transient effects, but merely serves as an overall check on the selected velocity. A previous calibration of the translation device examines the transient behavior, and can be found in Appendix V.

Spread rates were calculated by designating a section of the desired element and applying a linear regression to this section. Because of the unsteady nature of the flame and pyrolysis elements for these tests, the section

the flame and pyrolysis elements for these tests, the section was chosen to be near the end of each run, to minimize the disturbance in the plot from ignition. Although selection of the duration of the designated section varied for each run, the selection process was driven by the desire to find a portion of the plot which was representative of the trends occurring at the end of the drop. When the slopes of the paired elements (base and tip for the flames, burnout front and pyrolysis front for the pyrolysis zone) were not the same within the experimental error, the overall spread rate was defined to be the average of the spread rate for the given elements. The uncertainty of these spread rates is inversely proportional to the duration of data used for the curve-fit. This uncertainty is discussed in the Error Analysis (Appendix I). The uncertainty was determined to be approximately 76% in the cases of quiescent and 1 cm/sec flow, due to the short duration of data available for the regression. The uncertainty for subsequent tests was 1.53% or less.

IV. Results

Most tests were conducted using KimWipes as the fuel, with an atmosphere of 18% O_2, 82% N_2. All tests were conducted at a pressure of one atmosphere. Table 1 shows the test matrix for these tests:

Ignition Method	*0 cm/s*	*1 cm/s*	*2.5 cm/s*	*5 cm/s*	*7.5 cm/s*	*10 cm/s*	*10 cm/s with TC*
Hotwire	--	1_d	$2_u,1_d$	1_d	1_d	1_d	3_d
Chem.	3_u	1_u	1_u	1_u	--	1_d	--

Table 1 Test Matrix

Note that the velocities listed are the values of the desired free stream velocity for each test. The actual free stream velocity realized for each test point will be reported case by case. The relative velocity for each test is equal to the free stream velocity minus the flame spread rate.

The u and d subscripts in the above matrix indicate the direction of motion of the fuel translation device. The residual g-levels inherent in a ground based facility induced some element of buoyant flow in each test. The relative direction of the imposed flow could then be significant, because it is then either enhanced or reduced by the buoyant flow. Because the g-level experienced by the experiment in each test was not recorded, it is impossible to quantify this buoyant velocity. Estimates for these buoyant velocities based on assumed g-levels can be found in Appendix II.

Additionally, two tests were conducted using Ashless Filter Paper as the fuel. The flow velocity for both of these tests was 10 cm/s. One of these tests was run with an O_2 concentration of 18%, the other with 21%. The diluent for both tests was N_2.

The results of this study will first be presented by velocity, with comparison being made between the flames resulting from the two ignition techniques. Error bars are displayed for the flame and pyrolysis lengths for each test. These error bars represent the sum of the measurement errors from each component of the respective lengths.

Velocities are reported for each pyrolysis and flame element, as well as the mean- spread rates and growth rates of the flame and pyrolysis lengths. The mean-element flame and pyrolysis spread rates are defined as the average of the velocities of the flame tip/base, and the pyrolysis front/burnout front, respectively. The comparison to Jiang's steady-state mathematical model (Jiang, 1995) will also be presented for each velocity. The results of the Ashless Filter Paper tests will then be presented.

The final topic to covered will be the results of the tests which employed thermocouples. A comparison will be made with the temperatures predicted by Jiang's steady-state model. The effect of the thermocouples themselves on the tests will also be addressed by comparing these runs with tests of otherwise similar conditions which did not use thermocouples.

Results by Velocity

Sample Device Speed cm/s	Fuel KW or AFP	O_2 %	Ign. Type	Thermo Couple	Tip Spread cm/s	Base Spread cm/s	Flame Length Growth cm/s	Avg. Flame Elem. Spread cm/s	Pyrol Front Spread cm/s	Burn Front Spread cm/s	Pyrol Length Growth cm/s	Avg. Pyrol Zone Spread cm/s
0.00*	KW	18	Chem		-8.18	+1.20	-9.38	-3.50	+0.08	+0.04	+0.04	+0.06
0.00*	KW	18	Chem	No	-2.39	+1.19	-3.59	-0.60	+0.03	+0.03	0.00	+0.03
0.00*	KW	18	Chem	No	-2.56	+0.58	-3.14	-0.99	0.00	0.00	0.00	0.00
1.00^	KW	18	Chem	No	-1.32	+0.88	-2.20	-0.22	+0.12	+0.20	-0.08	+0.15
1.16^	KW	18	HW	No	+0.46	-0.01	+0.47	+0.23	+0.24	+0.24	0.00	+0.24
2.58^	KW	18	Chem	No	-1.53	+0.59	-2.12	-0.47	+0.15	+0.26	-0.11	+0.21
2.50^	KW	18	HW	No	+0.38	+0.26	+0.12	+0.32	+0.32	+0.22	+0.10	+0.27
2.55^	KW	18	HW	No	+0.20	+0.25	-0.05	+0.23	+0.42	+0.32	+0.10	+0.37
2.52	KW	18	HW	No	+0.48	+0.20	+0.28	+0.34	+0.35	+0.37	-0.02	+0.36
5.12	KW	18	Chem	No	+0.45	+0.47	-0.02	+0.46	+0.71	+0.71	0.00	+0.71
5.09	KW	18	HW	No	+0.47	+0.70	-0.23	+0.59	+0.68	+0.67	+0.01	+0.68
7.47	KW	18	HW	No	+0.86	+0.93	-0.07	+0.90	+1.24	+0.98	+0.26	+1.11
10.07	KW	18	Chem	No	+0.78	+1.36	-0.58	+1.07	+1.20	+1.09	+0.11	+1.15
9.92	KW	18	HW	No	+1.05	+0.99	+0.06	+1.02	+1.50	+1.12	+0.38	+1.31
9.89	AFP	18	HW	No	+0.46	+0.05	+0.41	+0.26	+0.13	+0.07	+0.06	+0.10
9.85	AFP	21	HW	No	+1.18	+0.06	+1.12	+0.62	+0.30	+0.17	+0.13	+0.24
10.05	KW	18	HW	Yes	+1.88	+0.89	+0.99	+1.39	+1.02	+0.97	+0.05	+1.00
9.88	KW	18	HW	Yes	+1.15	+1.05	+0.10	+1.10	+0.99	+0.93	+0.06	+0.96

1) All pyrolysis data taken at end of test time
2) Flow stops at about 3.7 sec for (nominal) device velocity of 10 cm/sec
3) ^ : Flame too dim to track at some time, but pyrolysis elements continued to spread
*4) * : Flame extinction: no movement of pyrolysis elements*

Table 2 Results by Velocity

Table 2 summarizes the test results. Due to the short duration of the available test time, steady-state propagation was not achieved in any test, though several

cases may have been near steady-state. The flame/pyrolysis element velocity data was taken by applying a linear regression to a portion of the data near the end of the test for each element. In cases where the flame became too dim to see before the end of the test, the portion selected for the curve-fit was a section near the end of the visible data. The duration of the data used for this curve-fit varied for each test, but an attempt was made to use the greatest amount of data for each regression possible that would capture the behavior of the element at the end of the test. The duration of the curve-fit ranged from approximately 0.5 seconds of data for the quiescent cases, to about 2 seconds of data for the highest velocities. Similarly, due to the transient nature of these tests, the mean element spread rates were defined as the arithmetic average of the velocities of the base and tip for the flames, and the burnout front and pyrolysis front for the pyrolysis zone. A measure of the steadiness for either the flame or pyrolysis zone is the growth rate of their length, which is the difference in the velocity of the component elements.

Quiescent Flow

The quiescent flow cases occurred when mechanical malfunctions with the flow device occurred. Three cases occurred for the chemical ignition technique, none using the hotwire ignition system. All three tests were performed with the translation device configured to operate in the "up" direction. This means that any buoyant flow caused by the residual g-levels was in the opposed direction.

The release of energy from the chemical ignition system created a non-uniform flameball which enveloped the leading edge of the fuel sample. The shape of this non-uniform ignition burst was significantly different for each of the three cases.

Following the non-uniform flameballs non-uniform pyrolysis fronts were observed. This was readily visible in the video images and the non-uniformity remained in the quenched samples retrieved at the end of the tests.

These flame images become too dim to see approximately 1.3 seconds into the test. The pyrolysis fronts never propagated after the ignition burst. The burnout fronts did not propagate after 1.5 seconds. At this point, the combustion reaction was considered to have stopped. Figures 11, 12, and 13 show the data plots from these tests.

Comparison of the three cases shows that the mean-area pyrolysis length for each test was between 1.3 cm and 1.5 cm. The shape of the ignition flameball was different in each of the three cases.

Velocity data was recorded for the flame elements in these tests. However, the error associated with these velocities was large, due to the small amount of time available for the curve-fit (Appendix I). Quantitative flame element velocity data for these tests was disregarded.

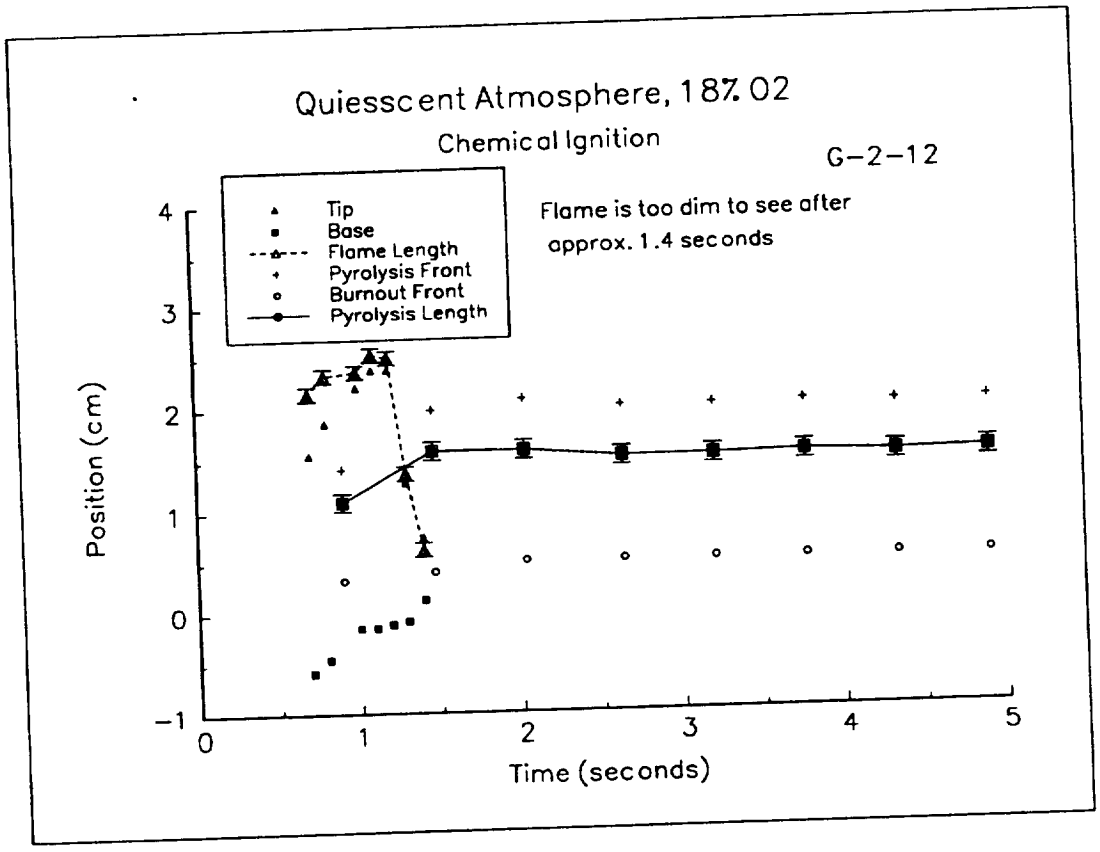

Figure 11

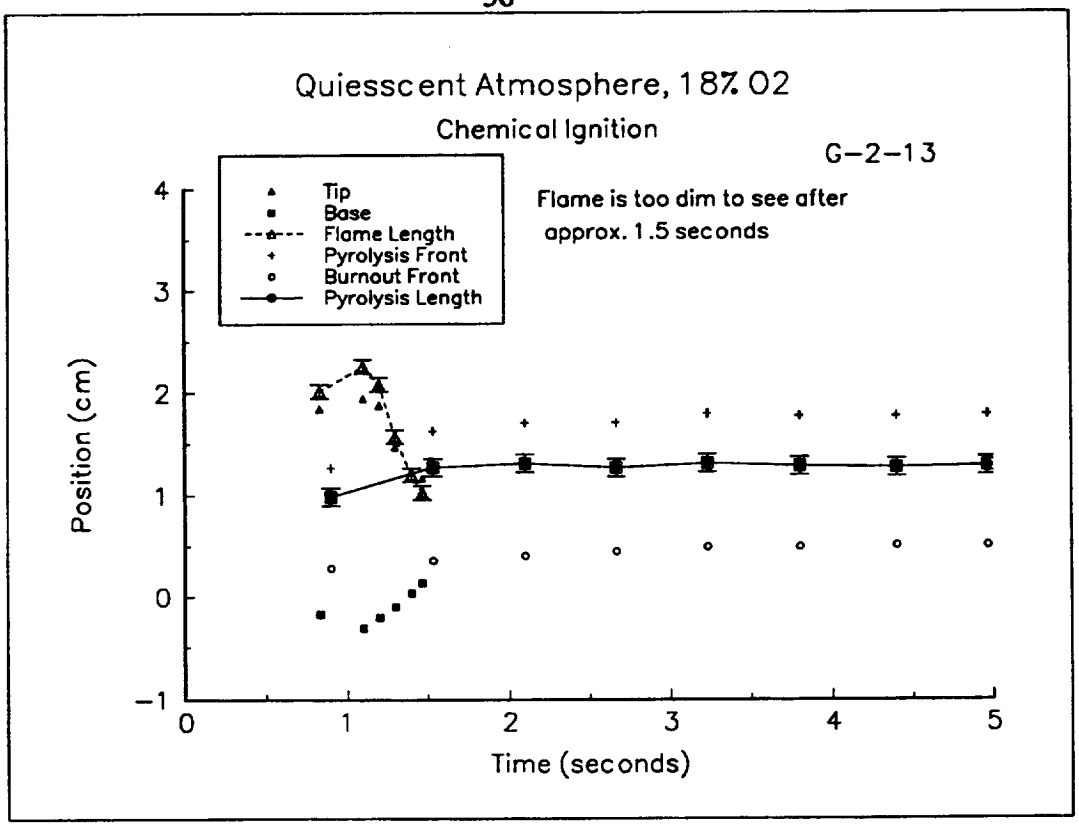

Figure 12

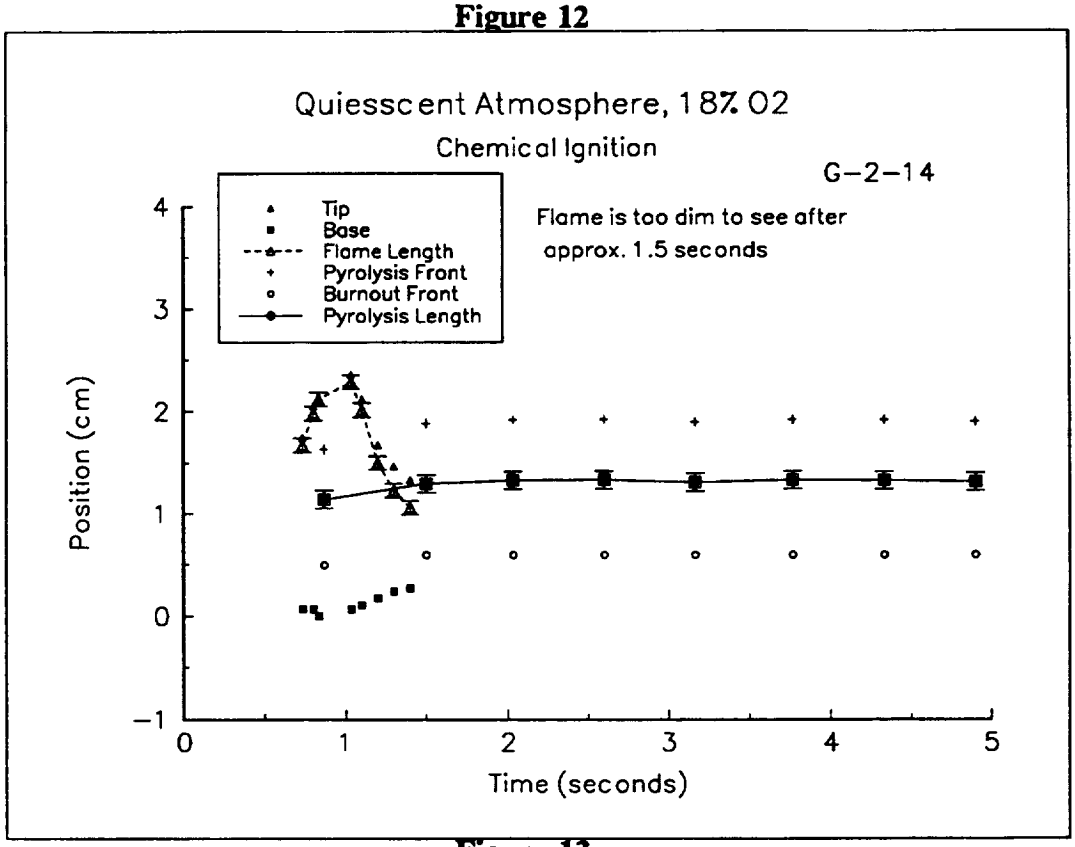

Figure 13

1 cm/sec Flow

The carriage velocities for these two points were measured to be 1.16 cm/sec for the hotwire ignition technique, and 1.00 cm/sec for the chemical ignition technique. The large error in the flow velocity for the hotwire case was attributed to a faulty command to the computer controller, because no other errors of this magnitude were observed in either the calibration or testing operation. Note that the hotwire test was done with the fuel device moving in the "down" direction, while the chemical test was carried out in the "up" direction. The buoyant flows induced by the residual g-levels then tended to further increase the relative velocity of the hotwire case, and reduce that of the chemical ignition case.

Figure 14 is a plot of the flame and pyrolysis elements for the hotwire-ignited test. This system produced a small, relatively uniform ignition flameball followed by a uniform pyrolysis front. Both the pyrolysis and burnout fronts propagated until the end of the drop. The mean-area pyrolysis length was steady (within the limits of the error analysis) at approximately 0.45 cm, and progressed at a speed of 0.24 cm/sec.

The flame became too dim to see at approximately 2 seconds into the drop. However, the pyrolysis zone continued to propagate, indicating that the combustion reaction was still occurring, although very weakly.

Figure 15 shows the results of the chemically-ignited test. This test showed a large non-uniform ignition burst, and subsequently a non-uniform

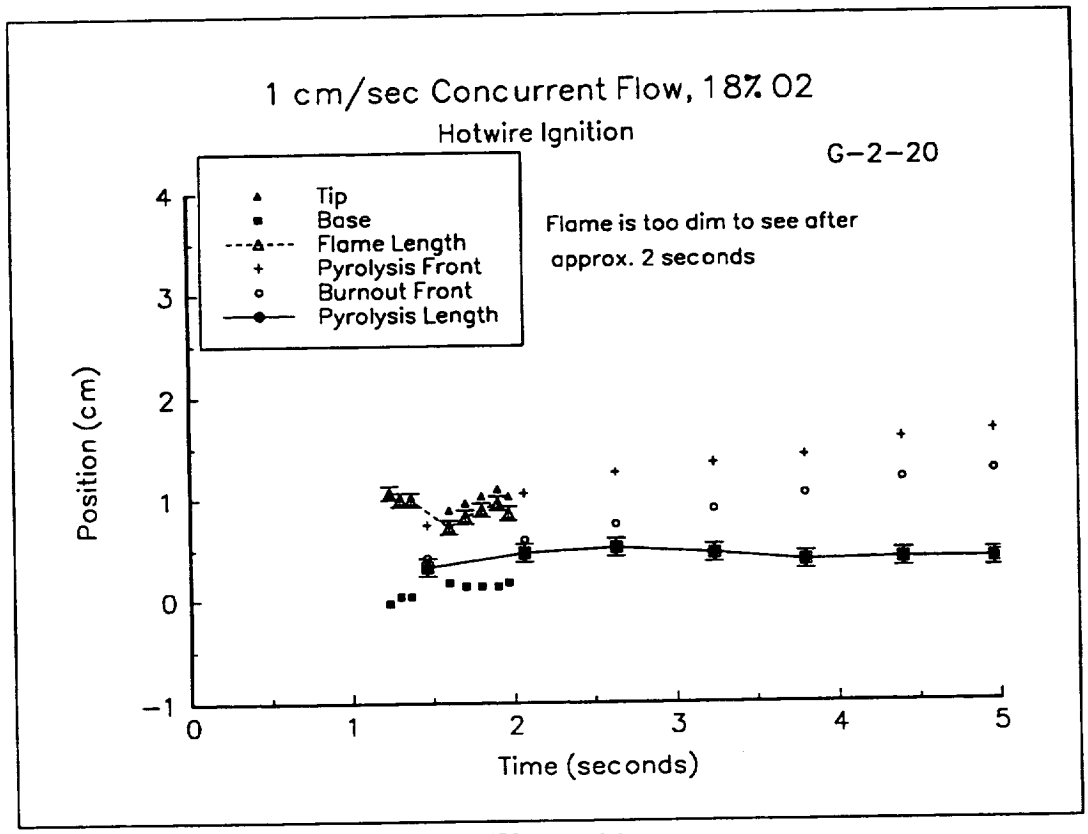

Figure 14

pyrolysis front. This initial pyrolysis zone was approximately four times larger than that produced by the hotwire system. The final average pyrolysis length was approximately 1.0 cm. The partially-burned sample from this test can be seen in Figure 16.

The initial flame length produced by the chemical system was about 2 cm, where that produced by the hotwire system was close to 1 cm. However, the flame from the chemical system quickly shrank to a length of about 0.75 cm, and became too dim to see at 1.5 seconds into the drop. This can be seen in Figure 17, which shows the flame elements from both tests together.

The error associated with the base velocity measurements for this flow

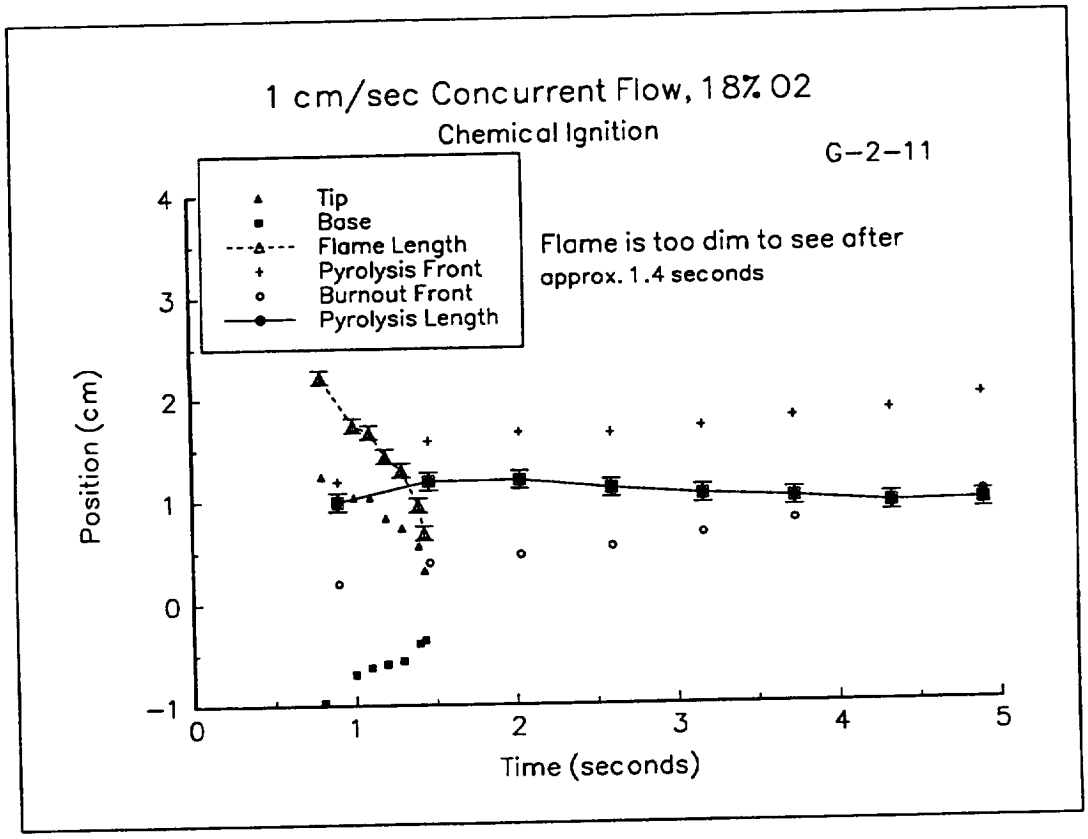

Figure 15

speed were quite large (122%), so quantitative measurements of the flame element velocities for these tests were disregarded.

The flame images from both tests do not indicate whether the flames would have sustained in a longer test. Although the flames were too dim to be seen with the imaging techniques employed here, the propagation of the pyrolysis zones indicate that the reactions were still taking place when the tests ended. The dimness of the flame and the decrease in the flame length suggest that the reactions were getting very weak, and may have stopped at some point. Jiang's model (Jiang, 1995), found no steady state solution at this flow velocity.

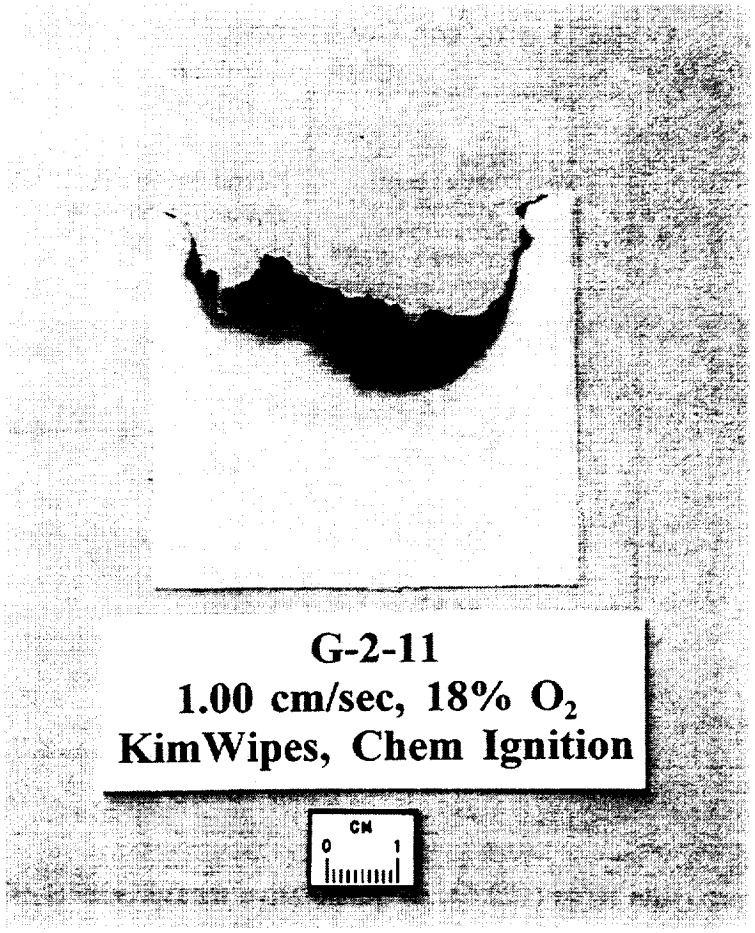

Figure 16 Partially Burned Sample

An interesting comparison can be made between the chemical ignition tests for the Quiescent and 1 cm/sec flow cases. The average pyrolysis lengths, which in both cases never propagate after the ignition burst, are very similar. Also, the visible flames become too dim to see by no later than 1.5 seconds for both cases. However, the flame length in the Quiescent case actually grows from an initial value of about 2.1 cm at 0.8 seconds to a value of 2.5 cm at 1.2 seconds, before quickly shrinking and dimming at 1.3 seconds. The flame

length in the 1 cm/sec case declines steadily from a value of about 2.1 cm at 0.8 seconds until it is too dim to see at about 1.3 seconds. A possible reason for this may be that the free-stream velocity of 1 cm/sec is too slow to transport sufficient oxygen to sustain the flame. However, this low speed flow would cause convective cooling which would not be present in the quiescent case. This could account for the decreased flame length.

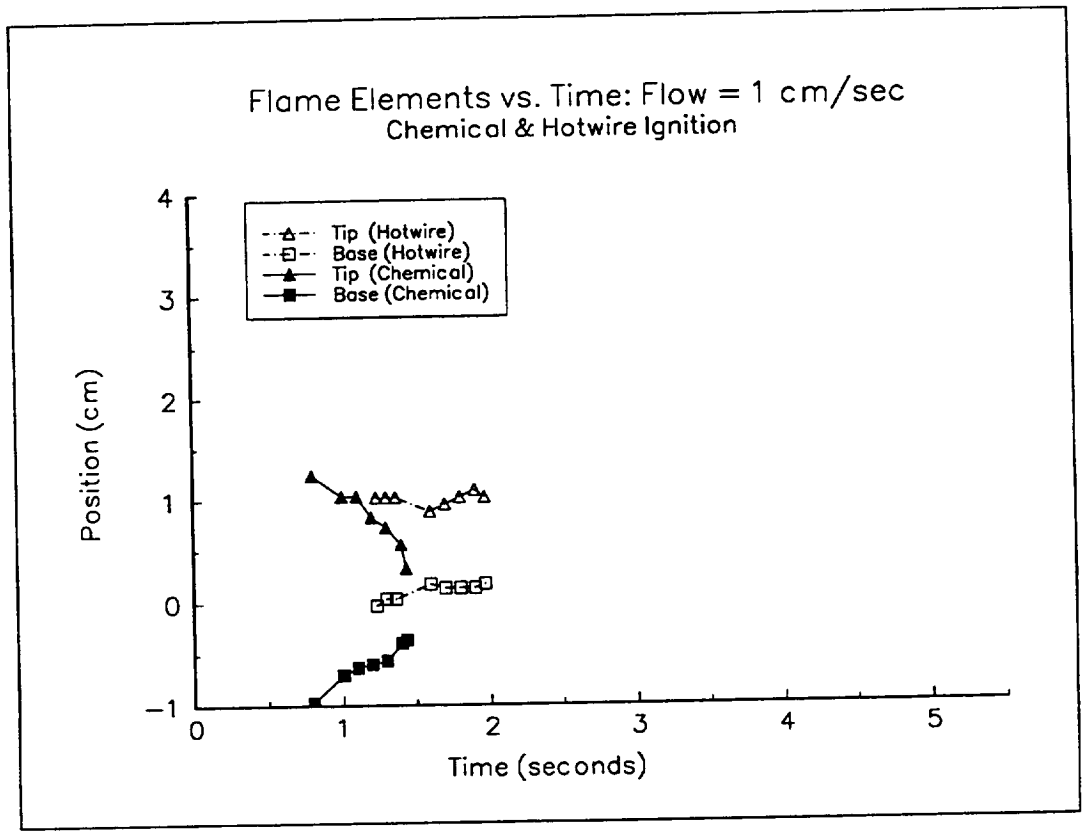

Figure 17

2.5 cm/sec Flow

Four experiments were performed with a nominal carriage velocity of 2.5 cm/sec, three with the hotwire ignition system and one with the chemical system. For the three hotwire ignition tests, two were conducted with the fuel translation device moving in the "up" direction, one in the "down" direction. The respective carriage velocities were 2.50 cm/sec and 2.55 cm/sec for the "up" cases (test numbers G-2-15 and G-2-16, respectively), and 2.52 cm/sec for the "down" case (test number G-2-17). The results of these tests can be seen in Figures 18, 19 and 20, respectively.

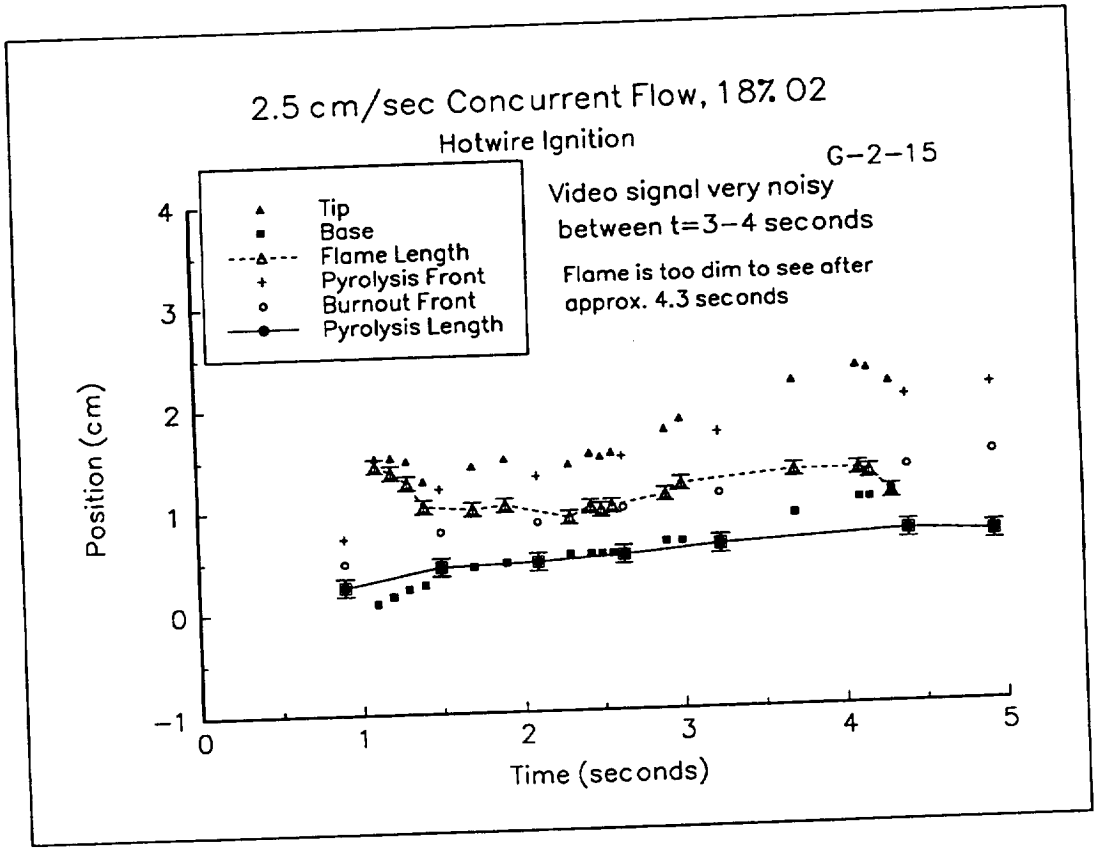

Figure 18

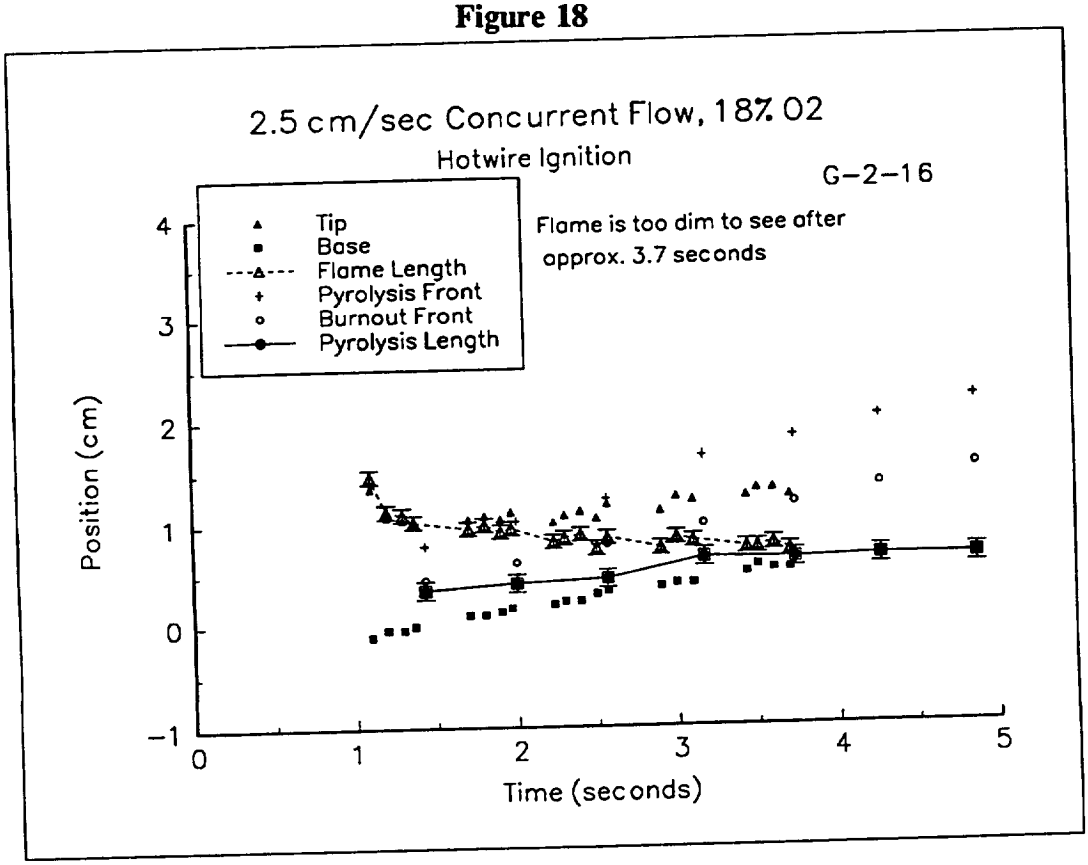

Figure 19

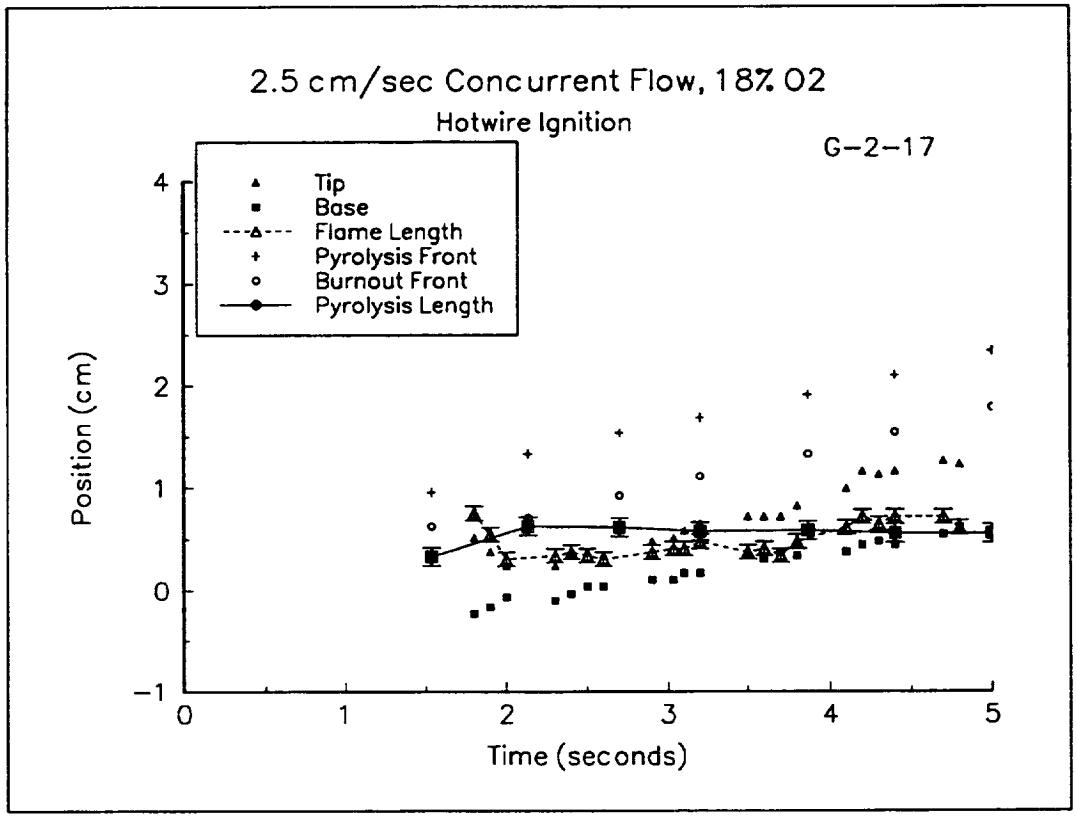

Figure 20

Comparison of the three cases in Figure 21 show the pyrolysis lengths of all three to be comparable from 2.5 seconds on, within the limits of the error analysis. The flame lengths are somewhat different, though, with G-2-15 and G-2-16 both having somewhat longer flames than G-2-17. It should be noted, though, that the flames of both G-2-15 and G-2-16 become too dim at approximately 4 seconds, while the flame in G-2-17, though somewhat shorter, stays bright enough to track for the entire drop. Also note that the flame tip for test G-2-17 was upstream of the burnout front for the entire test. This was not observed for either test G-2-15, or G-2-16.

It is difficult to make comparisons between the flame lengths of these

three tests, due to variations between the upward-moving tests (G-2-15 and G-2-16), which were thought to be conducted identically. The trend appears that these tests had longer flame lengths than test G-2-17, which was conducted in the downward direction. It may be that buoyant flows caused by the residual g-levels could explain this. Estimations of this buoyant velocity are shown in Appendix II. However, contrary to the experimental observations, the tests with the reduced velocities (due to buoyancy) were expected to have shorter flames than that of the test where the flow was enhanced by buoyancy. Unfortunately, the variation of the data prevents a conclusion on this matter.

Because the results of all three cases were observed with no other quantifiable differences to explain these effects, the mean-element spread rates and flame element measurements reported for subsequent comparisons will be the average of the results from all three tests.

The average carriage velocity for the hotwire ignition cases was 2.52 cm/sec. The carriage velocity in the chemical ignition case was 2.58 cm/sec.

As in the case of the 1 cm/sec chemical ignition case, the ignition burst from the chemical ignitor was much larger than those of the hotwire ignitor. The chemical ignitor yielded a non-uniform flameball, which produced a non-uniform pyrolysis front. The pyrolysis front did not propagate after approximately 2 seconds.

The hotwire ignitor produced small, fairly uniform ignition flame-balls which gave uniform pyrolysis fronts. Figure 22 shows the partially burned

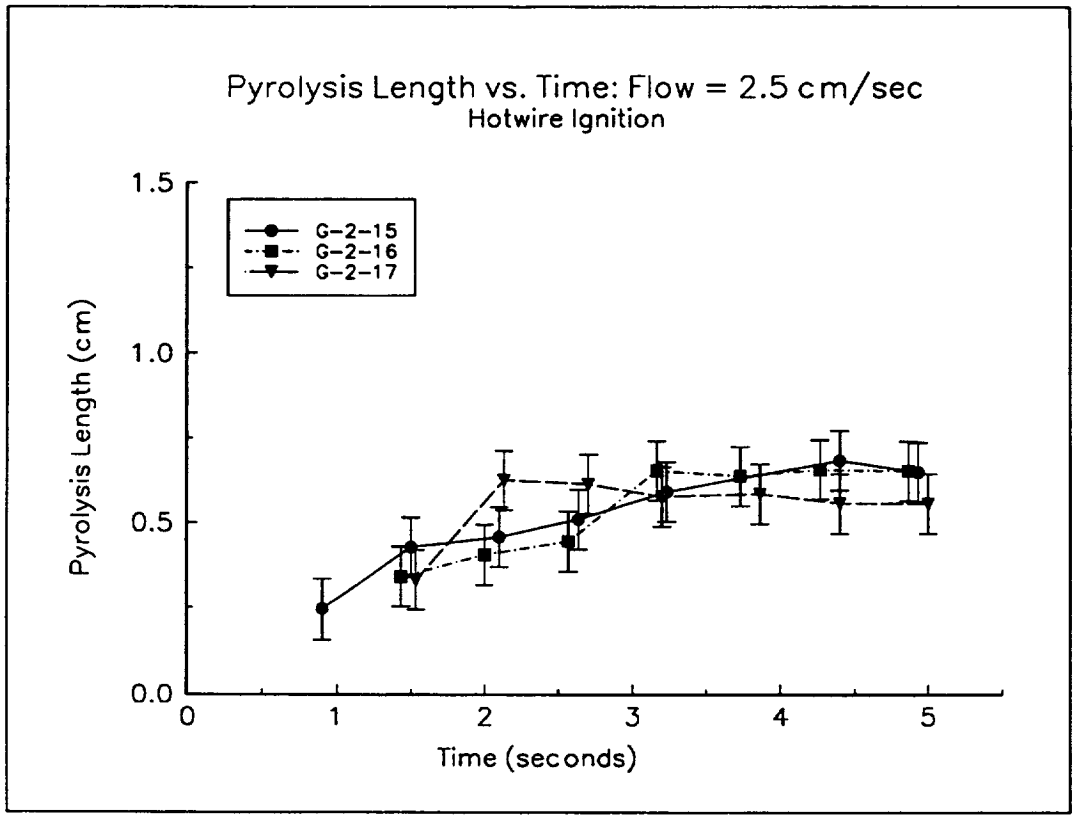

Figure 21

sample from test G-2-17. The uniform pyrolysis front shown in this sample was typical of the pyrolysis fronts for the hotwire-ignited tests. In all three cases, the pyrolysis fronts propagated throughout the entire drop time. The average of the mean-area pyrolysis lengths for the three tests at the end of the drops was 0.62 cm, and within the limits of the errors, appeared steady after about 3 seconds. The pyrolysis zone(s) advanced at an average velocity of 0.33 cm/sec.

The data from the chemical ignition test is shown in Figure 23. This test produced a flame length of about 2.5 cm at 1.1 seconds, which then shrunk at a rate of 2.12 cm/sec to 0.5 cm at 2 seconds. At that time, the flame

became too dim to see. The burnout front continued to progress throughout the full drop time, at a velocity of 0.21 cm/sec, indicating that the reaction was still taking place, although weakly. The final mean-area pyrolysis length for this run was approximately 0.85 cm, and was shrinking.

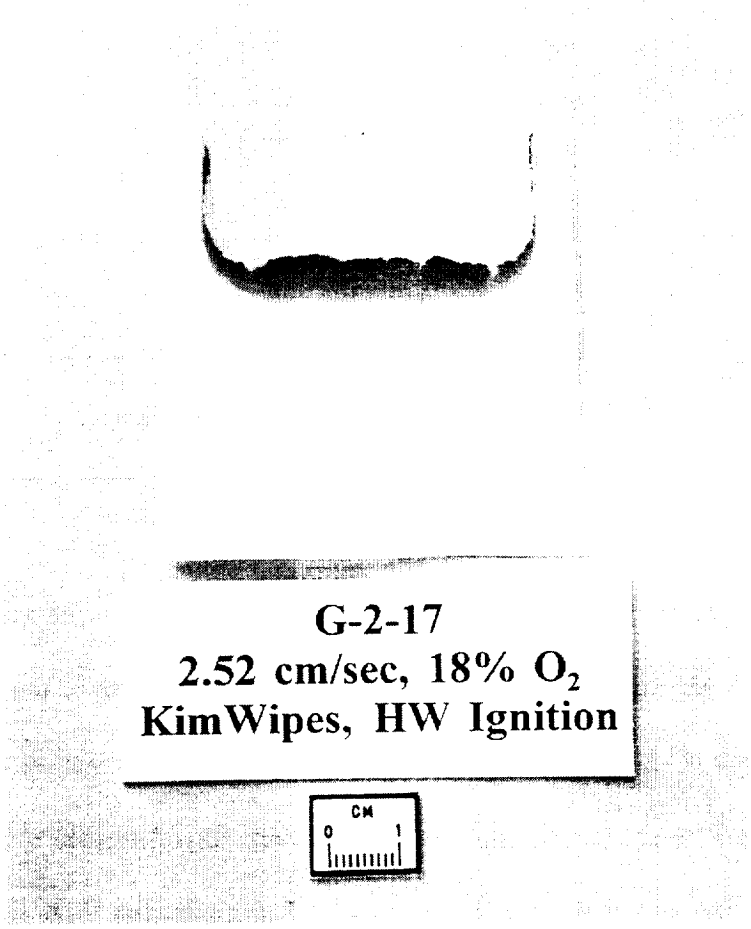

Figure 22 Partially Burned Sample

The hotwire-ignited tests gave flame lengths which were shorter than those of the chemically-ignited test near the beginning of the drop, with tests G-2-15 and G-2-16 showing an average flame length of 1.4 cm at 1.1 seconds

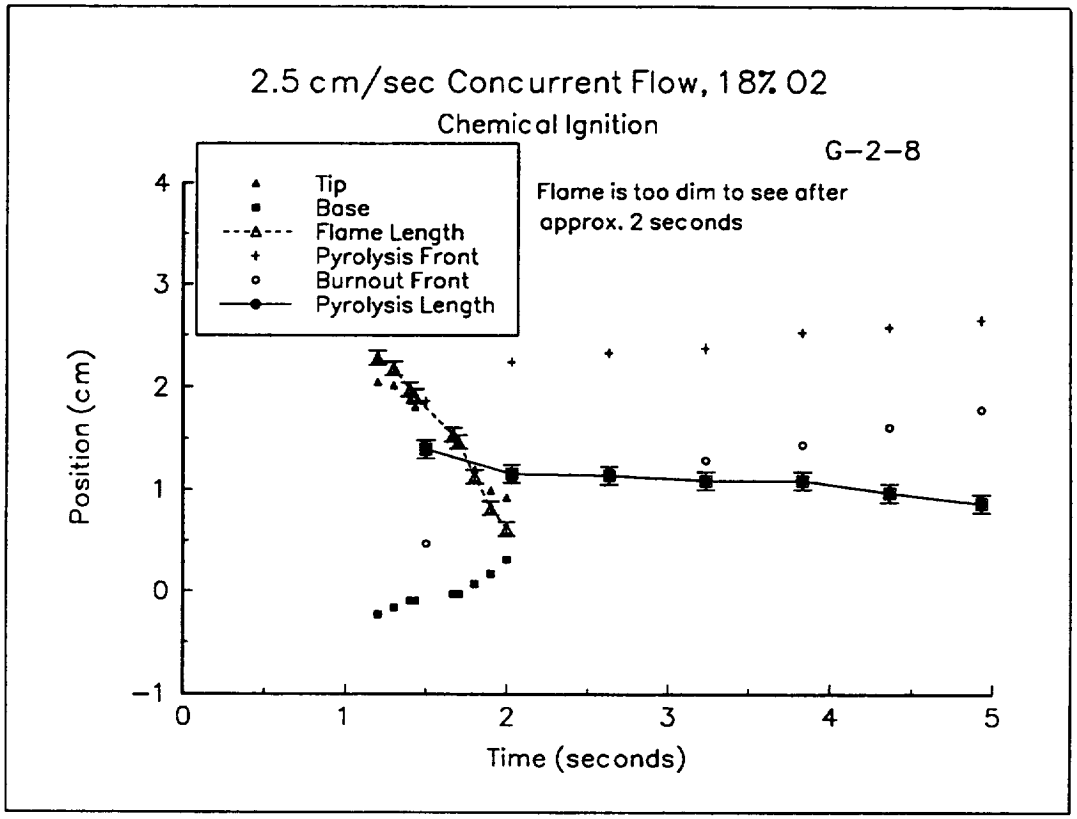

Figure 23

(due to imaging problems, flame data for test G-2-17 was not available until time t=1.8 seconds). Figure 24 shows the flame elements of the chemically-ignited test (G-2-8) together with those of one of the hotwire-ignited tests (G-2-16). The flames from the hotwire-ignited tests stayed visible much longer, though, with an average flame length at 3.7 seconds (the time at which one of the three cases became too dim) of 0.8 cm. The flame lengths from the three tests grew by an average of 0.12 cm/sec, and these flames spread at an average velocity (for the three tests) of 0.29 cm/sec. As previously mentioned, the pyrolysis zones continued to propagate through the entire drop.

Similar to the 1 cm/sec case, the results of the chemical ignition test

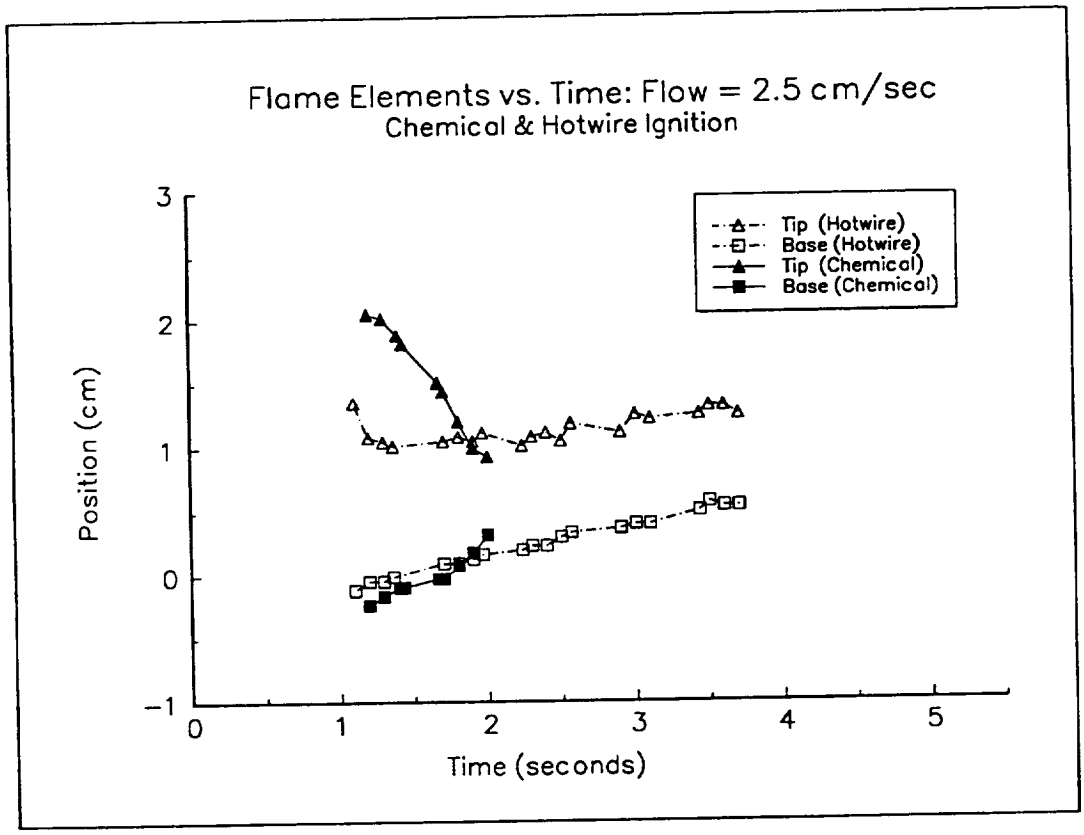

Figure 24

suggest that oxygen starvation caused by the large ignition burst caused these flames to be weaker than those produced by the hotwire system. The flow velocity was not large enough to bring sufficient oxidizer into the reaction region for a strong, visible flame. Jiang's model (Jiang, 1995) found a steady-state solution at the free stream velocity of 2.52 cm/sec, with a flame spread rate of 0.20 cm/sec.

5 cm/sec Flow

The actual carriage velocities for this case were 5.09 cm/sec (downward) for the hotwire test, and 5.12 cm/sec (upward) for the chemical

test.

The chemical ignitor yielded a large, non-uniform flameball. However, at this flow velocity, the resulting pyrolysis front was uniform. Figure 25 shows the flame and pyrolysis elements for this test. The mean-area pyrolysis length stayed constant within the error at approximately 1 cm for the duration of the test. The pyrolysis zone advanced at about 0.71 cm/sec over the final 2 seconds of the test.

The hotwire system produced a uniform ignition burst which gave a uniform pyrolysis zone. The results of this test (Figure 26) show the mean-

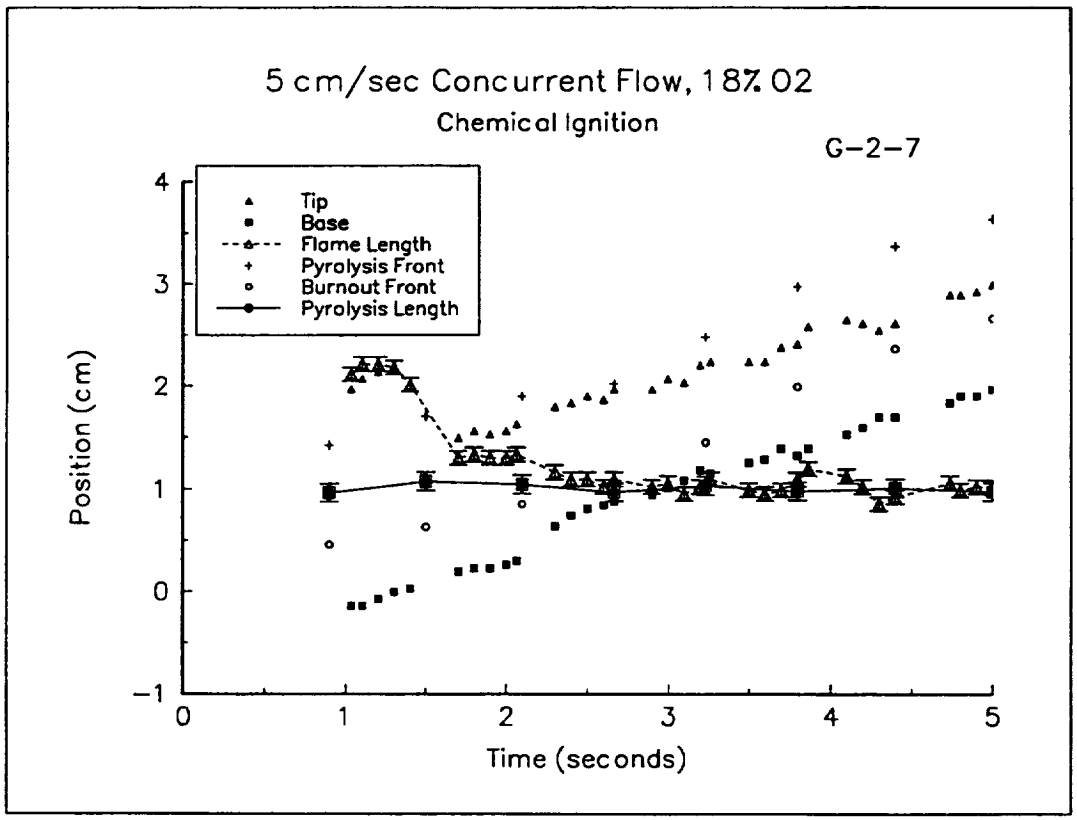

Figure 25

area pyrolysis length was constant at about 1 cm after 2 seconds. The pyrolysis zone for this case spread at about 0.68 cm/sec for the last 2 seconds of the test.

Similar to the 2.5 cm/sec cases, the chemical system gave a flame length which was initially longer than that produced by the hotwire system

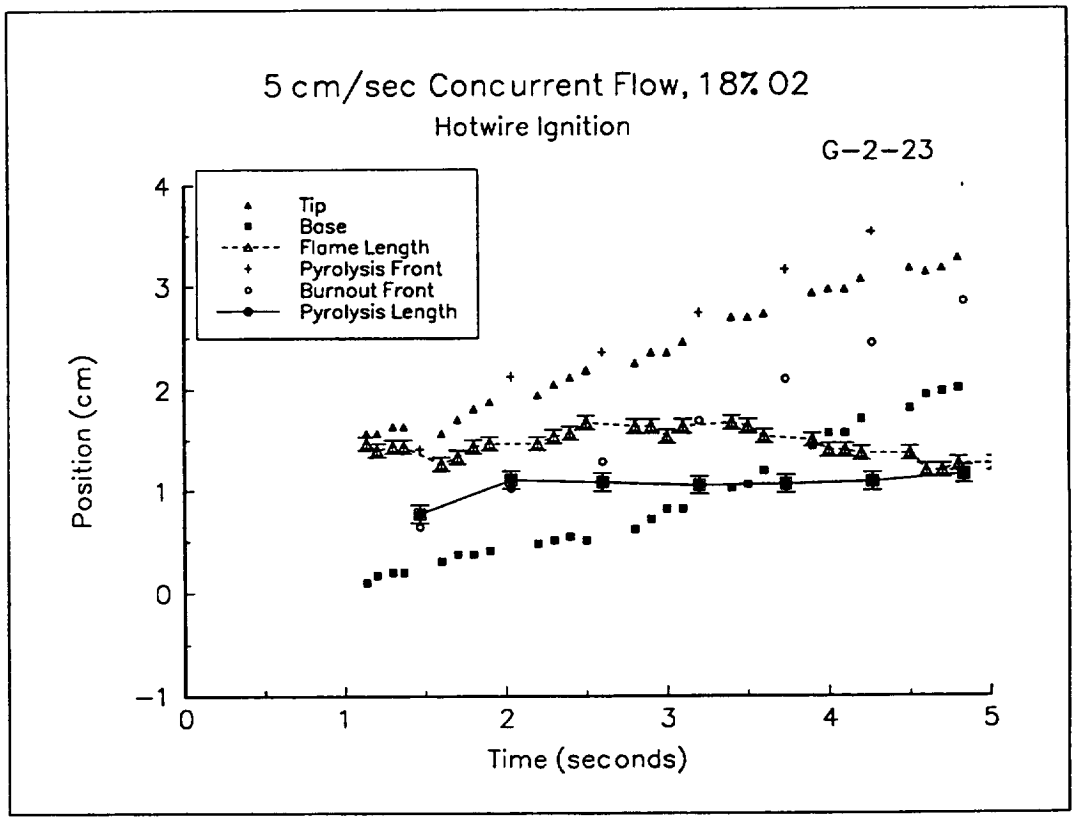

Figure 26

(Figure 27). At 1 second into the drops, the flame lengths were approximately 2 cm and 1.4 cm, respectively. However, by 2 seconds, the flames for the chemical case had receded to about 1.3 cm, while the hotwire flames were unchanged (within the experimental error). The flame from the chemical

system continued to decline to a value of about 1 cm by 2.5 seconds. This flame length remained somewhat steady for the remainder of the drop, and spread at a rate of 0.46 cm/sec. The flame from the hotwire system likewise remained fairly steady at a length of about 1.5 cm until about 3.8 seconds, when it declined slightly to about 1.2 cm for the rest of the drop. It progressed at a speed of 0.58 cm/sec. The difference in the flame lengths for the two tests suggests that the ignition effects are still affecting the flames at the end of the test time, though the effect was less than that experienced at lower free-stream velocities.

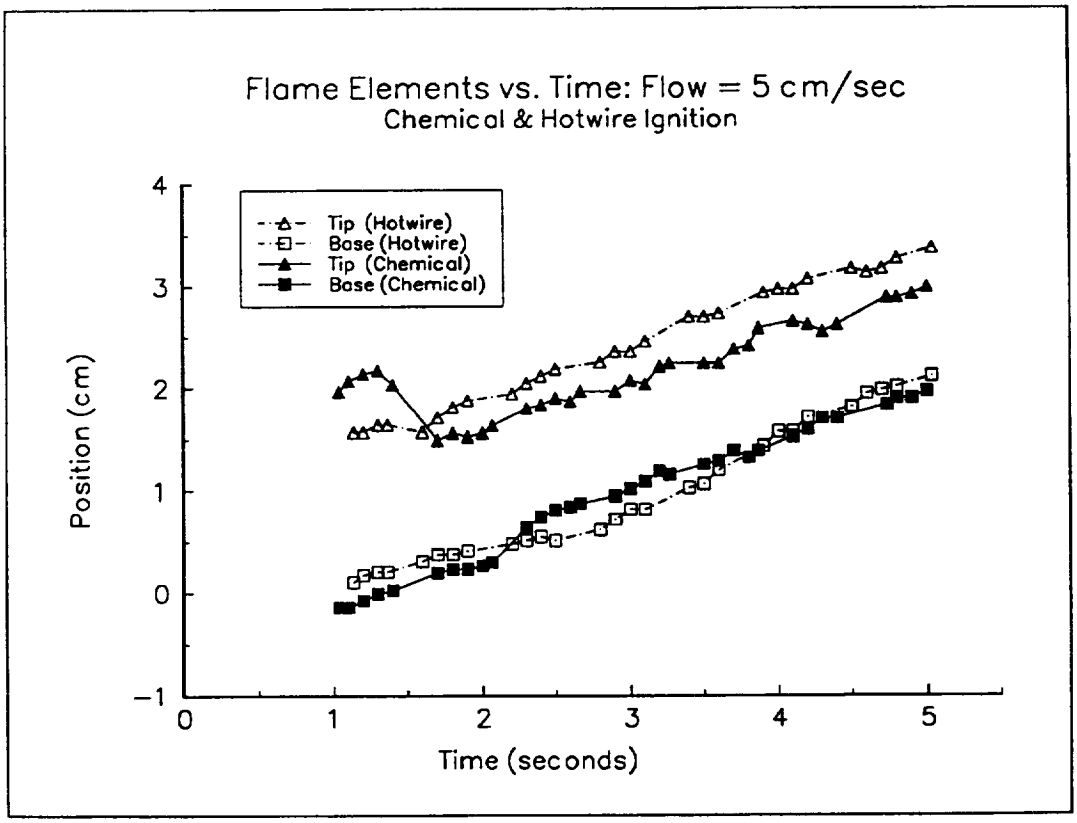

Figure 27

In both the chemical and hotwire cases, it appears as though the mean-

area pyrolysis lengths converged to a similar length of about 1 cm. Figure 28, which gives the mean-area pyrolysis lengths for the two tests as a function of time, shows that these values were steady and similar within the limits of the error.

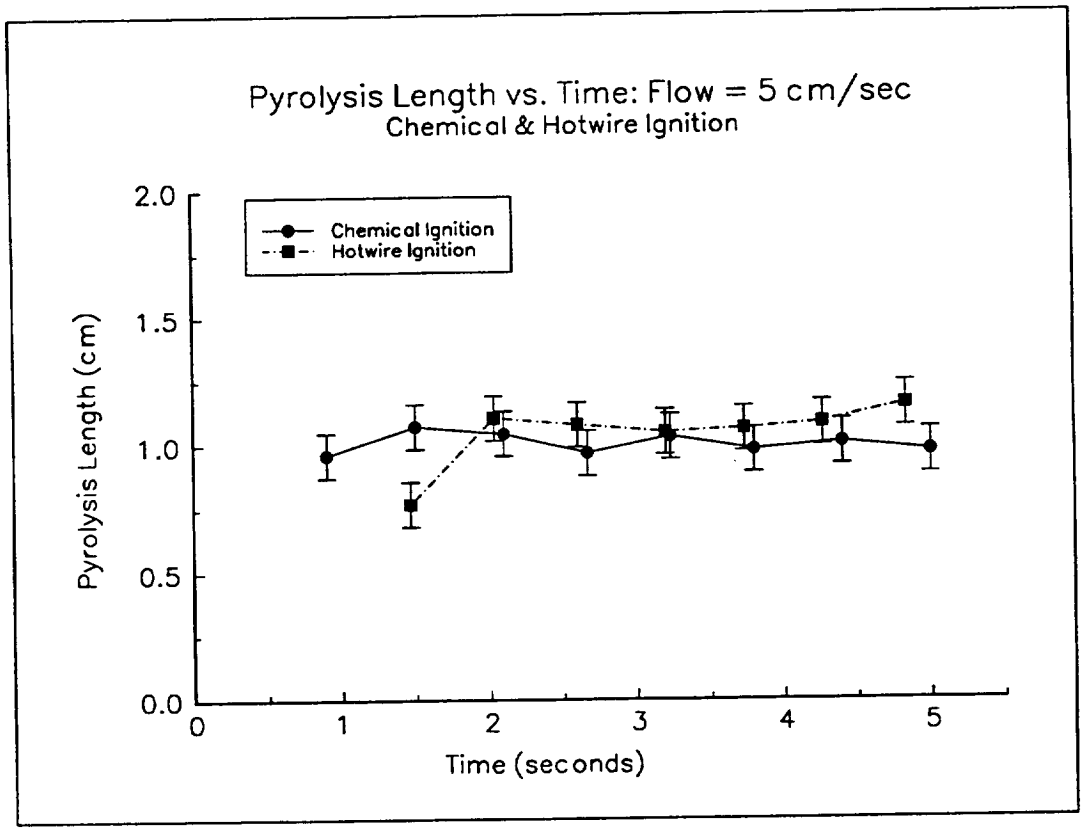

Figure 28

Jiang's steady-state model (Jiang, 1995) predicted a flame spread rate of 0.56 cm/sec for the free stream velocity of 5.12 cm/sec.

7.5 cm/sec Flow

Only one test was available for the carriage velocity of 7.5 cm/sec. This was conducted with a hotwire ignition system, with the carriage moving in

the "down" direction. Note that for this carriage velocity, the carriage was required to stop at approximately 4.7 seconds, due to the length of travel available for the carriage. The actual carriage velocity was verified to be 7.47 cm/sec.

The ignition burst and pyrolysis zone for this case were uniform, as in previous hotwire tests. The data for this test is displayed in Figure 29, and shows a mean-area pyrolysis length of approximately 1.2 cm at 1.5 seconds, which grew at a rate of about 0.26 cm/sec from 2.5 seconds until the end of the test. The final mean-area pyrolysis length was about 1.8 cm. The mean-element spread rate for the pyrolysis zone was approximately 1.11 cm/sec.

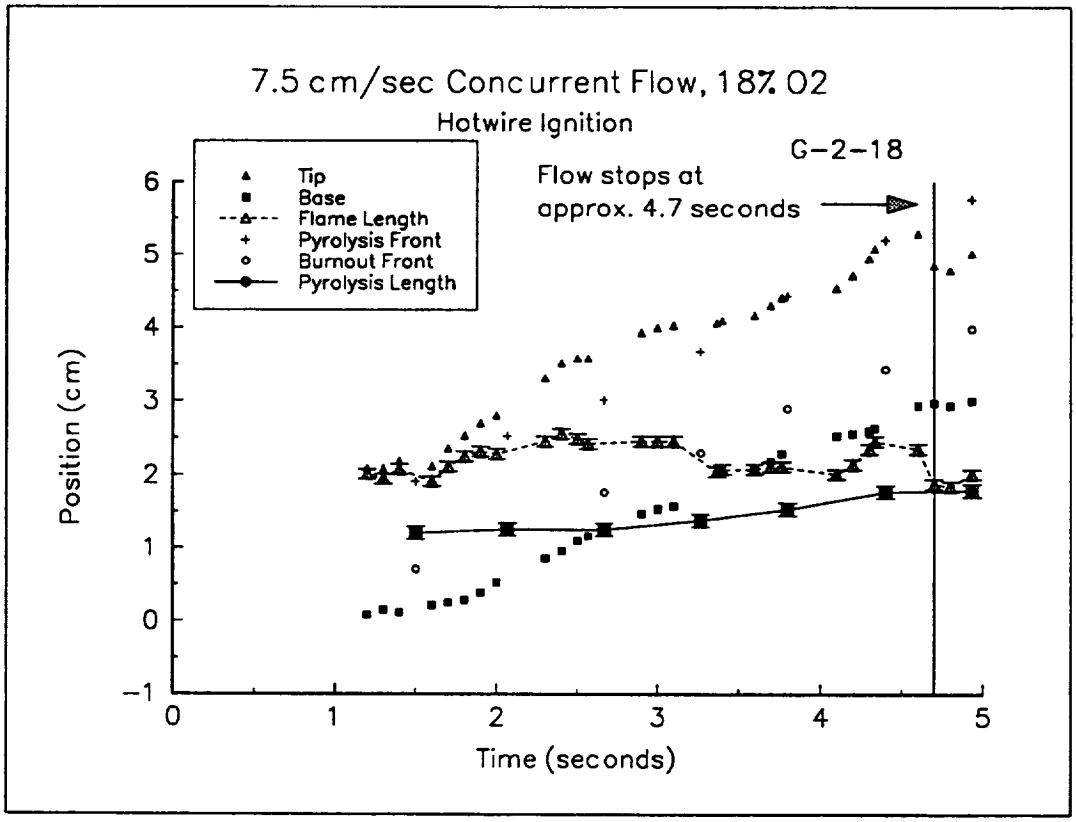

Figure 29

The flame length at 1.3 seconds was about 2 cm. The flame for this test exhibited considerable unsteadiness, but the average value of the flame length stayed around 2.1 cm. This mean-element flame spread rate was 0.90 cm/sec.

The changing flame and pyrolysis lengths indicate that this test did not reach steady state. By the end of the flow time, the value of the mean-area pyrolysis length is approaching value of the flame length, but it is clear that neither had reached a constant value in the available time.

Jiang's steady-state model (Jiang, 1995) gave a flame spread rate of 0.96 cm/sec.

10 cm/sec Flow

The actual carriage velocities for these tests were 9.92 cm/sec for the hotwire test and 10.07 cm/sec for the chemical test. At this carriage velocity, the maximum flow time available was approximately 3.7 seconds. In this case, both ignition systems were tested with the carriage moving in the "down" direction.

As in the other cases, the flame initially produced by the chemical system was longer than that produced by the hotwire system. Figure 30 shows the results of the chemical-ignition test. By 1.5 seconds, the flames from the chemical system had receded to a length of 2.9 cm, which was about the same length as the hotwire-ignited flames at that time. From that point until the time

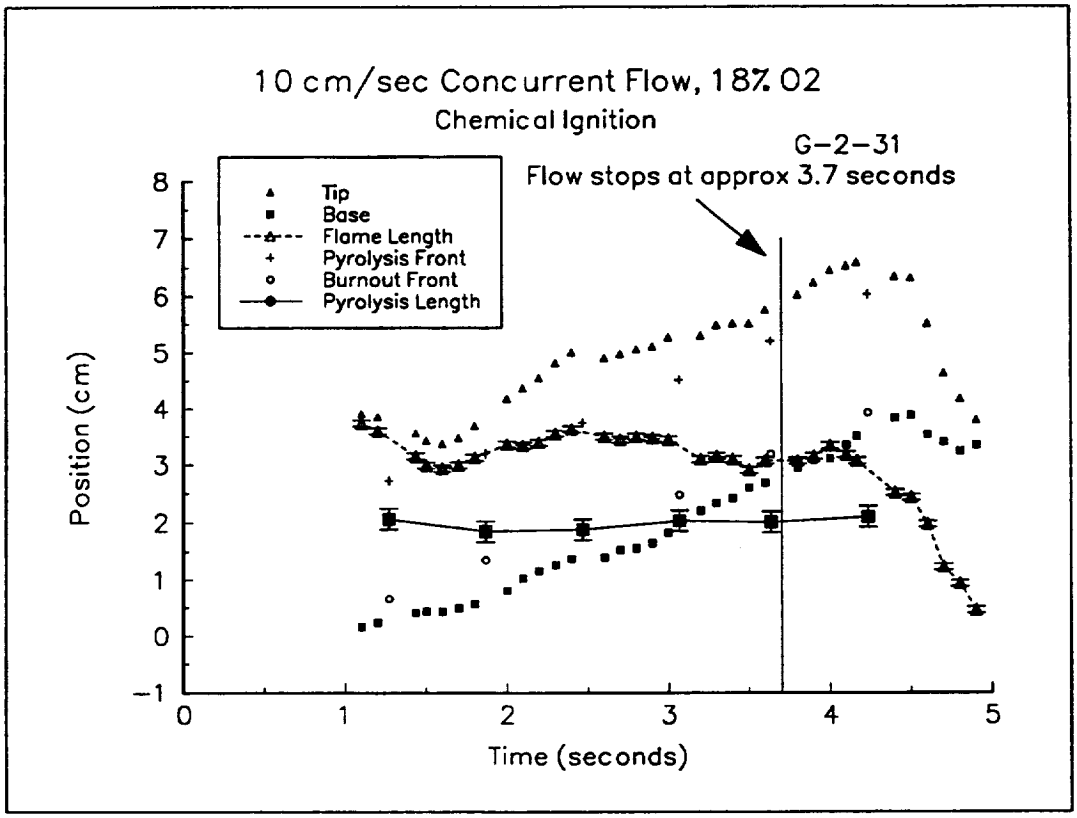

Figure 30

the flow stopped, the flames from the chemical ignitor averaged an approximate length of 3.2 cm. The mean-element flame spread rate was 1.06 cm/sec.

The flames from the hotwire system grew from 2.9 cm at 1.5 seconds to a length of 3.9 cm at 2.5 seconds (Figure 31). This length then stayed fairly constant for the remainder of the flow time. Figure 32 shows that the hotwire-ignited test exhibited a longer flame than the chemically-ignited test (after the ignition burst subsided), which is consistent with the tests at other flow velocities. The mean-element flame spread rate for the hotwire ignition test at this velocity was 1.02 cm/sec.

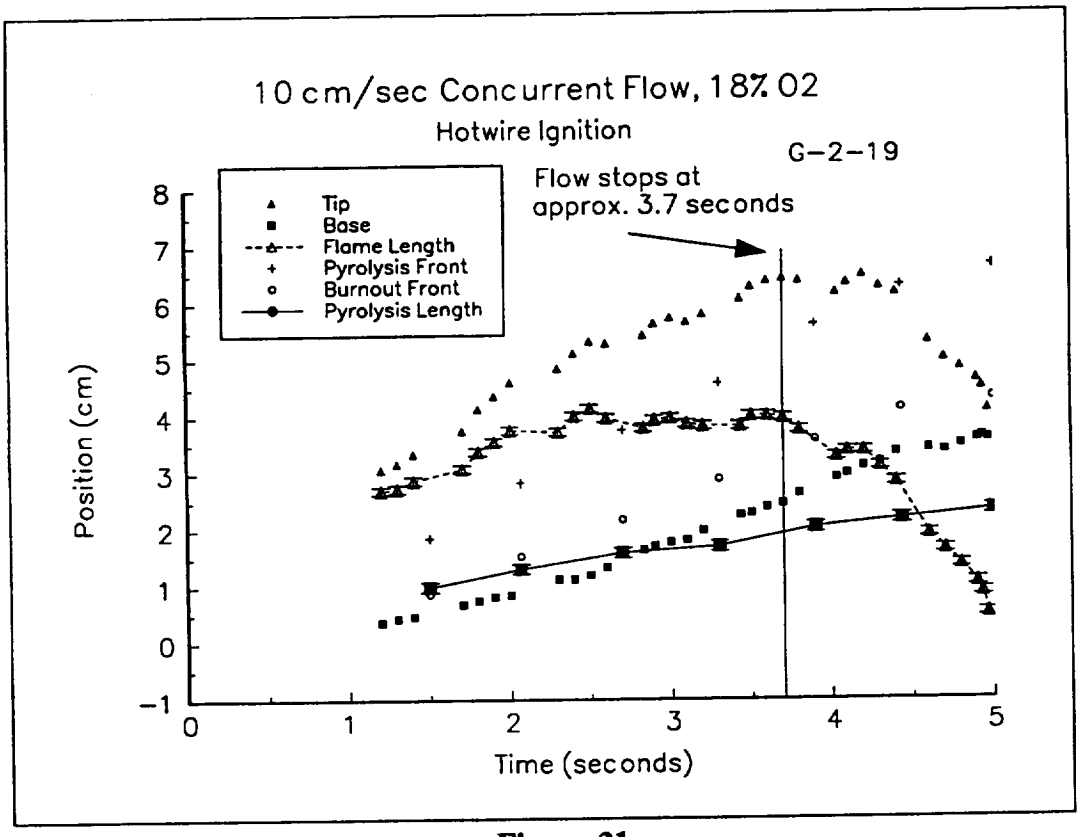

Figure 31

As in the case of the 5 cm/sec tests, the pyrolysis zones produced by both ignition systems were uniform, despite the non-uniform ignition burst in the chemical ignition case. Figure 33 shows the burned sample from test G-2-31. Like all previous tests, the pyrolysis length produced by the ignition burst is significantly longer for the chemical system than that produced by the hotwire system. This is clearly shown in Figure 34. (Note that the difference in the error bars for these two tests was because the tests were conducted with different optical arrangements, which lead to different errors. For details on this, see the Error Analysis in Appendix I). The average pyrolysis lengths at approximately 1.5 seconds were 2.0 cm for the chemically-ignited test and 1.0

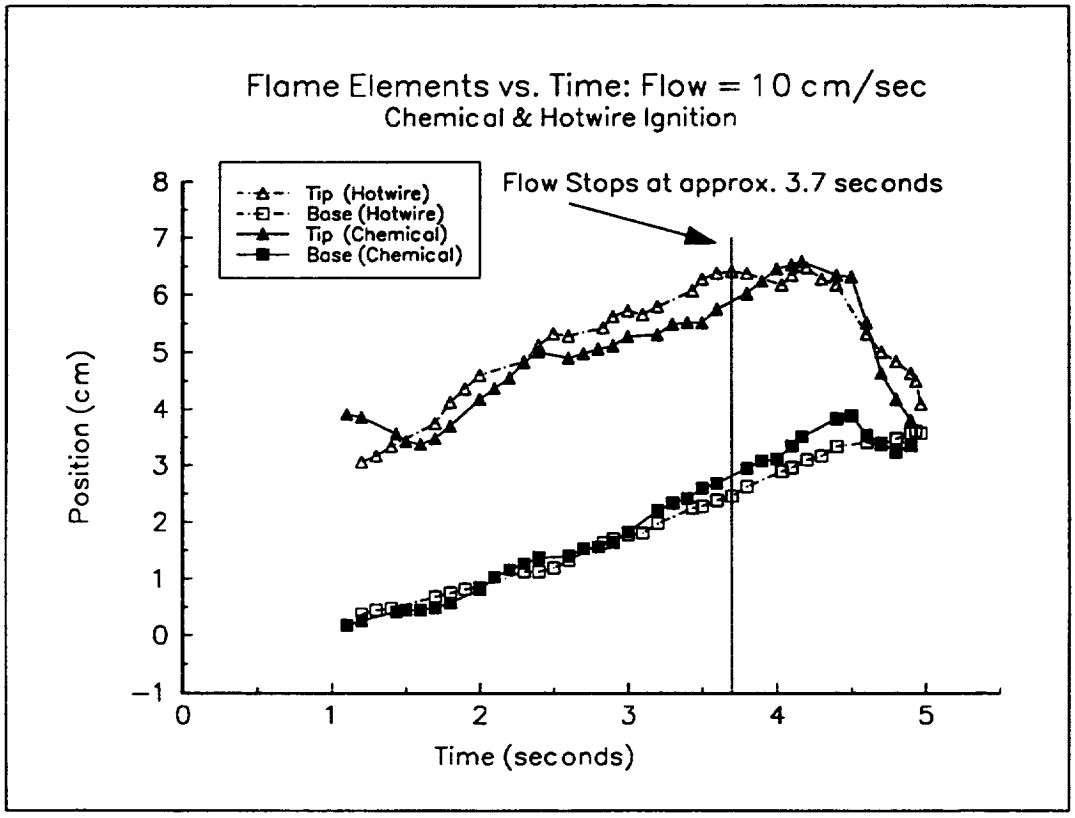

Figure 32

cm for the hotwire-ignited test. The pyrolysis zone for the chemical system maintained a fairly constant length (within the limits of the experimental error) throughout the test. The pyrolysis zone for the hotwire test grew steadily during the entire flow time, with the mean-area pyrolysis length increasing at the rate of 0.41 cm/sec. The final length of the pyrolysis zone for this test was about 2 cm at the end of the flow time. The mean-element pyrolysis spread rate for the chemical-ignited system was 1.15 cm/sec, while that of the hotwire system was 1.33 cm/sec.

An interesting similarity between the two tests was the behavior of the flames after the carriage stopped. (Because of the space limitations of the

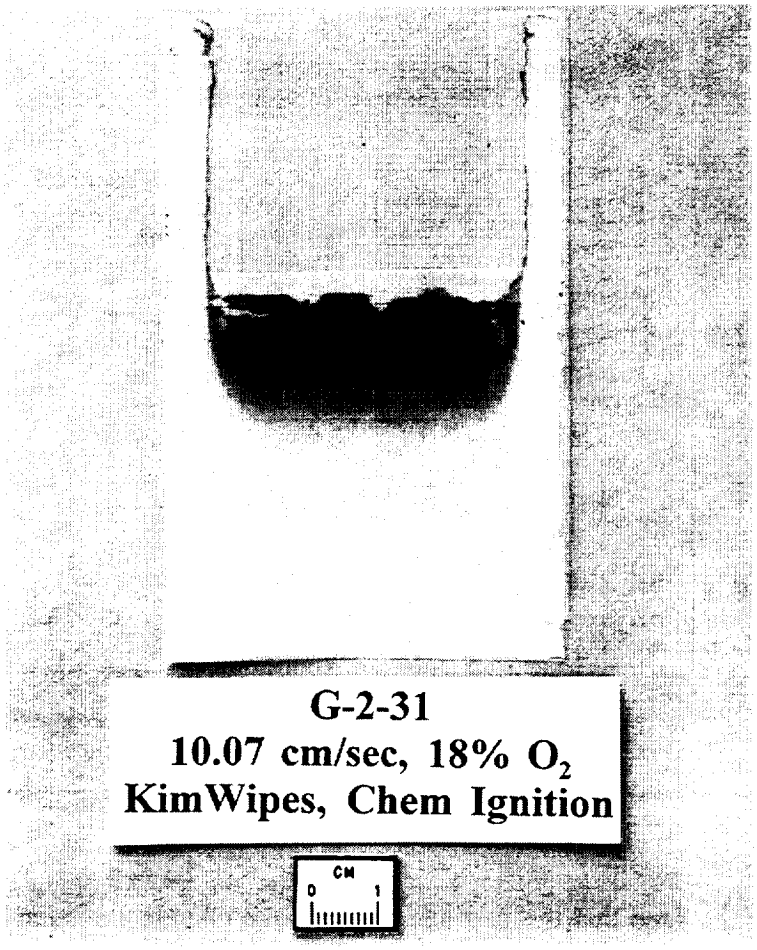

Figure 33 Partially Burned Sample

chamber, the maximum travel of the carriage was approximately 37 cm. If the device was operated at 10 cm/sec, this left about 1.5 seconds of drop time after the cessation of the flow.) When the carriage was brought to a sudden stop, the gas being "dragged" along in the boundary layer near the fuel sample still retained its momentum from the steady state carriage velocity, and continued (briefly) to propagate toward the bottom of the chamber. This created a momentarily reversed (opposed) flow in the flame region.

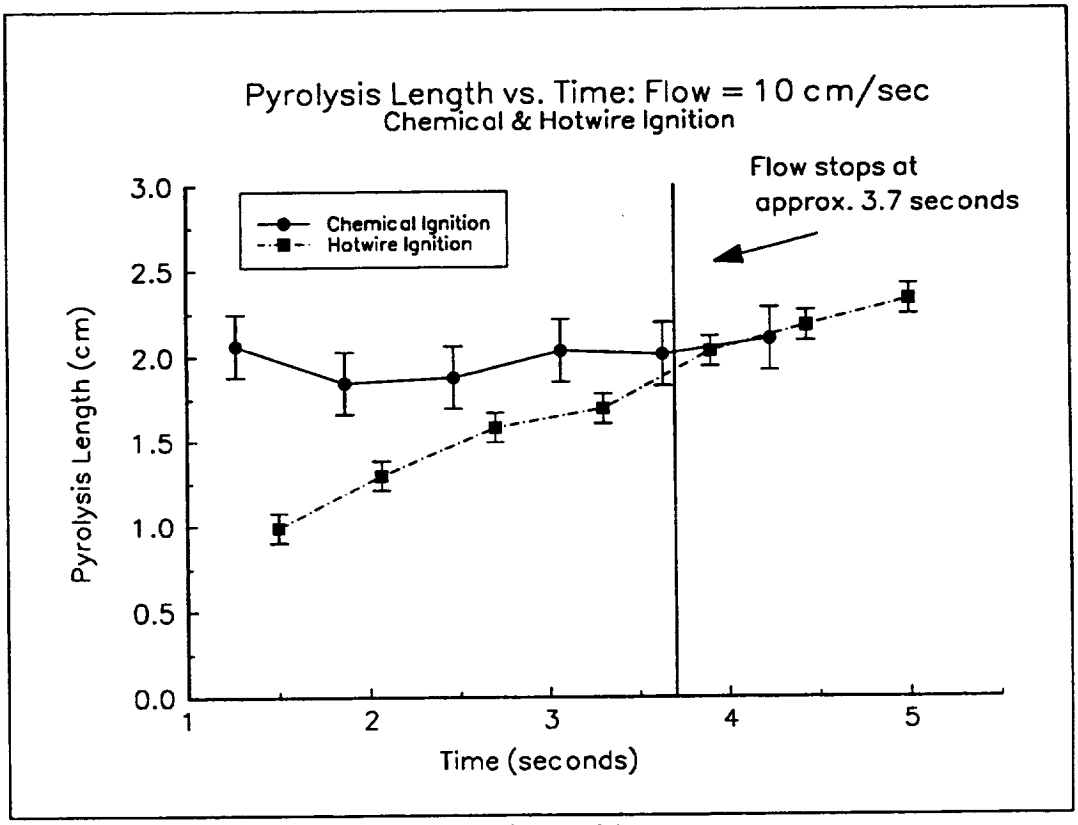

Figure 34

At the time that the carriage stopped, the chemical system flames were about 3.2 cm long, and the hotwire ignited flames were about 3.8 cm long. Both showed a fairly steady length (within error limits) for the next 0.4 seconds, at which both flames began a steady declined to a length of about 0.5 cm. However, the flames from both cases were still visible until the drop vehicle impacted. The length of the chemically-ignited flames receded at a rate of -4.43 cm/sec, while the hotwire-ignited flames shrunk at about -3.57 cm/sec. In both cases, this indicates that more than 1.5 seconds would be required to extinguish the flames by stopping the flow.

Results of Jiang's steady-state model (Jiang, 1995) at a free stream

velocity of 9.93 cm/sec show a flame spread rate of 1.38 cm/sec.

Ashless Filter Paper

Two tests were conducted using Ashless Filter Paper as the fuel. One test was done with an O_2 concentration of 18%, the other with 21% O_2. The pressure for both tests was one atmosphere, and the diluent for both cases was N_2. The carriage velocities for the two cases were 9.89 cm/sec and 9.85 cm/sec, respectively. The hotwire ignition system was employed in both of these tests.

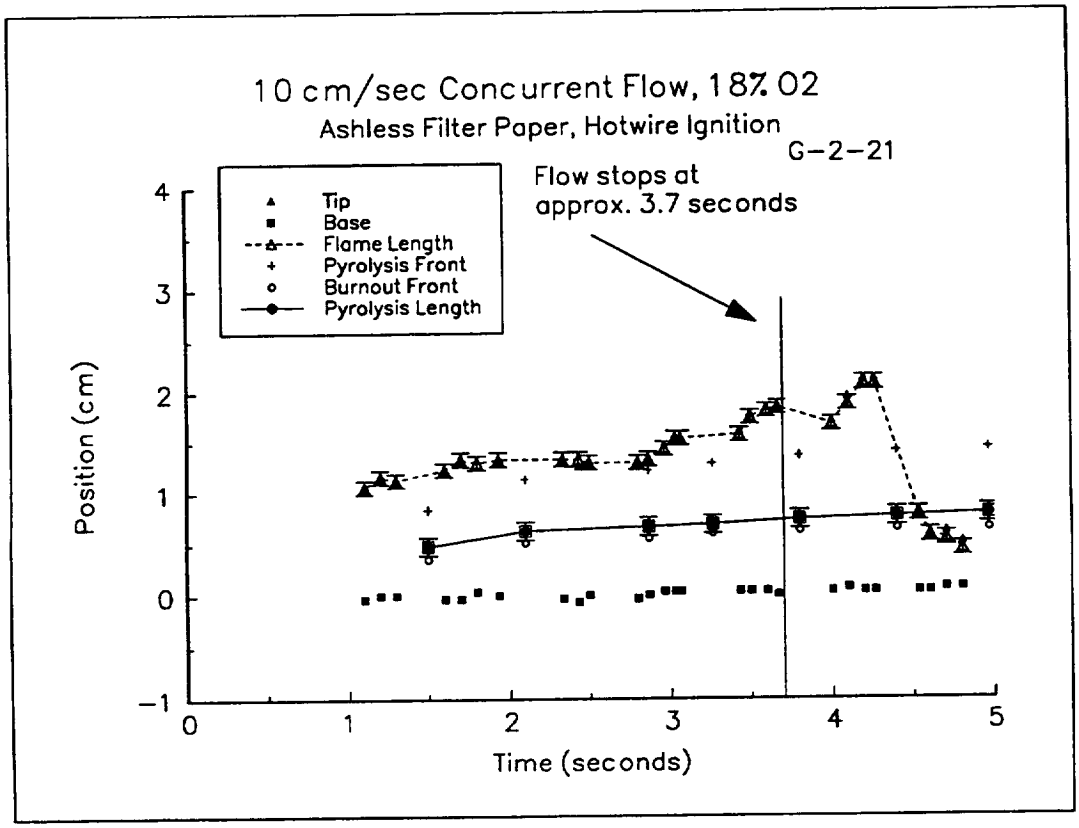

Figure 35

In both cases, the ignition provided by the Hotwire system was fairly uniform, and produced uniform pyrolysis zones. However, the pyrolysis zones for both tests were much shorter than that produced in any of the tests using KimWipes as the fuel. This was because the Ashless Filter Paper has an area density which is more than four times that of the KimWipe samples. The flame structure and pyrolysis zone are expected to take about four times longer to develop and reach steady-state for the Ashless Filter Paper than they would for the KimWipes.

The final mean-area pyrolysis length (at the end of the flow time) for the 18% O_2 was about 0.70 cm. Figure 35 shows the data from this test. The mean-element pyrolysis zone spread at 0.10 cm/sec, and the rate of growth for the mean-area pyrolysis length was 0.06 cm/sec.

The data from the test using an O_2 concentration of 21% (Figure 36) showed a mean-area pyrolysis length (also at the end of the flow time) of about 0.90 cm. For this case, the mean-element pyrolysis zone spread at a rate of 0.24 cm/sec, and the mean-area pyrolysis length grew at the rate of 0.24 cm/sec. Figure 37 shows the partially burned sample from this test.

Because of the density of this fuel, the flames for these two tests were also much shorter than that observed for the KimWipe-fueled flames. As expected, these flames were still growing at the end of the flow time, with the flames from the 18% O_2 test growing in length at a rate of 0.41 cm/sec, while the flames from the 21% O_2 test grew in length at a rate of 1.12 cm/sec.

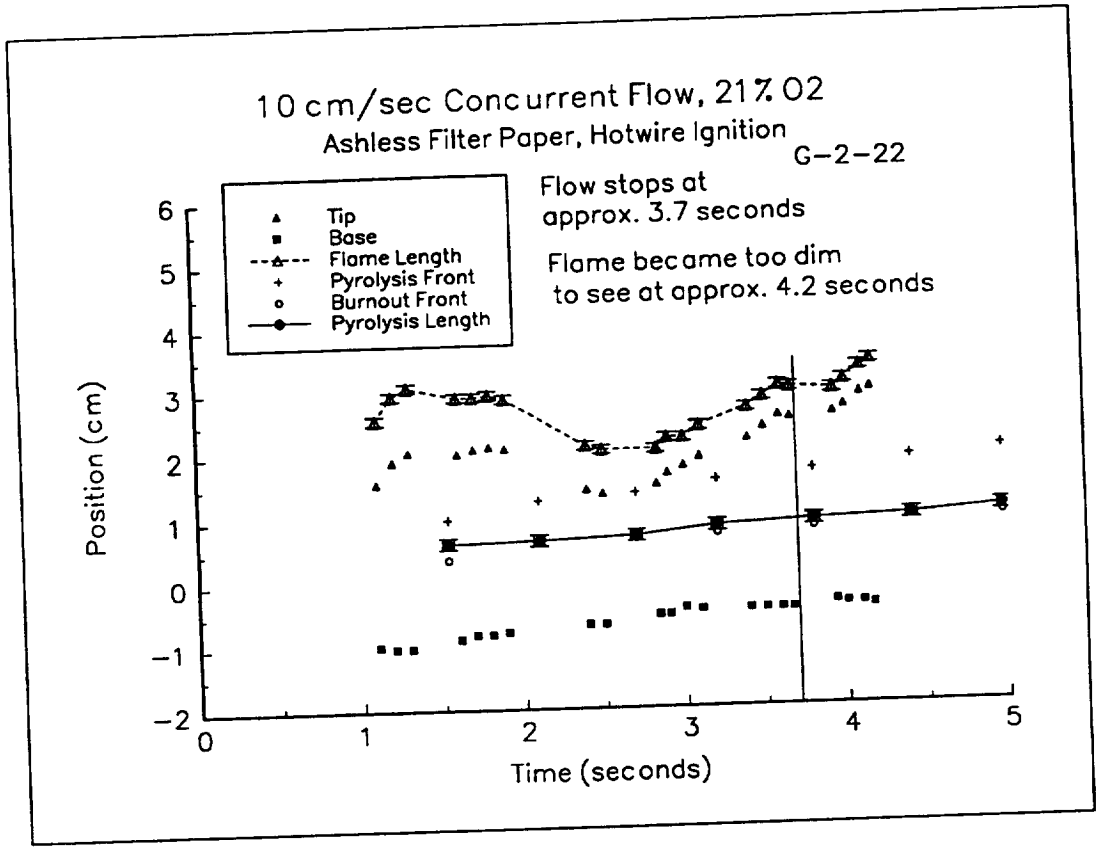
10 cm/sec Concurrent Flow, 21% O2
Ashless Filter Paper, Hotwire Ignition
G-2-22
Flow stops at approx. 3.7 seconds
Flame became too dim to see at approx. 4.2 seconds
Tip
Base
Flame Length
Pyrolysis Front
Burnout Front
Pyrolysis Length
Position (cm)
Time (seconds)
6
5
4
3
2
1
0
-1
-2
0
1
2
3
4
5

Figure 36

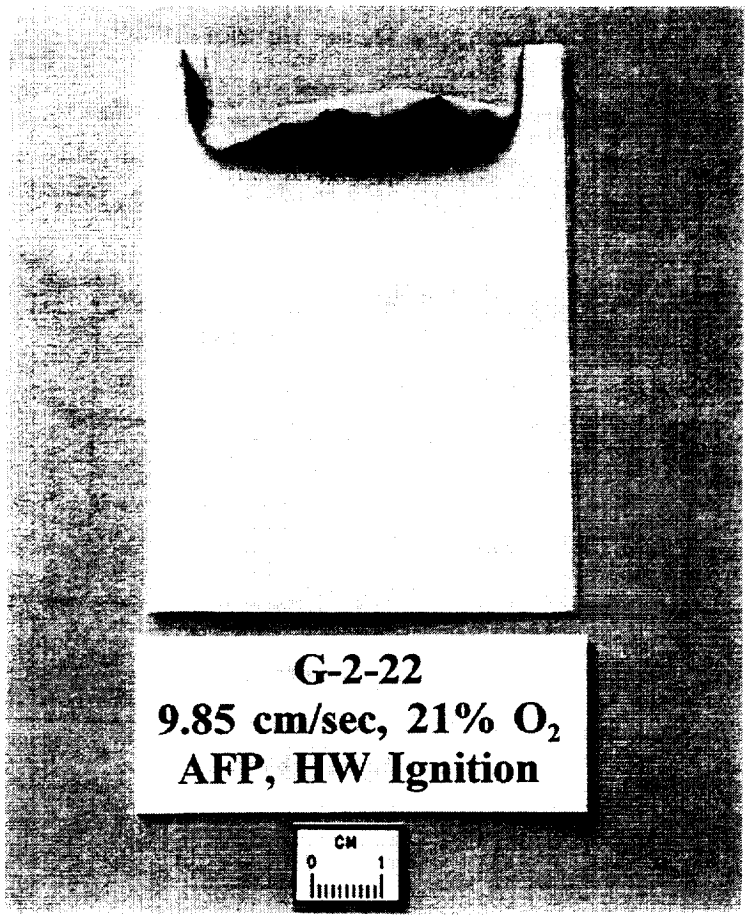

Figure 37 Partially Burned Sample

Thermocouple Data

Three experiments were conducted using thermocouples to obtain temperature information in two locations. For each test, one thermocouple was placed touching the surface of the fuel, and one was suspended in the gas phase above the fuel. All three tests were conducted using KimWipes as the fuel, with 18% O_2 (82% N_2), pressure of one atmosphere, and a carriage

velocity of approximately 10 cm/sec. All three tests were ignited using the hotwire system.

The first test using thermocouples (test number G-2-26) had them positioned with the solid phase thermocouple placed 3 cm behind the initial leading edge of the fuel, and 2 cm from the side. The gas phase thermocouple was placed 1 cm downstream from the solid phase thermocouple, 0.2 cm off the surface. It was desired to be as far away from the (initial) leading edge of the fuel to minimize the effects (on the temperature traces) of the ignition. The position of the thermocouples (in the streamwise direction) was chosen based on the results of test G-2-19, which was the hotwire ignition test with carriage velocity of (approximately) 10 cm/sec. It was determined from this test that with this positioning, the flame should propagate past both thermocouples before the end of the flow time. This determination was based on the assumption that the thermocouples themselves were a small enough heat sink to have a negligible effect on the flame spread rate.

Video failure prevented the acquisition of flame/pyrolysis element data for this run. It was therefore also impossible to verify the carriage velocity for this run. However, the thermocouple data for this run was successfully acquired.

The temperature traces for this run (Figure 38) clearly show the preheat of the fuel surface as the flame approached the thermocouples. This preheat temperature was fairly constant at a value of about 725 K between t=2.4

seconds and t=3.4 seconds. During this same period, the gas phase trace shows a fairly steady increase, reaching a value of about 875 K by t=3.4 seconds.

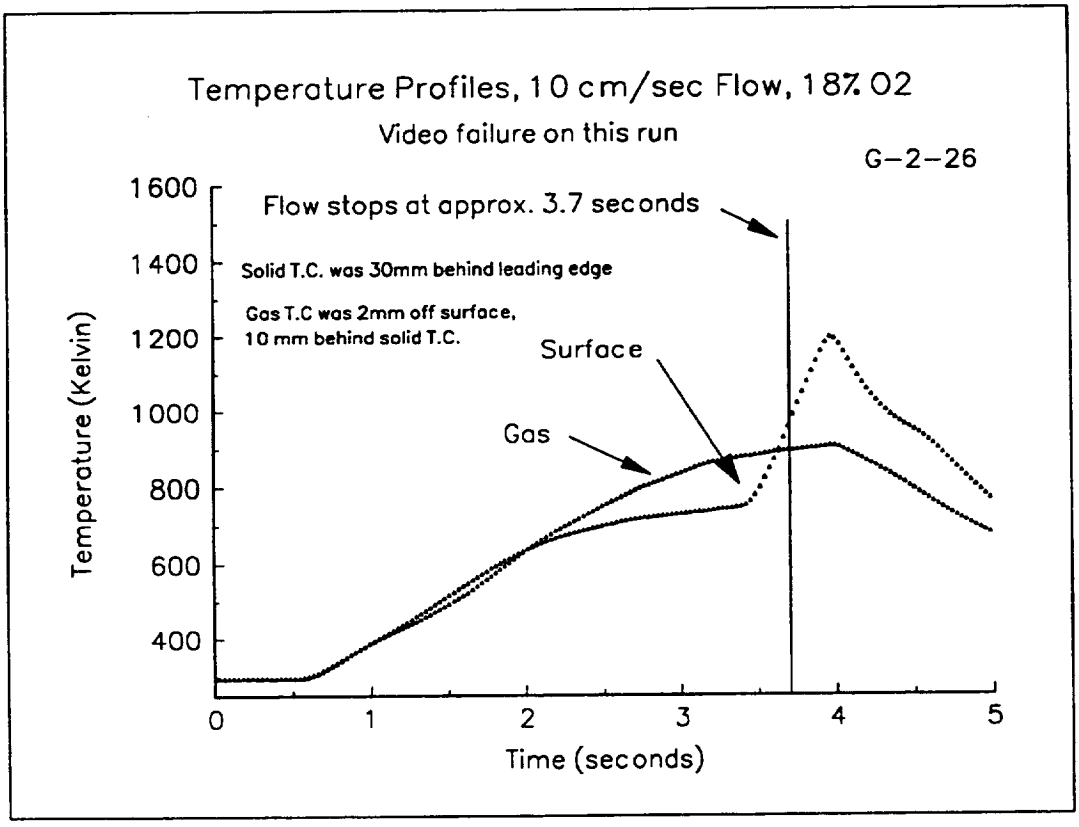

Figure 38

At about 3.4 seconds, the solid phase trace shows a sharp increase in temperature which continues past the time (approximately 3.7 seconds) where the flow stopped. The gas phase trace grew gradually to a value of about 900 K. The peak for both traces occurred at approximately t=4.0 seconds. It is apparent from this that the flame did not propagate as far as expected, and in fact the temperature peak did not progress past the thermocouples during the test time.

At the conclusion of this drop, it was immediately obvious that video

failure occurred. The drop package was then prepared for a drop the following day, with the modification that the gas phase thermocouple was now placed 1 cm above the fuel surface. This was done before results of the thermocouple traces were available for analysis, and it was not realized that the flame did not reach the thermocouples in the flow time available. Test G-2-27 was then conducted with the thermocouples in the same streamwise position, but with the gas phase thermocouple 1 cm off the fuel surface.

Analysis of the images from test G-2-27 show the carriage velocity to be 10.05 cm/sec. Examination of the thermocouple traces (Figure 39) show that the surface temperature reached a peak of about 715 K during the time that the flow was on. However, it did not reach that peak temperature as quickly as in the previous test.

The gas phase temperature trace showed a quick climb to about 690 K, where it leveled off somewhat between time t=1 second and t=2 seconds. It then rose to a peak temperature of about 1375 K at the very end of the flow time. The temperature climbed slightly after the cessation of flow, to a maximum of 1425 K at t= 4.2 seconds.

It can be seen from this that the flame didn't propagate far enough for the peak temperature to be recorded by the surface thermocouple during the available flow time. The fact that the surface temperature took longer to reach a quasi-steady preheat temperature in this test than it did in the previous test suggests that the placement of the gas phase thermocouple, which was raised

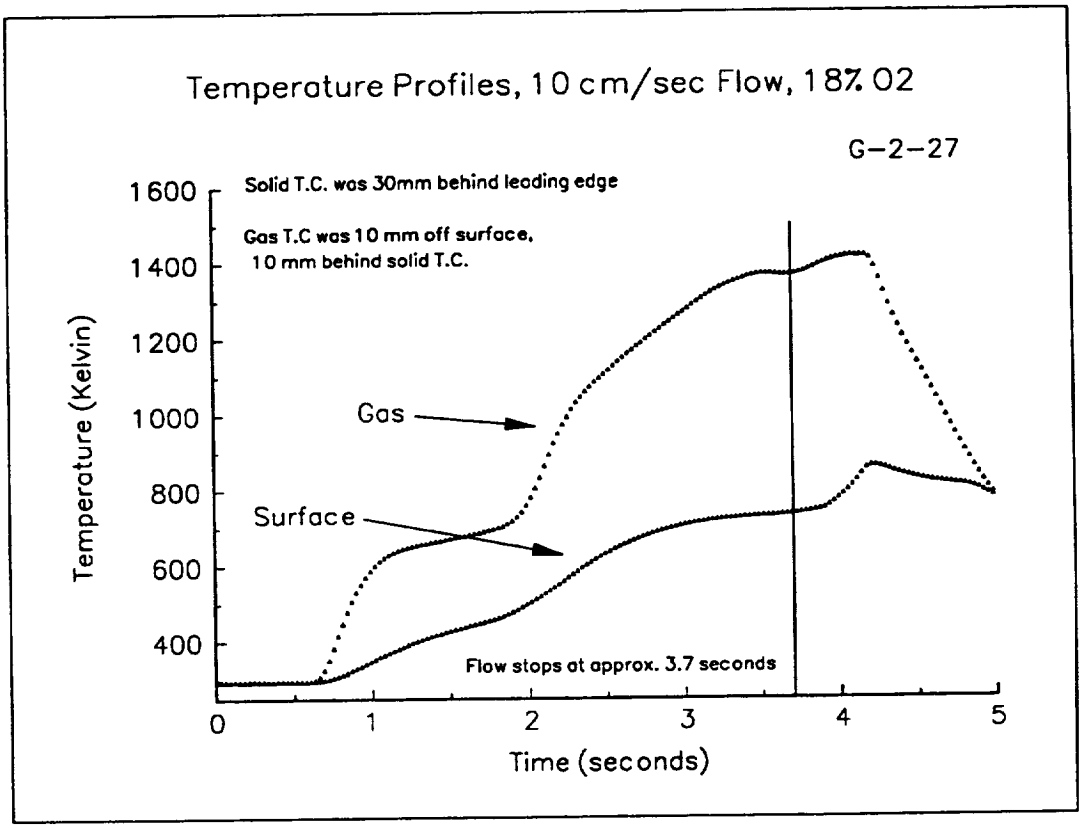

Figure 39

for this test from 0.2 cm off the surface to 1 cm, may have affected the rate at which heat was transferred to the upstream surface.

The flame/pyrolysis element data from test G-2-27, given in Figure 40, show a flame length which is fairly steady at about 1.5 cm between t=1 and t=2 seconds. The flame length then grows at a rate of 0.99 cm/sec to a length of about 3.2 cm at time t=3 seconds. From approximately t= 1.5 seconds until the flow stops, the mean-element flame spread rate was 1.39 cm/sec.

The mean-area pyrolysis length was approximately 1.75 cm at t= 1.4 seconds, and stayed approximately this length for the entire test. The mean-element pyrolysis zone spread at a rate of 1.00 cm/sec. The leading edge of

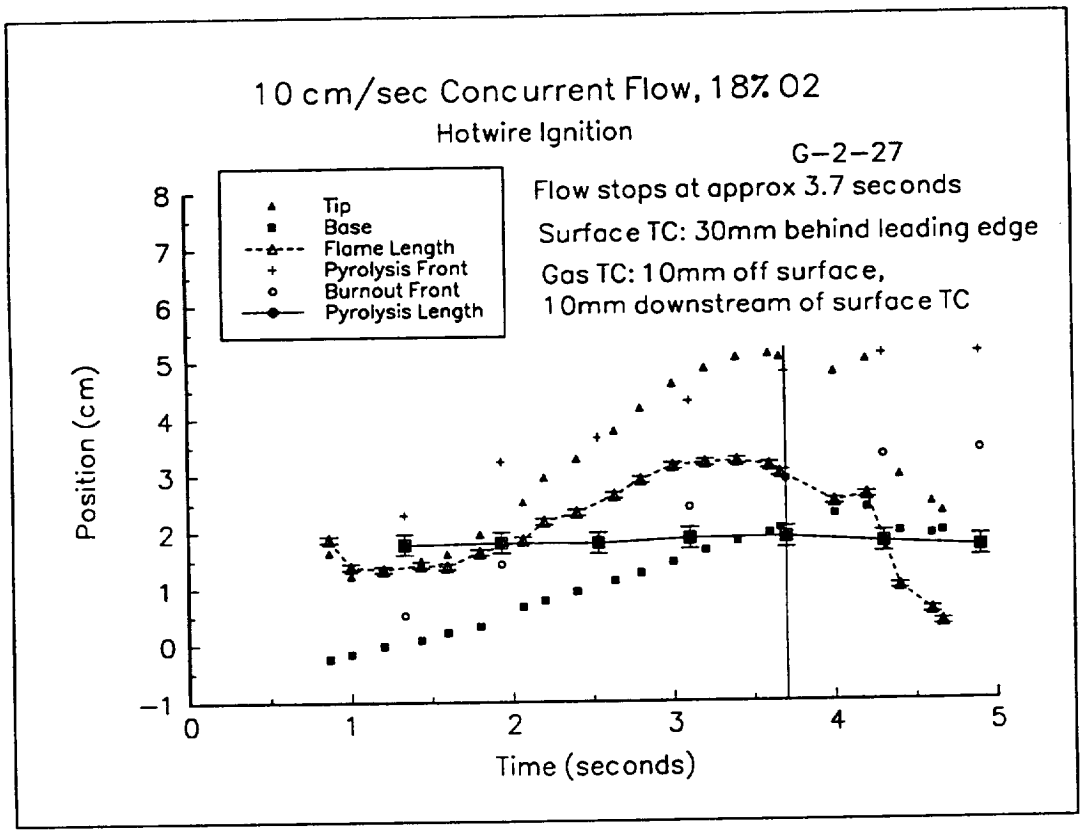

Figure 40

the diamond-shape of the thermocouple leads can be seen in the final pyrolysis zone as a quenched area, suggesting that the thermocouple leads were acting as a heat sink, thereby locally lowering the flame (and fuel surface) temperatures.

For the last thermocouple test (number G-2-28), it was desired to mount the thermocouples in a place to insure that the flame would propagate past both of them during the flow time. The surface thermocouple was placed 1.5 cm from the initial leading edge of the fuel. The gas phase thermocouple was again placed 1 cm downstream of the solid thermocouple, and elevated 1 cm off the surface. Both thermocouples were placed 2 cm from the samples' side edge.

The temperature traces from this test are shown in Figure 41. Both thermocouples show a steady rise in temperature from about time t=0.4

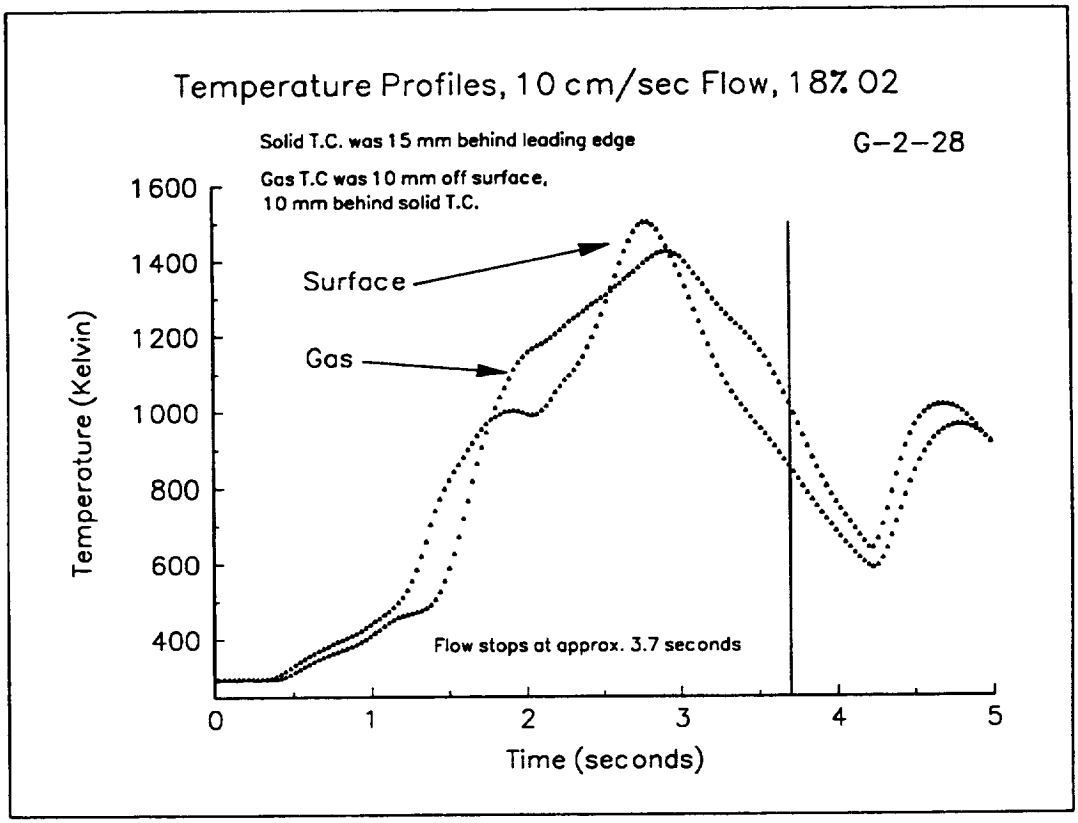

Figure 41

seconds until t=1.2 seconds. During this time, the surface temperature exceeds that of the gas phase. Both traces then show a steep increase until about t=1.8 seconds, at which time the gas phase temperature climbs past the surface temperature. The surface temperature briefly plateaus at approximately 1000 K, while the gas temperature at that moment is approximately 1150 K. Both traces then climb at fairly steady rates, until the surface trace peaks at 1503 K and the gas trace peaks at 1426 K. These peaks occur at the times t=2.7

seconds and t=2.9 seconds, respectively. Figure 42 shows a representation of the position of the flame relative to the thermocouples at the times t = 1 second, and t = 2.7 seconds.

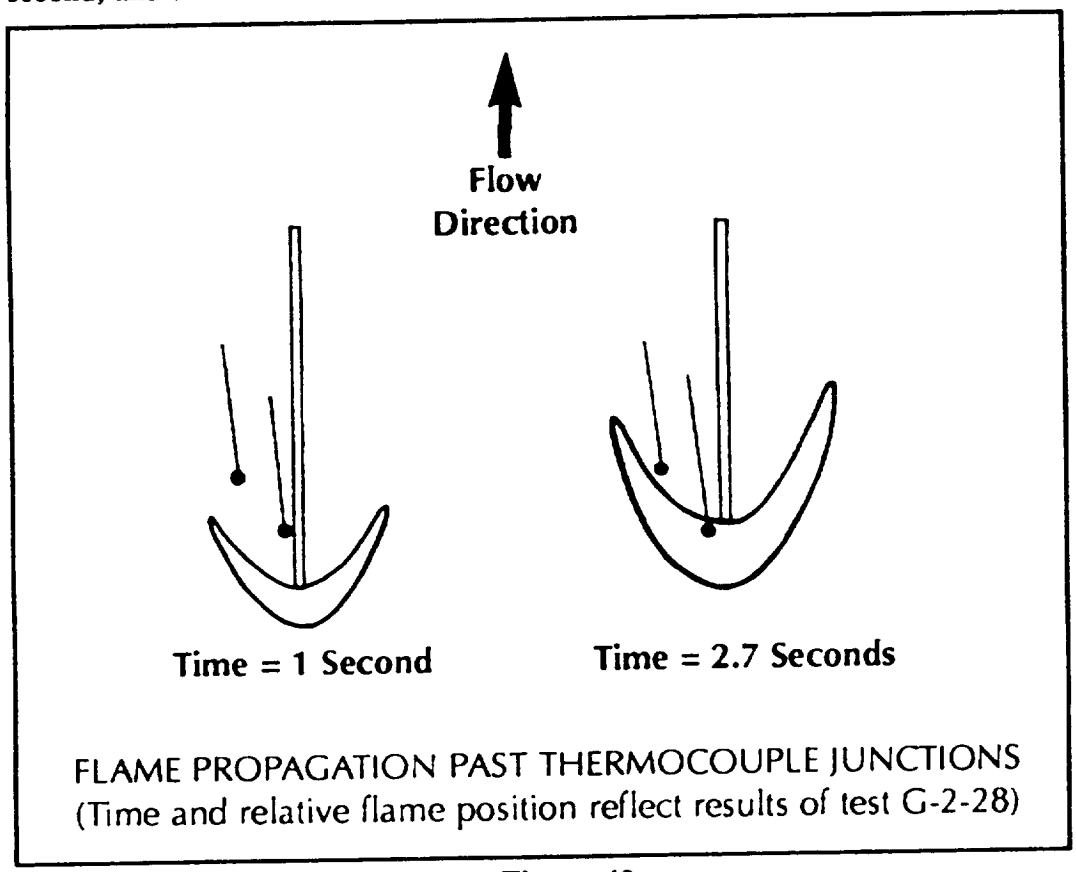

Figure 42

After reaching their peak temperatures, both traces decrease fairly steadily through the remainder of the flow time, reaching an inflection point (after the flow stopped) at about 4.2 seconds. The gas and surface temperatures at that point were about 700 K and 650 K, respectively. Both traces then climb rapidly, reaching a second gas phase peak of about 1040 K and a second surface peak of about 970 K at 4.7 seconds. Both traces decrease from that point until the end of the drop. This second peak occurred after the

carriage stopped, during the period of reversed flow caused by the momentum of what was the boundary layer when the device was moving.

Analysis of the video images show the actual carriage velocity to have been 9.88 cm/sec. Figure 43 shows the flame length to be about 1.2 cm at t=1

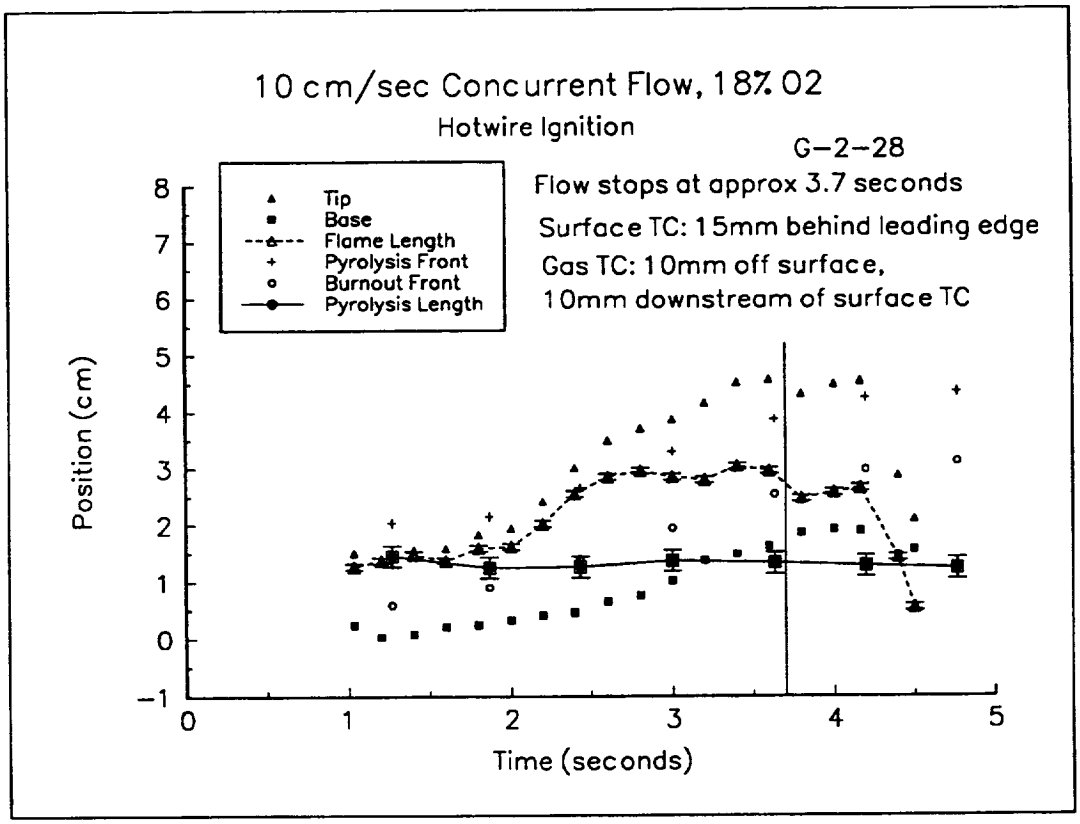

Figure 43

second, and rose slowly to about 1.5 cm by t=2 seconds. It then increased to about 3 cm by t=2.7 seconds, where it remained fairly steady for the remainder of the flow time. The flame length then dipped to about 2.5 cm at 3.7 seconds, and at 4.1 seconds decreased rapidly. The mean-element flame spread rate (near the end of the flow time) was 1.10 cm/sec.

The mean-area pyrolysis length for this test was steady (within the error) at about 1.3 cm from 1.9 seconds until the end of the flow time. The mean-element pyrolysis zone spread rate was 0.96 cm/sec. As in the previous test, the pyrolysis zone of the remaining sample shows the diamond shape pattern of the surface thermocouple leads as a non-pyrolized area (Figure 44).

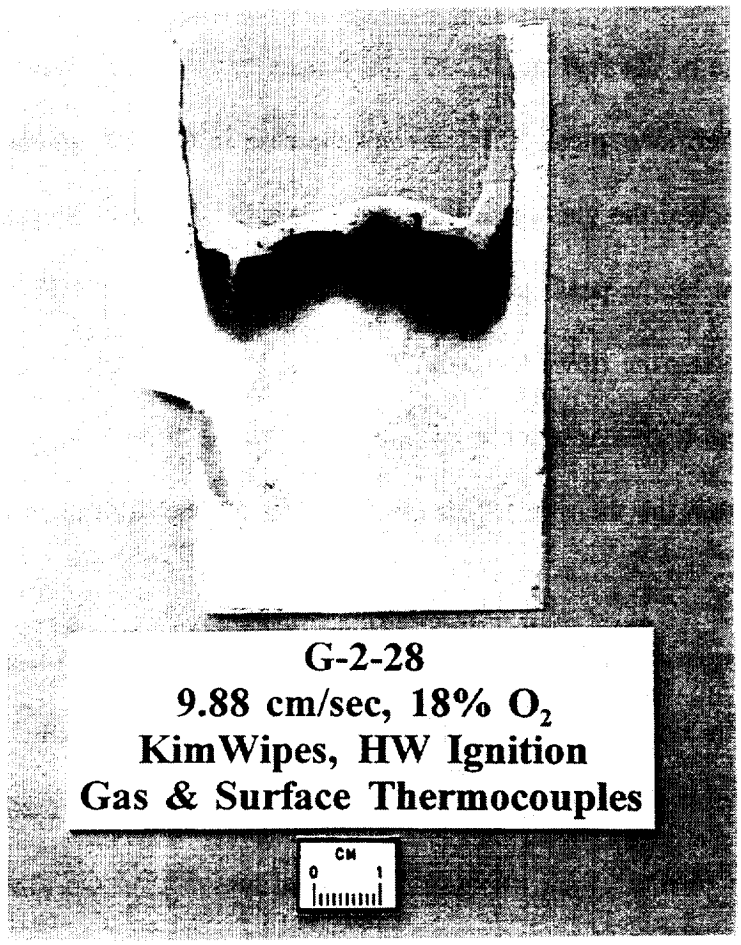

Figure 44 Partially Burned Sample

Comparison of the flame element plots of tests G-2-27 (Figure 40) and G-2-28 (Figure 43) show the initially measured flame lengths to be fairly

similar, approximately 1 cm (at time t=1 second) for both tests. These flame lengths stay similar for most of the test.

However, the mean-element flame spread rates (as measured from approximately 2 seconds until the end of the flow time) differ, with G-2-28 having a rate of 1.10 cm/sec, and G-2-27 having a rate of 1.39 cm/sec. Since G-2-28 had the thermocouples half the (streamwise) distance to the initial leading edge of the fuel as G-2-27, the flames had sufficient time to propagate past both thermocouples. This was not the case in G-2-27, where the flame had just reached the gas phase thermocouple when the flow stopped. This can also be seen by the peak gas temperatures, which about 1420 K in G-2-28, and 1380 K (during the flow) for G-2-27. The fact that the thermocouples for test G-2-28 spent a greater amount of time closer to the flames suggests that heat losses through the thermocouples may account for the difference in the spread rates.

Comparison of the flame element plots from these two tests with the results of the hotwire-ignited test at a similar velocity without thermocouples (test G-2-19, Figure 31) show that the flames in the test with the thermocouples took longer to reach their maximum observed length than did those in the test without thermocouples. The maximum observed flame length for the tests with the thermocouples with the thermocouples was about 3.10 cm, whereas the maximum length seen in the test without thermocouples was about 3.95 cm. The implication of this is that the addition of the thermocouples may account

for the significantly shorter flames of tests G-2-27 and G-2-28.

Jiang's steady-state model calculated a gas phase peak (measured 1 cm off the surface) of 1442 K, and a peak temperature from the surface of 1597 K. The peak temperatures recorded in test G-2-28 were 1426 K and 1503 K for the gas phase and surface, respectively.

V. Discussion

Hotwire Ignition vs. Chemical Ignition

Several trends became evident in the tests of the two ignition systems. One of the obvious differences was the manner in which the ignition energy was released. The hotwire system consistently produced a fairly small, uniform

Figure 45 Ignition Burst from Hotwire System

ignition burst, concentrated around the leading edge of the fuel sample (Figure 45). This contrasts with the much larger, non-uniform burst of the chemical ignition system (Figure 46). Additionally, the non-uniformity of the chemical burst was non-repeatable with the application techniques used in these tests.

Figure 46 Ignition Burst from Chemical System

At low speeds, the large flameball from the chemical system produced initial pyrolysis zones which were much larger than that which would be expected for a steady state flame at that speed. This means that in the limited time available for these tests, the flame didn't progress far enough to escape the pyrolysis region created by the burst. The weakness of the flames (compared to that produced by the hotwire system) at speeds of 2.5 cm/sec or lower may be partially attributable to the fact that the flame was attempting to sustain itself on fuel that was already partially pyrolyzed. Due to the short duration of the tests, it is uncertain whether the flame would have propagated past the initial pyrolysis zone, and achieved steady state. The fact that these

flames were getting visibly dimmer (and in some cases became too dim to see) suggests that the reaction may have eventually ceased.

Another effect which may have contributed to the chemical flames being weaker than the hotwire flames may have been that the large ignition burst of the chemical ignitor consumed much of the oxygen in the region near the newly established flame. It is possible that the flame was attempting to grow and propagate through a region with reduced oxygen concentration. The combination of the flame advancing over previously partially pyrolyzed fuel, and a locally reduced oxygen concentration could serve to explain the differences in both visible intensity and flame length that were observed between the two ignition systems. Though flame lengths were observed to be smaller (after the initial burst dissipated) for all the chemical tests compared to the hotwire cases, the effects were the most obvious at the free stream velocities of 1 cm/sec and 2.5 cm/sec. At the higher velocities, somewhat shorter flame lengths were still observed for the chemical cases, but the higher flow velocities probably enhanced the transport of fresh oxidizer into the reaction zone to the point that the effect was less apparent.

Clearly, the magnitude of the ignition burst was greater for the chemical system than realized from the hotwire system. This was expected, due to the additional potential energy of the nitrocellulose strip. What was not entirely expected was non-uniformity of the ignition burst from this system, and the inability to reliably repeat the shape of this flameball. Typically, the

nitrocellulose ignited first at one or both edges of the sample, and propagated inward. Sometimes, the ignition burst propagated inward from both sides at about the same time; other times, one side would propagate toward the center faster than the other.

A likely explanation for the variability of the shape of the ignition burst is small differences in the application of the nitrocellulose strip. The technique used involves the placement of the strip at the leading edge of the fuel sample, followed by placement of the ignitor wire flat against the length of the strip. The strip was then dissolved into the paper using drops of acetone applied from an eyedropper. This served to bond the chemical strip to the paper and to the straight ignitor wire.

The problem with this is that there was no way to reliably deposit the same amount of acetone to the ignitor strip in exactly the same place for each sample. The acetone dissolved the strip instantly, and then tended to spread out over an area of the sample. The area which was subsequently (briefly) soaked with the acetone/nitrocellulose mixture was determined by the amount of acetone applied. This then affected the concentration (though not the total amount) of dissolved nitrocellulose in a given area of the fuel sample.

The hotwire ignition system did not suffer from this problem. The main problem with this system was that it is difficult to guarantee perfect thermal contact between the entire ignitor wire and the paper sample. This could account for small differences in the shape of the ignition bursts of the Hotwire

tests. However, ignition bursts for these tests were generally quite uniform, so this problem probably had a minimal effect on these tests.

Temperature Profiles

The small amount of test time limits the interpretation of the thermocouple data. In order to have the flame propagate past both probes in the available time, it is necessary to mount them relatively close to the ignition region. Because of this problem, the different streamwise positions of the thermocouples in runs G-2-27 and G-2-28 can prove to be useful.

The traces from G-2-27 (which had the surface probe mounted 3 cm from the initial leading edge of the fuel) show the surface temperature gradually increasing to a preheat temperature of about 720 K. The behavior of this preheat zone (which was also observed in test G-2-26, although at a slightly earlier time) is not readily apparent in the surface trace from test G-2-28, probably because the probes for that test were mounted at half the streamwise distance from the initial leading edge. This means that the surface probe was within a distance from the ignitor that was approximately equal to the final pyrolysis length measured at the end of the test. Therefore, this probe (for G-2-28) never had the chance to experience the normal development of the preheat zone, though it clearly passed through the base of the flame (at about 2.7 seconds) and recorded a peak flame temperature.

Similarly, the gas phase trace for the first 1.8 seconds of test G-2-28

shows a much quicker rise in temperature than the same time for test G-2-27. This is to be expected, due to the closer proximity to the ignition region. The slope of the gas phase trace for G-2-28 from time 2.2 seconds until it reached its peak at about 2.9 seconds is 318 K/sec. The gas phase slope of G-2-27 between 2.7 seconds and 3.5 seconds was 246 K/sec. This corresponds in both cases to the approach of the flame reaction zone to the probe. Both probes subsequently reached peaks of approximately 1400 K.

The significant difference is that this peak was reached at 3.5 seconds for G-2-27, and 2.9 seconds for G-2-28. This means that G-2-27 was nearly at the end of its' flow time, while G-2-28 still had about 0.8 seconds of flow time left. This allowed sufficient time for the base of the flame to propagate past the surface phase probe, while that did not occur in G-2-27.

When taken together, the traces from G-2-27 and G-2-28 can be seen to form a somewhat clearer picture of both the preheat/pyrolysis temperature behavior, as well as the peak (and cooldown) temperature profiles. However, as the comparison of the flame element plots of these tests with that of test G-2-19 (without the thermocouples) shows, the intrusion of the thermocouples themselves shortened the flames and may have lowered the flame temperatures. Figure 47 is an image from test G-2-28, showing the shorter flame on the same side of the fuel as the thermocouples (left side of edge view). The partially burned sample (Figure 44) clearly showed a quenched region around the thermocouples.

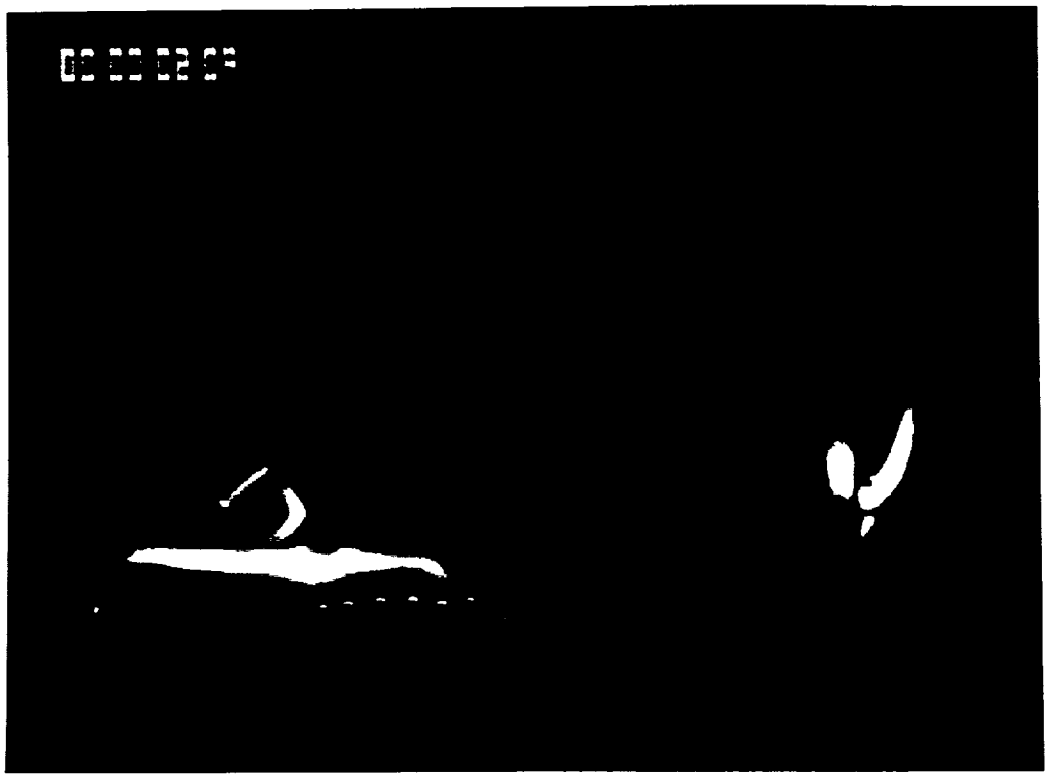

Figure 47 Flame Images from test G-2-28
(Freestream Velocity=9.88 cm/sec, 18% O_2)

To further support this observation, an estimation was made of the heat losses due to the thermocouples, and compared to an estimation of the energy released by the combustion of the fuel. Details of all assumptions and calculations associated with these estimations can be found in Appendix III. This estimation used the one-dimensional, steady-state heat conduction equation and Fourier's Law to estimate losses due to conduction. Radiation losses from the thermocouples were accounted for by modeling the thermocouple junction and the un-insulated portion of the leads as black-body emitters. The heat loss rate due to the thermal inertia of the thermocouple junction and leads was also

calculated.

The rate of energy release from the combustion of the fuel was estimated to be about 188 Watts for test G-2-19, which was the hotwire-ignited test with a freestream velocity of about 10 cm/sec. Test G-2-28, which was conducted under similar conditions except for the addition of the thermocouples, released energy at the rate of approximately 156 Watts. The estimate of the heat loss rate associated with raising the temperature of the junction and leads to the final measured temperature was about 2.7 Watts. The heat loss rate from the thermocouples due to conduction and radiation was approximately 7.3 Watts. The combined loss rate of almost 10 Watts is about a factor of three smaller than the calculated difference of about 32 Watts between the tests, but still supports the hypothesis that heat losses through the thermocouples are sufficient to affect the flame.

VI. Comparison with Steady-State Model

Flame Spread Rates

Figure 48 shows the steady-state flame spread results from Jiang's

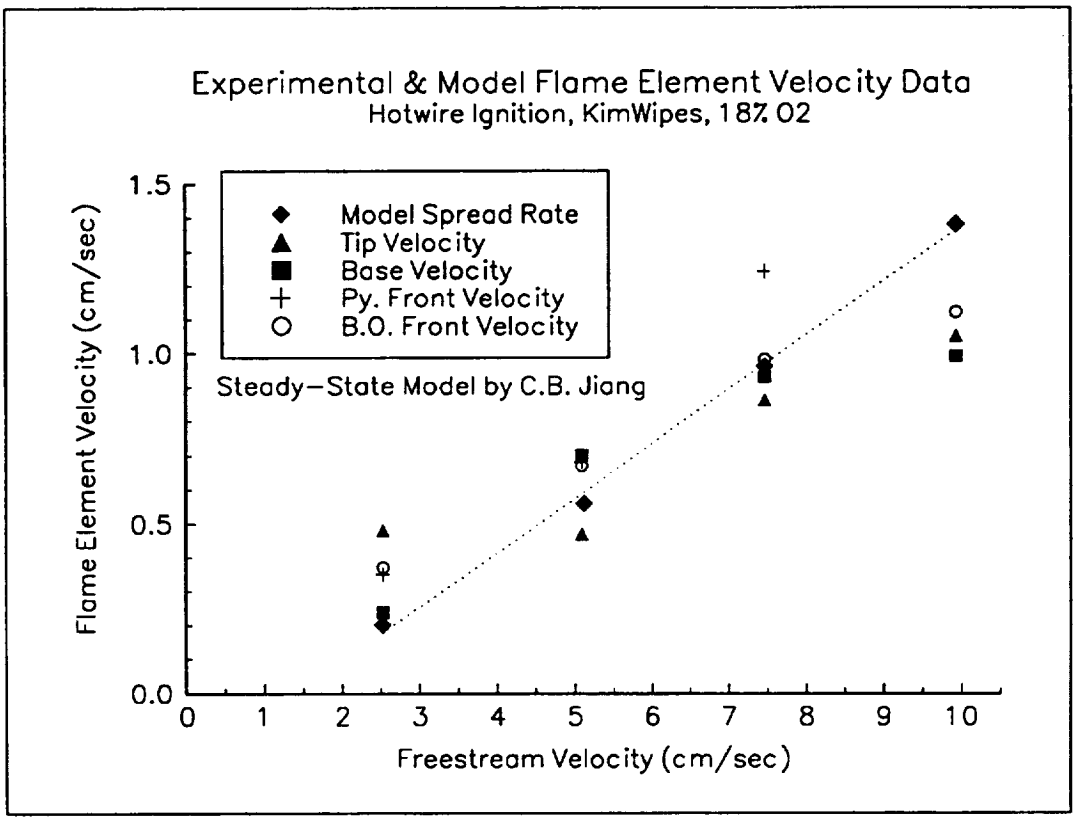

Figure 48

model plotted with the velocities of the flame and pyrolysis elements measured experimentally for the hotwire ignition system. The dotted line is the curve-fit for the theoretical data. Due to the fact that none of the tests definitively reached steady-state, direct comparisons with the model are difficult.

However, one approach to comparing the steady-state model with the observed data is to make no assumptions about the validity of the mathematical

model, but to look for points in the experimental data which appear to have been at or close to steady-state, and see if the model accurately predicts these. The cases which (as previously discussed) appeared to be the closest to steady-state were the cases with (nominal) free-stream velocities of 5 cm/sec and 7.5 cm/sec. With that assumption, the theoretical spread rate of 0.56 cm/sec is about 19% more than the experimental tip velocity of 0.47 cm/sec, and 20% less than the experimental base velocity of 0.70 cm/sec. The pyrolysis and burnout fronts had experimentally measured velocities of 0.68 cm/sec and 0.67 cm/sec, respectively, both of which are about 17% greater than the theoretical spread rate. The experimental data for this case, which was shown in Figure 25, shows that the pyrolysis length was not changing much, but the flame length was decreasing with time, and was approaching the length of the pyrolysis zone near the end of the test time.

For the freestream velocity of about 7.5 cm/sec, the observed tip and base velocities of 0.86 cm/sec and 0.93 cm/sec were both within about 10% of the theoretical spread rate of 0.96 cm/sec. The observed burnout front speed of 0.98 cm/sec was close to the theoretical spread rate, but the experimental pyrolysis front was advancing at the rate of 1.24 cm/sec, which is about 29% faster than the theory predicts. The experimental data (Figure 29) shows that the flame and pyrolysis lengths were also approaching similar values when the flow time ended.

Flame Length

Flame lengths are determined from Jiang's model by using fuel consumption rate contours. By designating a specific reactivity contour to be the border of the visible flame, a flame length is defined. This can then be verified experimentally by selecting a contour to match the visible flame length from a test conducted at the same free-stream velocity. This contour can then be compared to the visible flame lengths at other free-stream velocities, to confirm the accuracy of the model's predictions.

The problem with this technique is that it assumes that steady-state experimental flame length data is available for at least two points, one to choose the contour and one to verify the model. As previously discussed, it is difficult to determine whether any of the tests reached steady-state. However, a "loose" comparison will be made, using the hotwire-ignition tests at free-stream velocities of (approximately) 5 cm/sec and 7.5 cm/sec.

Examination of the data from test G-2-23 (Figure 26) shows a final flame length of about 1.3 cm for the free-stream velocity of 5.12 cm/sec. Similarly, test G-2-18 (Figure 29) shows a final flame length of about 2.2 cm for the free-stream velocity of 7.47 cm/sec.

Figure 49 shows the fuel consumption rate contours for Jiang's model at a free-stream velocity of 5.12 cm/sec. A contour of approximately $10^{-3.5}$ g/cm^3/sec would yield a visible flame length of about 1.3 cm.

This contour value can then be applied to the plot in Figure 50, which

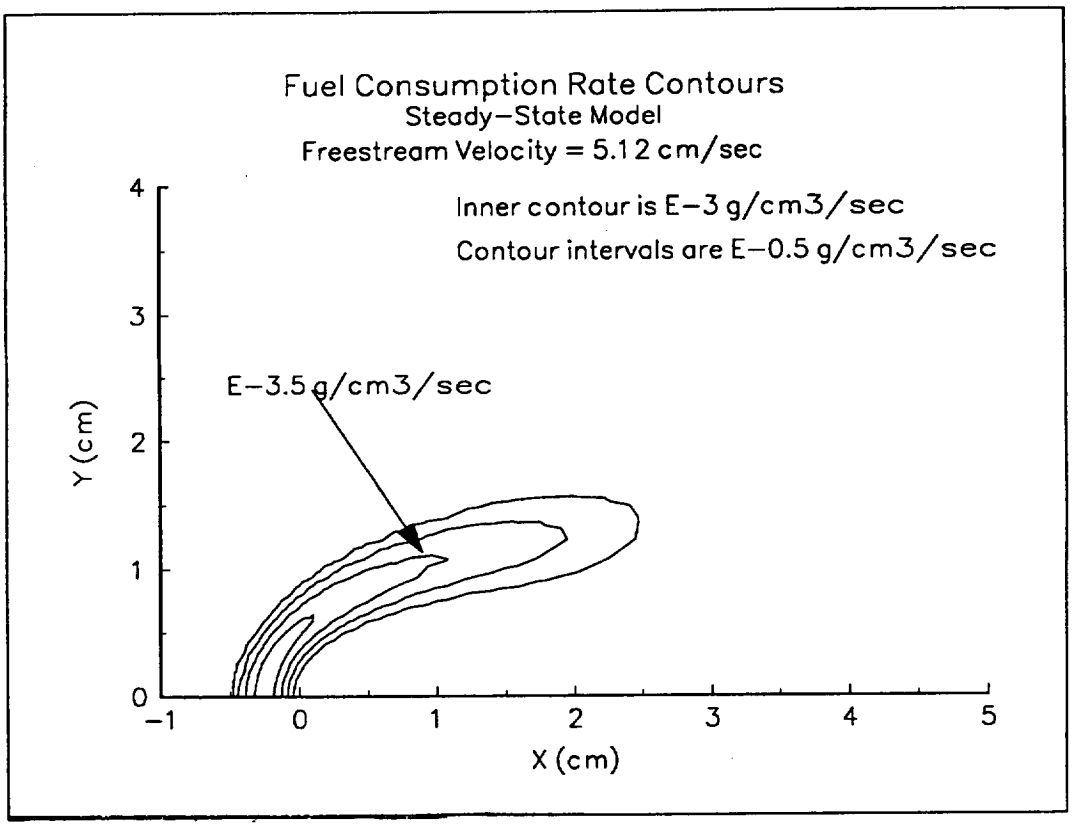

Figure 49 Fuel Consumption Rate Contours: Steady-State Model Free-Stream Velocity of 5.12 cm/sec

shows the theoretical steady-state fuel consumption rate contours for the free stream velocity of 7.47 cm/sec. This then yields a theoretical visible flame length of about 2.3 cm, which is approximately equal to the observed flame length of 2.2 cm for test G-2-18.

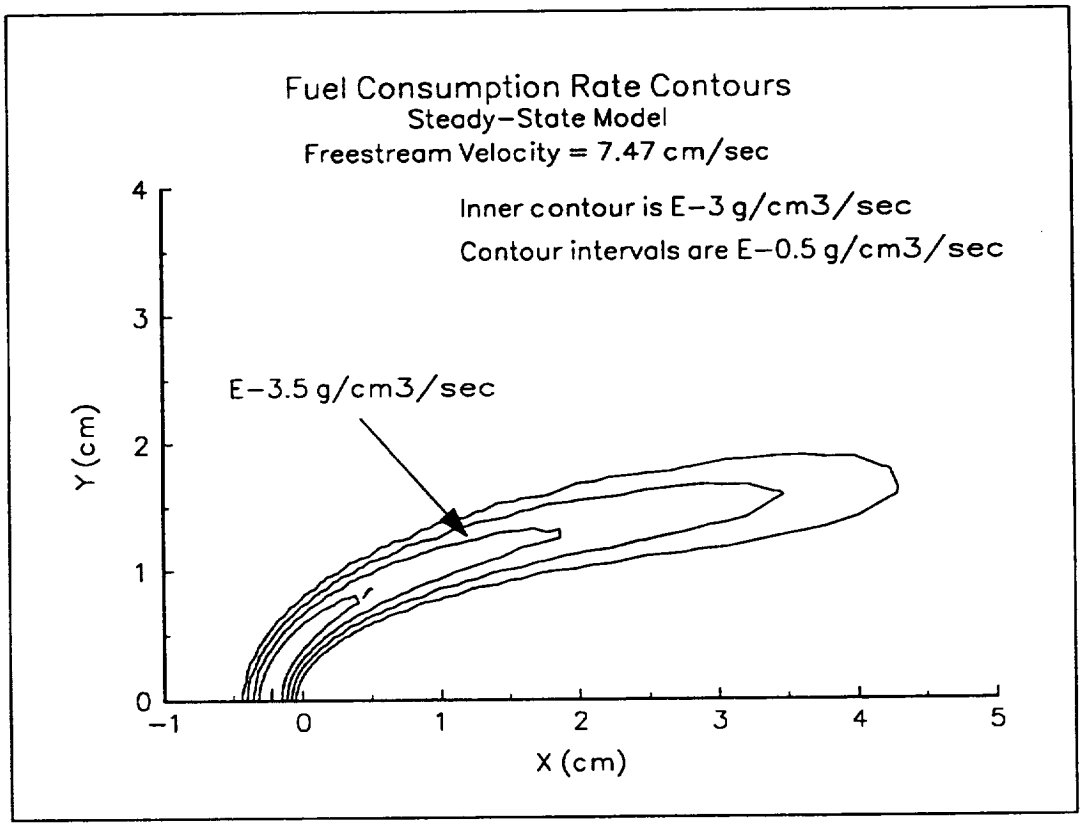

Figure 50 Fuel Consumption Rate Contours: Steady-State Model Free-Stream Velocity of 7.47 cm/sec

Peak Temperature

Peak temperatures were acquired experimentally only for the free-stream velocity of 9.88 cm/sec (Test G-2-28, Figure 41). These show a peak gas phase temperature of 1426 K, and a peak surface temperature of 1503 K. Jiang's steady-state model predicts a gas phase temperature of 1442 K, which is less than 1.2% above the empirical value. The model also predicts a peak surface temperature of 1597 K, which is 6.25% above the experimental temperature.

VII. Conclusions

The results of the comparison between the hotwire and chemical ignition systems show that the hotwire system gives a more reproducible ignition than that of the chemical system. The effect of the non-uniformity of the ignition burst from the chemical system is more significant at the lower speeds which were tested. Improvements in the application technique for the chemical ignition system may eliminate some of this non-uniformity. Additionally, it may be possible to minimize the time required to achieve steady-state propagation by fine-tuning the ignition system to give initial pyrolysis and flame lengths which are close to the steady-state values.

Steady-state propagation was difficult to achieve in these tests, due to the limits of the available test time. This was especially true for the highest flow speeds tested, where the available test time was further reduced due to size limitations of the fuels sample translation device. The results show that the two cases which were the closest to steady-state were the tests with (nominal) freestream velocities of 5 cm/sec and 7.5 cm/sec. Even in these cases, though, not all measured elements were advancing at the same rate.

The results from the two tests which were closest to steady-state were compared to the steady-state calculations of Jiang (Jiang, 1995). Comparison of the spread rates was difficult, because it was not clear that the experimental data had reached steady-state.

Thermocouple data was gathered for several tests with thermocouples in

different positions for the flow velocity of about 10 cm/sec. Due to the restriction of how far the flame could propagate in the available test time, it was necessary to place these thermocouples fairly close to the ignition source. Although the effects of the ignition process can be seen in the temperature traces, peak gas phase and surface temperatures were recorded for one test. These values compare well (within about 6%) of the steady-state temperatures calculated by Jiang (Jiang, 1995) for the same locations.

However, the experimental data shows that the presence of the thermocouples influenced the flame by decreasing the flame length, and slowing the propagation of the flame and pyrolysis elements. This was also seen by the quenched area in the partially burned sample, corresponding to the placement of the thermocouples. Estimations were made of the rate of heat loss due to the thermocouples, and compared to the rate of heat release from the combustion of the fuel samples in cases with and without thermocouples. These estimations do not account for all of the losses, but they demonstrate that heat losses from these thermocouples were not negligible.

VIII. Recommendations

Due to the relatively small number of drops available for this study, it was not possible to repeat a significant number of tests under identical condition. As the three hotwire-ignited tests for the free-stream velocity of 2.5 cm/sec indicate, significant variation can occur from test to test. This is particularly true for weak flames (near the flammability limits), where small, perhaps uncontrollable perturbations in the test conditions can have a large effect on the results. Therefore, multiple repetitions of the very low speed tests may be necessary to give an accurate indication of the results.

Should the chemical ignition system be selected for further use, a more repeatable technique for bonding it to the fuel sample needs to be developed. The application of the acetone using an eyedropper does not guarantee an even distribution of the nitrocellulose onto the fuel sample.

Further characterization of the ignition system may help minimize the time needed to reach steady-state. To do this, it would be necessary to know the steady-state flame and pyrolysis lengths for each test condition. The ignition system could then potentially be tailored to deliver initial flame and pyrolysis lengths which were close to the required lengths.

Finally, it would be useful to have an accelerometer mounted on the test vehicle. This would allow a quantitative characterization of the buoyant velocity induced by any residual g-levels.

IX. References

DeRis, J.N., "Spread of a Laminar Diffusion Flame," Twelfth Symposium (International) on Combustion, Combustion Institute, Pittsburgh, pp. 241-252 (1969).

DiBlasi, C., "Process of Flames Spreading over the Surface of Charring Fuels: Effects of the Solid Thickness," *Combustion and Flame*, 97, pp.225-239(1994)

Ferkul, P.,"An Experimental Study of Opposed Flow Diffusion Flame Extinction Over a Thin Fuel in Microgravity", Master's Thesis, Dept. of Mechanical and Aerospace Engineering, Case Western Reserve Univ., NASA CR-182185, May, 1989

Ferkul, P. V. and T'ien, J. S., "A Model of Low-Speed Concurrent Flow Flame Spread Over a Thin Fuel," *Combustion Science and Technology*, **99**, 4-6, pp.345-370, (1994).

Friedman, R., Sacksteder, K. R., "Fire Behavior and Risk Analysis in Spacecraft," (1988) NASA TM-100944

Grayson, G. D., Sacksteder, K. R., Ferkul, P. V., and T'ien, J. S., "Flame Spreading Over a Thin Fuel in Low Speed Concurrent Flow: Droptower Experimental Results and Comparison with Theory," *Microgravity Science and Technology*, **VII/2**, pp.187-195, (1994).

Jiang, C.-B., "A Model of Flame Spread Over a Thin Solid in Concurrent Flow with Flame Radiation," Ph.D. Thesis, Dept. of Mechanical and Aerospace Engineering, Case Western Reserve Univ., May, 1995.

Klimek, R. B., Paulik, M. J., "Color Image Processing and Object Tracking Workstation," (1992) NASA TM-105561

Lekan, J., Neumann, E. S., Sotos, R.G., "Capabilities and Constraints of NASA's Ground-Based Reduced Gravity Facilities," Second International Microgravity Combustion Workshop, NASA Conference Publication 10113, pp.45-53 (1992)

Mendenhall, W., Sincich, T., Statistics for Engineering and the Sciences, Dellen Publishing Co., 1992

Olson, S. O., "The Effect of Microgravity on Flame Spread Over a Thin Solid Fuel," Master's Thesis, Dept. of Mechanical and Aerospace Engineering, Case Western Reserve Univ., NASA TM-100195, May, 1987

Olson, S.O., Ferkul, P.V., and T'ien, J.S., "Near-Limit Flame Spread over a Thin Solid Fuel in Microgravity," Twenty-Second Symposium (International) on Combustion, Combustion Institute, Pittsburgh, pp. 1213-1222, 1988).

Pettegrew, R. D., "Construction and Calibration of a Flammable Sample Translation Device," Senior Project, Dept. of Mechanical and Aerospace Engineering, Case Western Reserve University, May, 1993

Sacksteder, K. R., and T'ien, J. S., "Buoyant Downward Diffusion Flame Spread and Extinction in Partial Gravity Accelerations," *Twenty-Fifth Symposium (International) on Combustion*, to appear (1995).

Frey, A.E., and T'ien, J.S., "A Theory of Flame Spread over a Solid Fuel Including Finite-Rate Chemical Kinetics," Combustion and Flame, 36, pp. 236-289, (1979).

White, F. M., Heat and Mass Transfer, Addison Wesley Publishing Co. Inc., 1988

Appendix I

Error Analysis

This appendix will characterize and, where appropriate, quantify the uncertainties which may have affected the results of this work. Distinction is made between experimental error, data acquisition/reduction error, analysis error, and the uncertainty of the physical phenomena under study.

1.) Experimental Errors

Test Environment

Prior to filling the chamber with the desired test atmosphere, the chamber was evacuated to less than 0.001 atm, which was the resolution of the measurement equipment. All tests were conducted at one atmosphere pressure, and all but two tests were conducted with atmosphere concentrations of 18% O_2, 82% N_2. One test was conducted each at 21% O_2, 79% N_2, and 50% O_2, 50% N_2. All tests except the 50% O_2, 50% N_2 test employed premixed precision gas mixtures to minimize errors in partial pressure mixing. The error of these mixtures, as reported by the manufacturer, was +/- 0.002 %. For the one test which required partial pressure mixing, the error for each component equal to the resolution of the measurement device, which was previously reported to be 0.001 atm. Because this test was unsuccessful, this error is insignificant.

The chamber was filled slowly, to approximate an isothermal procedure.

After one atmosphere was reached, the chamber was allowed to equilibrate for several minutes, and the pressure was re-checked to insure it was at one atmosphere.

Ignition System

For the chemical ignition system, the nitrocellulose strips were weighed using the same scale used on the fuel samples. All strips were cut to be 10 mg, +/- 2%. The length of the strips was chosen to be 5 cm, so that the strip would span the entire sample. When necessary to trim the strips, material was taken from its width.

Timing of the ignition system was verified by connecting the ignition circuit with an oscilloscope, and measuring duration that the system was energized. It was found that an error of +/- 20 milliseconds occurred, which is attributable to the mechanical relays in the system.

Thermocouples

Temperature data in this study was obtained using 3 mil diameter, Type K thermocouples. Theses were connected to an integrated data-acquisition system, consisting of a signal amplifier and a 12-bit A/D converter card. The sampling rate of this system was 33.33 Hz. The accuracy of this system was listed by the manufacturer to be +/- 1.0 degrees.

Flow Velocity

The carriage velocity in these tests was verified two ways. A calibration of the flow translation device was done prior to its installation in

the combustion chamber; for details on this calibration, see Appendix II. This calibration showed that the device reached steady state speeds within 0.1 seconds. At steady state, the velocities measured were within 2% of the set velocities, in the calibrated range of 0.5 cm/sec to 10 cm/sec.

Additionally, the average carriage velocity was verified on each run through analysis of the video images. This was done by measuring the travel of the carriage against a fixed scale mounted in the field of view. To do this, an illuminated frame near the beginning of the run was selected. A cursor was placed on the scale, and the pixel coordinate on the screen, scale value at this spot, and time (as measured by a digital timer superimposed on each frame of the video) were recorded. The video was then advanced to an illuminated frame near the end of the run, and the cursor was placed at the same pixel coordinate. The new value on the scale at this point and the time on this frame then give sufficient information to calculate an average velocity over the measured interval. Analysis of each run showed that the carriage velocity was always within 2% of the set velocity, except for test G-2-20, which had a verified carriage velocity of 1.16 cm/sec. The deviation of 16% from the prescribed velocity of 1 cm/sec was the only instance of a carriage velocity having a difference of greater than 2% from the set velocity. A possible explanation for this could be input error in the programming of the stepper motor controller.

For the cases where the carriage velocity was selected to be 7.5 cm/sec

or 10 cm/sec, the limit of the amount of available flow time was imposed due to the limited length of travel of the fuel translation device. The maximum length of travel for this device was 40.9 cm. However, this maximum length was never reached because the carriage had a tendency to "settle" down the shafts approximately 2-3 cm when the carriage was returned to the top position. This could have been avoided by keeping the stepper motor energized and in "holding" mode from the time the sample was loaded until the beginning of the test. However, this may have caused overheating problems with the stepper motor, and it was decided to accept the loss of 2-3 cm of travel to prevent possible damage to the motor. Because of variations in the amount of "settling" experienced by the carriage for each test, it was impossible to determine the exact distance traveled for a given test. This only affected the high speed tests because for the carriage velocities of 5 cm/sec and slower, the carriage did not travel through more than at most approximately 26 cm in the available micro-gravity time.

2.) Data Acquisition

Flame Element Data

Flame element data was acquired by recording the video images onto a laser disc, and digitizing them frame by frame. A magnification, or scale factor was then found, using the Scale program, by counting the number of pixels between the farthest visible marks on a scale which was mounted in the

field of view.

Because of the difference in focal length between the front view and edge view, it was necessary to measure a scale factor for each view. Mid-way through the test series, an attempt was made to optimize the imaging procedure by moving the camera closer to the test sample and using a different lens. This also meant that the scale factors were changed as well. As a check on the accuracy of the scale factors themselves, these were recalculated for all tests. The front and edge view scale factors were found to be consistent to within 0.6% each time.

The flame element's position data was found by tracking a preset light or color intensity. Because of significant differences in the intensity of the flames under different test conditions, a potential source of error was the selected light or color intensity level. Another difficulty arose in the variation of the image intensity of weak flames. Due to the large energy release at ignition, flames in low speed flows appeared bright initially, but quickly faded in intensity. To examine this issue, the flame images from a single test were analyzed using two color intensity threshold levels. To allow comparison of flame lengths between tests, a single color intensity value was used on all tests. This value was chosen by examining some of the weaker images, and choosing a color intensity which corresponded to flames that were just slightly dimmer than what was visible to the author's eye. The effect of using this threshold level was then examined by comparison with data from the same test, using an

optimal color intensity value. Comparison of these threshold levels show a difference of approximately 16% in flame length between the two methods. For details on this comparison, see Appendix IV.

Because of the presence of the flashing light, the automatic tracking mode was impractical. Since the manual tracking mode consisted of the operator placing a cursor on the interface between the dark and the illuminated pixels, some error was incurred. This error was found by attempting to measure the same point 30 times. It was found that the same point could be measured within +/- 1 pixel each time. For the tests carried out with the original lens, this amounted to a maximum possible error of 0.034 cm. For the tests using the new lens, the maximum error was 0.027 cm. Because the flame length was found by subtracting the position of the flame tip from that of the flame base, the error for this flame length was the sum of the errors for both the tip and the base. The error in the flame length was displayed in the data plots in the form of error bars.

Many of the tests with carriage velocities below 5 cm/sec produced flames which became too dim to see at some point during the test. When the light level of these flames fell below the selected threshold level, the image could no longer be tracked. A combustion reaction may have still been occurring, albeit too dim to see. A better indication of whether the reaction was still taking place can be found in the pyrolysis and burnout front data.

Pyrolysis Data

Because of the nature of the pyrolysis images, the previously used tracking software was not applicable. The data was then acquired by advancing to an illuminated frame where the pyrolysis front was clearly visible, then drawing a horizontal line on the screen using the Scale program. This line was then placed in the position corresponding to the visible edge of the burnout front. If the burnout front was uneven, an average value was used. The pixel co-ordinate and time were then recorded. The area of the pyrolysis zone was then calculated using Sigma Scan, a commercial image measurement package. The area was found by tracing around the visible area of the pyrolysis zone using a mouse-driven cursor. When the trace was closed, the software would count the number of pixels enclosed. This area was then converted to an average pyrolysis length by dividing it by the sample width. The average position of the pyrolysis front was found by adding the average pyrolysis length to the burnout front position. The error in these measurements was found by attempting to measure the same point 30 times. It was found that the burnout front could be measured to +/- 0.0615 cm for the original lens, and +/- 0.0485 cm for the second lens. The error in the average pyrolysis length was found to be +/- 0.088 cm for the original lens, and +/- 0.183 cm for the second lens. The greater error in the average pyrolysis length for the second lens was due to poor illumination of the pyrolysis area. The error in the mean-average pyrolysis length for each test was displayed in the form of error bars.

Because the average pyrolysis position was found by adding the measurement of the burnout front position and the average pyrolysis length, the errors from these sources must be added. This calculated average pyrolysis position then had the greatest inaccuracy, with an error of +/- 0.150 cm for the original lens, and +/- 0.232 cm for the second lens.

3.) Data Analysis

Data Plotting

When the flame element data was originally plotted, the visible length of the flame appeared to periodically shrink and then return to original length, coinciding with the frequency of the flashing light. This was caused by the automatic gain control (AGC) on the video camera. When the image was fairly dim (ie., when the light was off), the AGC adjusted itself to a higher setting to accept more light. When the light flashed on, the AGC adjusted down to a lower setting to compensate for the bright light. Now, when the light went off, the AGC had to respond again to the lower light level. It was during this period of gain response time that the "apparent" flame length was momentarily shortened. Once the AGC responded, the flame "returned" to normal length. This response time was reported by the camera manufacturer to be approximately 0.25 seconds. Therefore, the 7-8 affected frames after each cycle of the flashing light were disregarded.

Flame & Pyrolysis Element Velocities

Because of the limit of the available test time, steady-state propagation was not achieved. To characterize the velocities of the different flame and pyrolysis elements, a linear regression was applied to sections of the element position data near the end of each test. These sections were chosen to represent the behavior of the element near the conclusion of the test. The duration of the data used for these regressions varied with each test, but typically covered the final 1-2 seconds of test time.

A statistical analysis was performed on the linear regressions from four

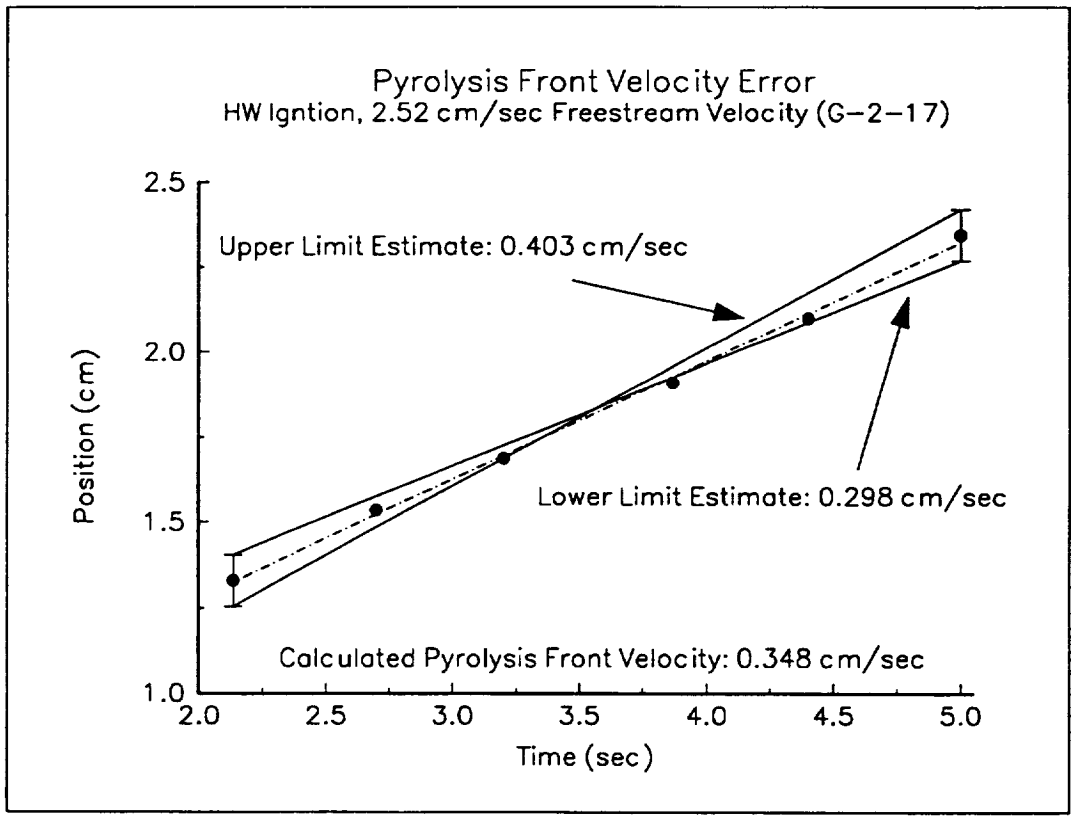

Figure 51

tests using the Axum software package. The tests selected for this analysis were tests G-2-20, G-2-17, G-2-7, and G-2-19, which had freestream velocities of 1.16 cm/sec, 2.52 cm/sec, 5.12 cm/sec, and 9.92 cm/sec, respectively. This statistical analysis yielded R^2 correlation coefficient for the regressions, which are reported in Table 3.

The error in the velocities of the flame and pyrolysis elements was found by determining the minimum and maximum curve-fits that could be made through the error bars. Figure 51 illustrates this by showing the portion of the pyrolysis front position data from test G-2-17 which was used for the linear regression, as well as the error bars and the lines which represent the two possible extremes for the curve-fit.

The R^2 correlation coefficient is an indication of the accuracy of the curve fit. The value of this coefficient is always between 0 and 1, and implies a percentage of the variation of the data which can be attributed to the dependence of one variable on the other. An example of this is an R^2 value of 0.75, which implies that the straight line model relating the dependent variable to the independent variable accounts for 75% of the variation in the values of the dependent variable (Mendenhall and Sincich, 1992).

Freestream Velocity (cm/s)	*Element*	*Element Velocity (cm/s)*	*Error (%)*	*R^2 Factor*	*Curve-Fit Time (sec)*
1.16	*Flame Tip*	*+0.46*	*20.0*	*0.756*	*0.367*
1.16	*Flame Base*	*-0.01*	*122.1*	*0.004*	*0.367*
1.16	*Pyrolysis Front*	*+0.24*	*17.8*	*0.943*	*3.500*
1.16	*Burnout Front*	*+0.24*	*7.3*	*0.994*	*3.500*
2.52	*Flame Tip*	*+0.48*	*5.4*	*0.923*	*1.300*
2.52	*Flame Base*	*+0.20*	*13.0*	*0.886*	*1.300*
2.52	*Pyrolysis Front*	*+0.35*	*14.9*	*0.998*	*2.867*
2.52	*Burnout Front*	*+0.37*	*5.7*	*0.999*	*2.867*
5.12	*Flame Tip*	*+0.45*	*2.9*	*0.973*	*2.600*
5.12	*Flame Base*	*+0.47*	*2.7*	*0.993*	*2.600*
5.12	*Pyrolysis Front*	*+0.71*	*9.0*	*0.985*	*2.333*
5.12	*Burnout Front*	*+0.71*	*3.7*	*0.987*	*2.333*
9.92	*Flame Tip*	*+1.05*	*1.9*	*0.977*	*1.700*
9.92	*Flame Base*	*+0.99*	*2.0*	*0.992*	*1.700*
9.92	*Pyrolysis Front*	*+1.50*	*5.4*	*0.998*	*1.833*
9.92	*Burnout Front*	*+1.12*	*3.0*	*0.999*	*1.833*

Table 3 Element Error & Correlation Coefficient

Table 3 displays the results of the statistical analysis of the linear regressions, as well as the duration of data used for the curve-fit. This shows that the errors in the element velocity associated with the linear regression decrease as the duration of the data used in the curve-fit increases.

The flame and pyrolysis spread rates were defined as the average of the velocities of the respective elements, while the flame and pyrolysis length growth rates were defined as the difference between the velocities of the respective elements. Because of this, the errors for each of these rates is the

sum of the errors in the velocities of the elements. Table 4 gives the errors of the spread and growth rates for the previously mentioned tests.

Freestream Velocity (cm/s)	*M.E. Flame Spread Rate (cm/s)*	*M.E. Flame Spread Error (%)*	*Flame Growth Rate (cm/s)*	*Flame Growth Error (%)*	*M.E. Pyrol Spread Rate (cm/s)*	*M.E. Pyrol Spread Error (%)*	*Pyrol Growth Rate (cm/s)*	*Pyrol Growth Error (%)*
1.16	*+0.23*	*142.1*	*+0.47*	*142.1*	*+0.24*	*25.1*	*+0.00*	*25.1*
2.52	*+0.34*	*18.4*	*+0.28*	*18.4*	*+0.36*	*20.6*	*-0.02*	*20.6*
5.12	*+0.46*	*5.6*	*-0.02*	*5.6*	*+0.71*	*12.7*	*0.00*	*12.7*
9.92	*+1.02*	*3.9*	*+0.06*	*3.9*	*+1.50*	*8.4*	*+0.38*	*8.4*

Table 4 Mean-Element Spread & Growth Rate Error (%)

The results summarized in Table 4 demonstrate that, due to the small time available to curve-fit the data, the quantitative measurements of the 1 cm/sec and quiescent cases should be disregarded.

Appendix II

Buoyant Flow Approximation

Because of the residual g-level present in any ground-based facility, some component of buoyant flow existed in each test. An estimation was made of this buoyant flow velocity, based on an assumed constant residual g-level of 10^{-5}g. White (White, 1988) gave an approximation of the buoyant flow velocity to be:

$$U_B = \sqrt{\beta g l (\Delta T)}$$

This expression assumes that the only pressure gradient present is hydrostatic pressure, and that the thermal boundary layer thickness is larger than the viscous boundary layer (Prandtl number less than one).

Using this expression, the buoyant velocity was estimated for each (nominal) carriage velocity tested. The reference length used in these calculations was the measured flame length for the hotwire-ignition test at each carriage velocity. The flame temperatures used were the peak temperatures (for each velocity) as calculated by Jiang's steady-state model (Jiang, 1995), except for the case of the 10 cm/sec carriage velocity, where an experimental flame temperature was available. These results are shown in Table 5.

Carriage Velocity (cm/sec)	*Estimated Buoyant Velocity (cm/sec)*	*Difference in Opposite Directions (%)*
1.0	*0.086*	*18.7*
2.5	*0.095*	*7.9*
5.0	*0.108*	*4.4*
7.5	*0.132*	*3.6*
10.0	*0.174*	*3.5*

Table 5 Buoyant Velocity Estimates

The tests where this effect was particularly significant were the 2.5 cm/sec tests, because several tests were performed in the up direction, with another performed in the down orientation. The estimate of the induced buoyant velocity for this case was about 0.10 cm/sec(a difference of about 8% between the two directions).

If the relative flow velocity were changed in a simple way by the buoyant flow, flame lengths would be expected to be shortened in a slower flow and longer in an enhanced flow (Ferkul, 1994). Because of the variation between the two cases (at the same nominal velocity) where the carriage was moving up, it is difficult to distinguish the difference between these tests and the case where the carriage was moving down. However, the trend seemed to be that the upward cases, where the flow is reduced by buoyancy have longer flames than the downward case. The reason for this discrepancy is not clear

from the available data.

Appendix III

Thermocouple Heat Loss Approximation

To estimate the total heat loss rate due to the presence of the two thermocouples used in this study, the loss rates due to thermal inertia, conduction, and radiation were considered. The total estimated rate of heat loss was then compared to the difference in the heat release rate from a test with the thermocouples, and one without. The following is a synopsis of the estimation of each of these rates, including all assumptions.

Thermal Inertia

The heat loss rate due to thermal inertia was calculated by first determining the mass of the junction bead, as well as that of each lead. The junction bead was assumed to have a diameter of 0.02286 cm (three times the diameter of the leads), and to have a density equal to the average of the densities of the leads (8.665 grams/cm^3). The density of the chromel lead was 8.73 grams/cm^3, while the density of the alumel lead was 8.60 grams/cm^3. The total mass of the leads and junction (for both thermocouples) was calculated to be 0.0112 grams.

The specific heat for each element was given by the manufacturer to be 0.4479 Joules/(gram*C) for chromel, and 0.5233 Joules/(gram*C) for alumel. These values were specified for a temperature of 20 C, which is well below the temperatures experienced in the tests. However, no other information was

available on these alloys at the time of these calculations.

The total heat required to raise both thermocouple junctions and their leads to 1500 K was estimated to be 6.53 Joules. For test G-2-28, both thermocouples showed a rise in temperature from 0.4 seconds until reaching a peak temperature at approximately 2.8 seconds (2.7 seconds for the surface, 2.9 seconds for the gas phase). The length of time required to reach the final temperature was then about 2.4 seconds, and the total energy required of 6.53 Joules was divided by this time to give a heat loss rate of 2.72 Watts.

Conduction

To estimate the heat loss rate due to conduction, the thermocouple leads were modeled using the one-dimensional, steady-state heat equation with Dirichlet boundary conditions. The solution to this problem is a linear temperature distribution, which when differentiated once gives the temperature gradient.

The size of this temperature gradient depends both on the temperature difference and on the length through which the gradient acts. For the purposes of this calculation, it was assumed that the entire diamond-shape configuration was at the flame temperature of 1500 K, and that 1 cm into the wire insulation (downstream of the diamond-shaped leads) the temperature was equal to the ambient temperature of 300 K. This yielded a gradient of -1200 K/cm.

Fourier's Law was then applied, using the calculated gradient. The

values used for the thermal conductivities were 0.922 Watts/cm*K for chromel, and 1.64 Watts/cm*K for alumel. Similar to the values of the specific heat used in the thermal inertia calculations, these values were specified at 20 C, but were considered usable for the purpose of this estimate. Using these assumptions, the total heat loss rate through conduction for both thermocouples was estimated to be 3.2 Watts.

Radiation

To estimate the loss rate due to radiation, the thermocouple junction and leads were modeled as black-body emitter, with a surface area of the spherical junction and the exposed leads of 0.1445 cm^2. The temperature used was 1500 K. The heat loss rate due to radiation was estimated to be 4.15 Watts.

Heat Release Rate

To estimate the rate of heat released from the combustion process, the speed of the burnout front was multiplied by the sample width and the area density (full thickness) to give a mass burning rate. This was multiplied by the heat of combustion for KimWipes, which is 16740 Joules/gram (Frey & T'ien, 1979) to give the heat release rate. The heat release rate for test G-2-19, which did not have thermocouples, was found to be about 188 Watts, while the heat release rate from test G-2-28 (the test with thermocouples) was found to be about 156 Watts. The difference in these rates is then about 32 Watts.

The estimated heat loss rate of about 10 Watts does not account for all of the difference in the two tests. However, it does show that heat losses from the thermocouples were not negligible, and did have an effect on the flames in this experiment.

Appendix IV

Effect of Threshold Value on Flame Element Data

The intensity resolution of the Tracking program used to track the flame elements in this study was 8 bits, meaning that the program could distinguish 2^8=256 levels of light or color intensity, with a value of 0 corresponding to zero light, and 255 being full scale intensity. To allow comparison between different tests, a constant color threshold intensity of 15 was used to analyze the data from all the tests. This value was chosen to allow distinction of the dimmest flames. To evaluate the effect of changing the threshold intensity value, test G-2-7 (18% O_2, chemical ignition, freestream velocity of 5.12 cm/sec) was evaluated using two different threshold levels.

Selection of the new threshold level to evaluate test G-2-7 was made using a program called Profiles, which allowed the user to draw a line using a mouse-driven cursor, and to place this line at any position on the screen. The program then gave a profile of either the color or total light intensity along the selected line. The line was then placed across the edge of the base and tip sections of the flame images, which aided in the selection of the proper intensity level. Because the flame images were fairly bright for this test, a threshold value of 40 was selected to use for this comparison.

Figure 52 shows a plot of the flame lengths for test G-2-7 using both threshold values. As expected, the flame length using the brighter threshold value of 40 was shorter than the length found using the dimmer threshold value

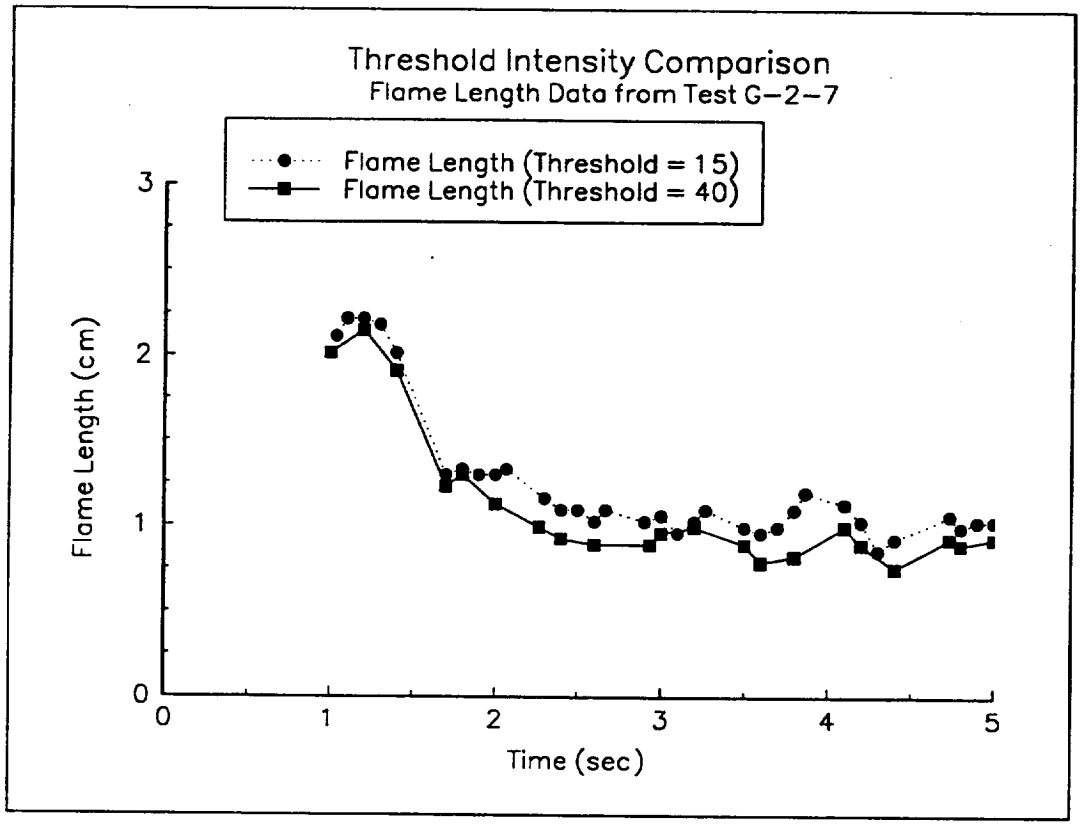

Figure 52

of 15. From the time t = 2.3 seconds until the end of the test, the plot of the flame length using the threshold of 15 had a mean value of 1.04 cm, while the flame length measured with a threshold value of 40 had a mean value of 0.89 cm. This means that increasing the intensity value by 9.7% increased the flame length by 14.2%. This shows that the measurement of the position of the flame elements (and therefore, the flame length) is sensitive to the selected threshold level. Comparison between flames can then only be done if the flame elements were tracked using the same threshold levels.

Appendix V

Calibration of the Fuel Translation Device

The fuel translation device used in this study was calibrated for nominal carriage speeds of 0.5, 1, 2, 5, and 10 cm/sec. However, the signal rate of the stepper motor controller could only be programmed in multiples of 50 Hz. Due to this limitation, the best available step inputs yield theoretical velocities of 0.51, 1.00, 2.00, 5.02, and 10.03 cm/sec. For simplicity, the velocities shall herein be referred to as 10, 5, 2, 1, and 0.5 cm/sec, respectively.

Final calibration was performed using a high-speed video system to image the device while operating at the previously mentioned speeds. This gave a visual record of the position of the carriage with respect to time. The images were processed using the Tracking computer software to track the position of a marker placed on the carriage.

The video camera was located 3 meters from the device, with the line of sight perpendicular to the direction of the carriage motion. A large focal length (limited by the laboratory where the calibration was performed) was established to minimize parallax error. A 50 mm lens was used so that the entire travel distance of the carriage would fill the field of view.

The device was calibrated with the traverse direction in the horizontal position. At the beginning of the data tape, a level is shown against one of the bearing shafts to verify the orientation of the device. To establish a length scale, a large ruler (with arrows marking 40 cm) is then shown. A mechanical,

digital timer (capable of resolving increments of 0.01 seconds) was also imaged to verify the framing rate.

The device was imaged against a black backdrop. Adequate lighting was achieved using a 100 watt incandescent light. To give the video analysis system a good target to track, a marker consisting of a white triangle on a black background was mounted on the carriage, facing the camera.

Because this system produced an image which was 256 pixels wide, while covering a travel distance of 42 cm, the spatial resolution of the system was 0.16406 cm/pixel. It was decided to set the framing rate for each trial to be such that two frames would be recorded at each position discernable within the limits of the spatial resolution. It was calculated that the ideal framing rates were 122, 61, 24, 12, and 6 frames/sec, corresponding to the carriage velocities of 10, 5, 2, 1, and 0.5 cm/sec, respectively. However, an additional constraint was the fact that the video system could only be set to record at preset rates of 1000, 500, 250, 125, and 50 frames/second. Therefore, the 10 and 5 cm/sec runs were imaged at 125 frames/sec, and the rest at the slowest speed of 50 frames/second. Five trials in both directions were imaged for each of the calibrated velocities.

To study the repeatability of the device, a pair of limit switches were mounted at both ends of the device. These were connected in series with a 30 Volt power supply and the mechanical timer. The switches were wired in the normally closed configuration, meaning that the timer would run unless one of

the switches were activated. The procedure was to start with the carriage compressing one of the switches, opening the circuit. The timer was then zeroed, and the motor was activated. As the carriage released the switch, the timer would start. The system was programmed to run until the carriage would trip the limit switch a the other end, stopping the timer. This test was repeated 25 times in each direction for each calibrated velocity.

It should be noted that, due to the fact that the sample holder had not yet been installed on the device, the length of travel available for the calibration was greater than that which was be available for actual usage. The actual total travel distance of the carriage was 40.9 cm.

The results of the calibration showed that the device always operated within 6% of the selected carriage velocity. Figures 53 through 57 (displayed at the end of this appendix) show the results of one trial for each calibrated velocity. These are broken into plots of the first 0.5 seconds of each test (to show the transient effects), and the steady-state portion of each test, lasting from 0.5 seconds to 4.0 seconds. The average carriage velocity was also verified (using a scale mounted in the field of view) for each experiment. With the exception of the 1.16 cm/sec case (which was attributed to a faulty controller command), all average carriage velocities were found to be within 2% of the selected values.

The results of the repeatability tests show that the standard deviation for each carriage velocity is on the order of 10^{-2} seconds or less. The fact that the

standard deviations were all comparable implied that the errors which caused these deviations were time invariant. As the length of run time increased, the fixed error became less and less significant. Therefore, the uncertainty in the repeatability of the carriage travel time decreased as the carriage speed decreased. Since the distance that the carriage travels was fixed, the uncertainty in the mean velocity (neglecting transient effects) correspondingly decreased.

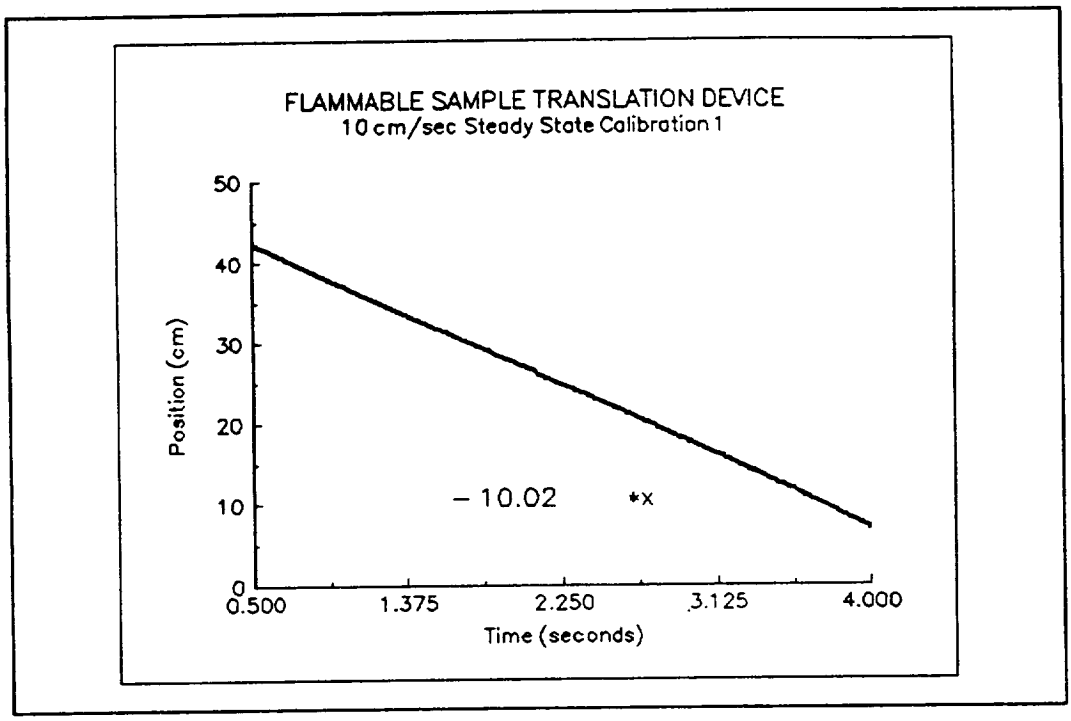

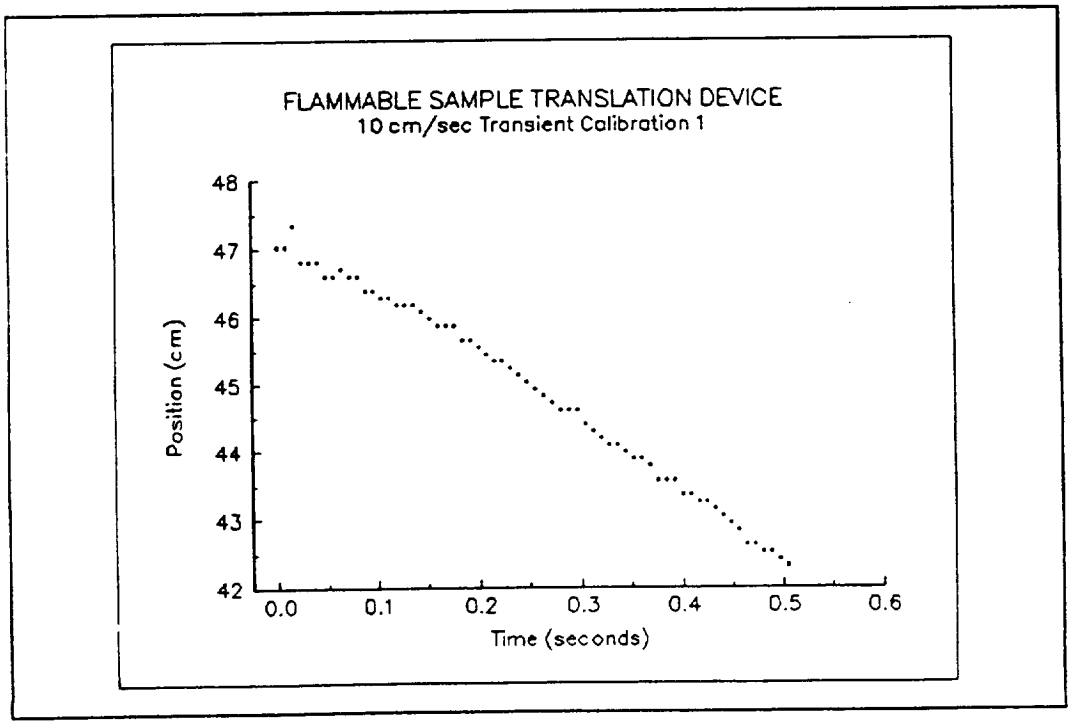

Figure 53 Steady-State and Transient Calibration, 10 cm/sec

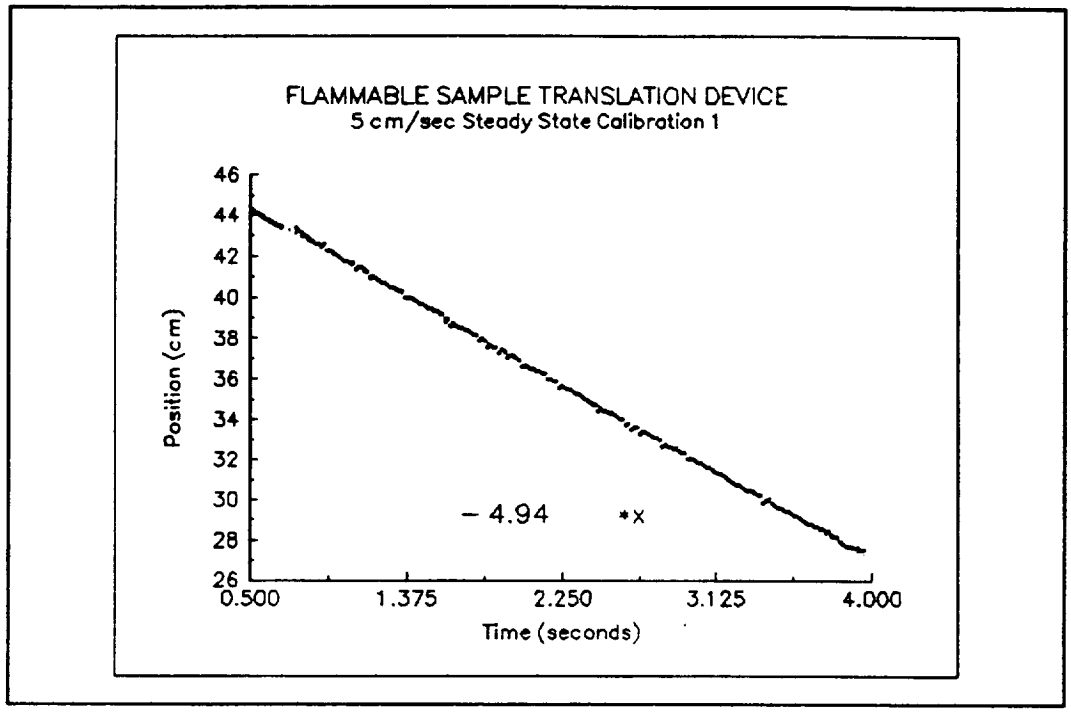

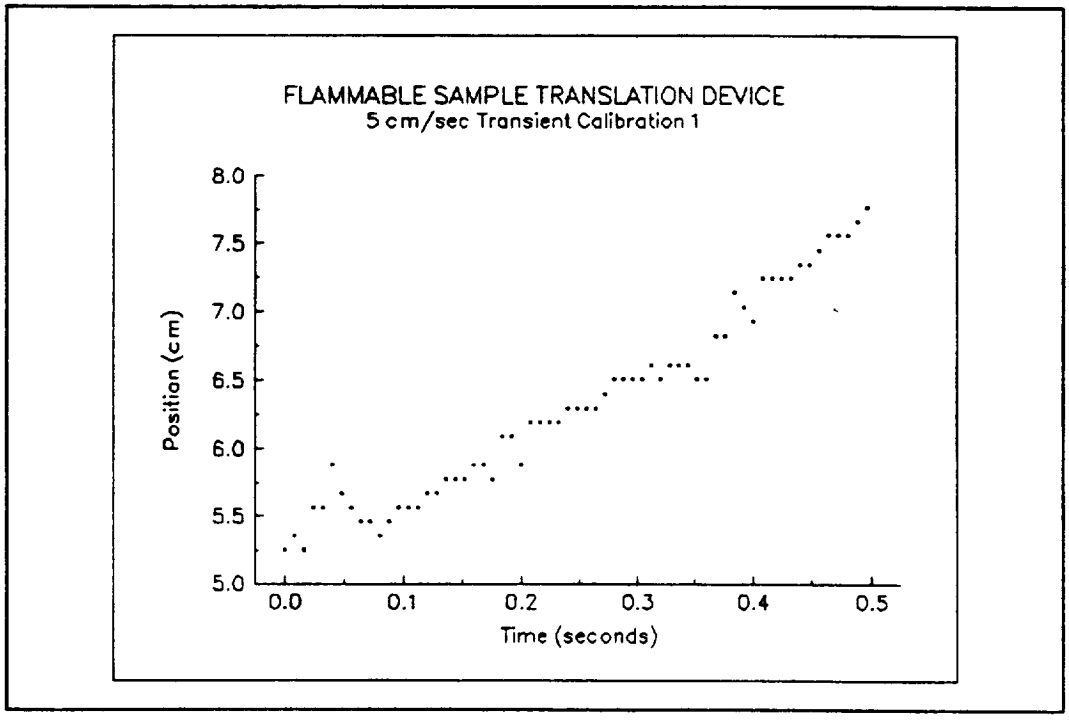

Figure 54 Steady-State and Transient Calibration, 5 cm/sec

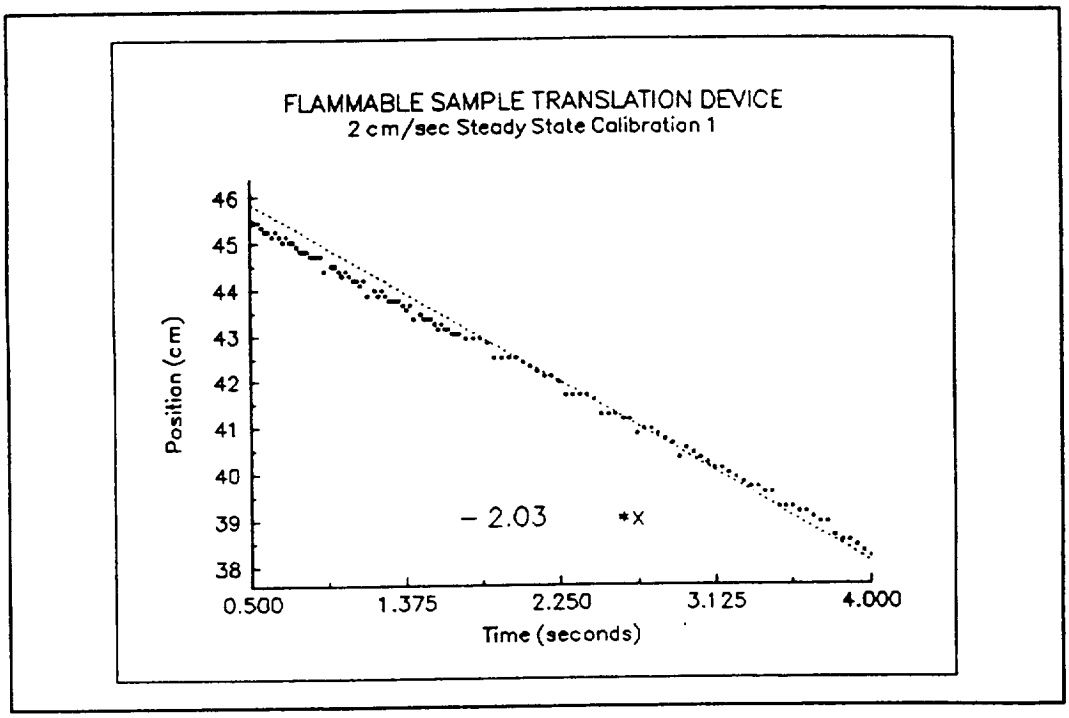

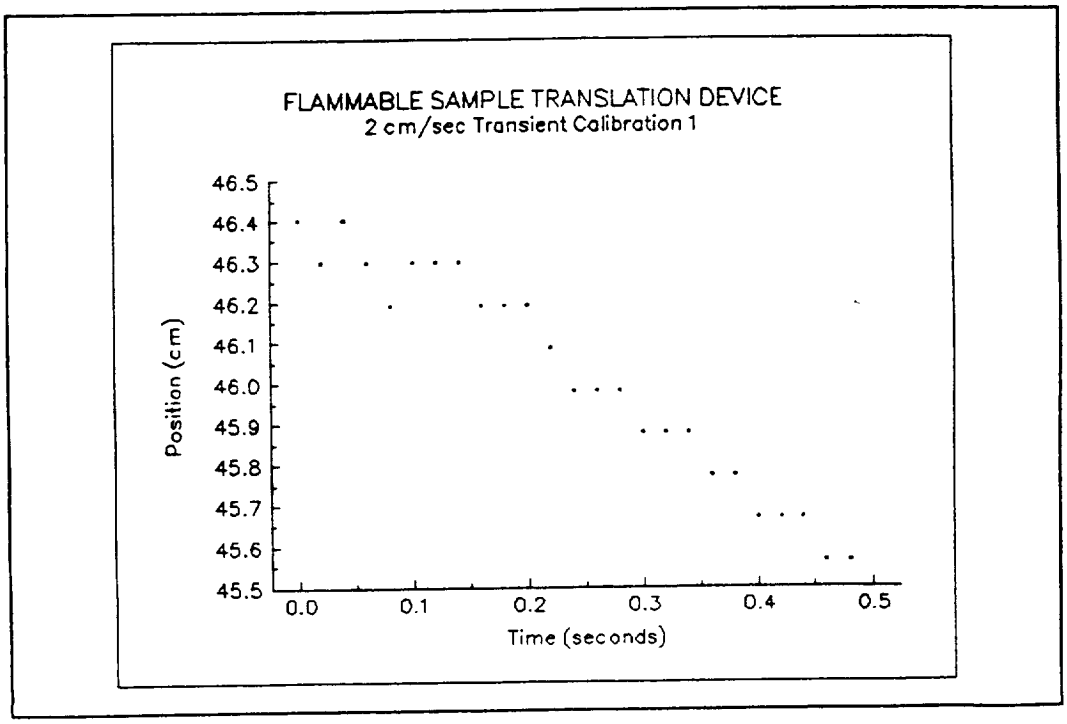

Figure 55 Steady-State and Transient Calibration, 2 cm/sec

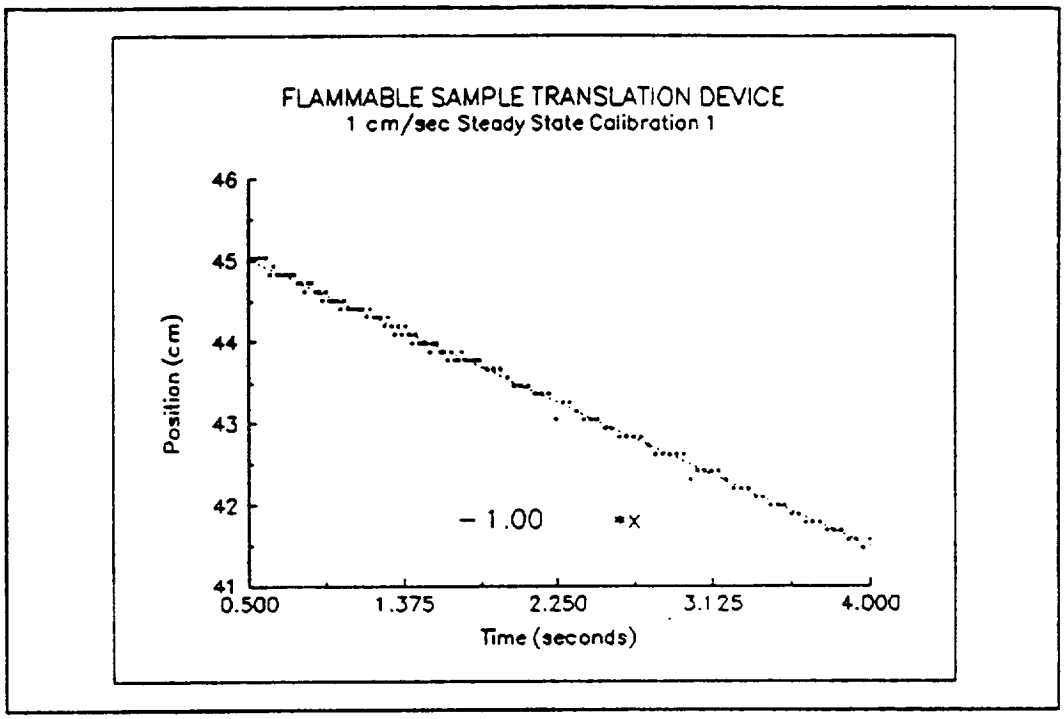

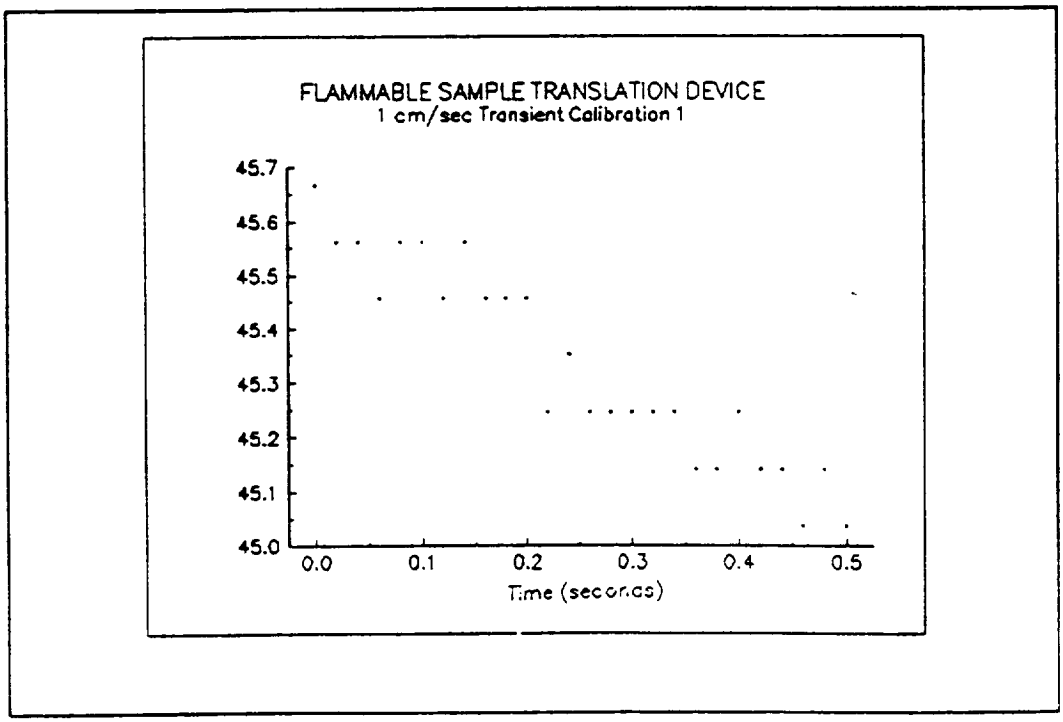

Figure 56 Steady-State and Transient Calibration, 1 cm/sec

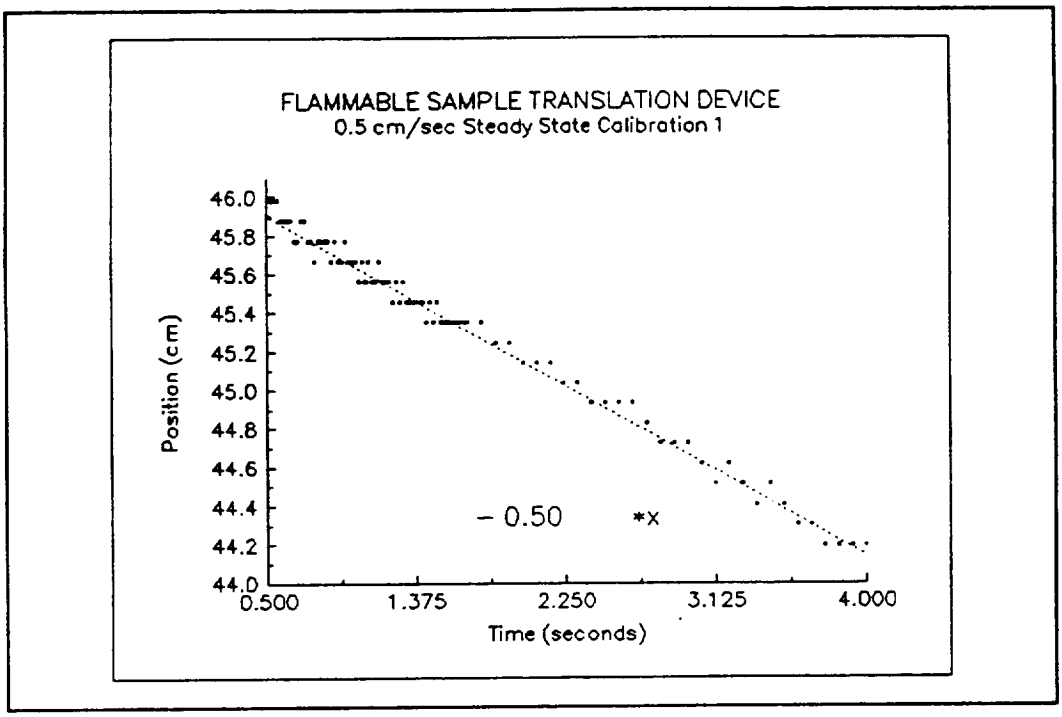

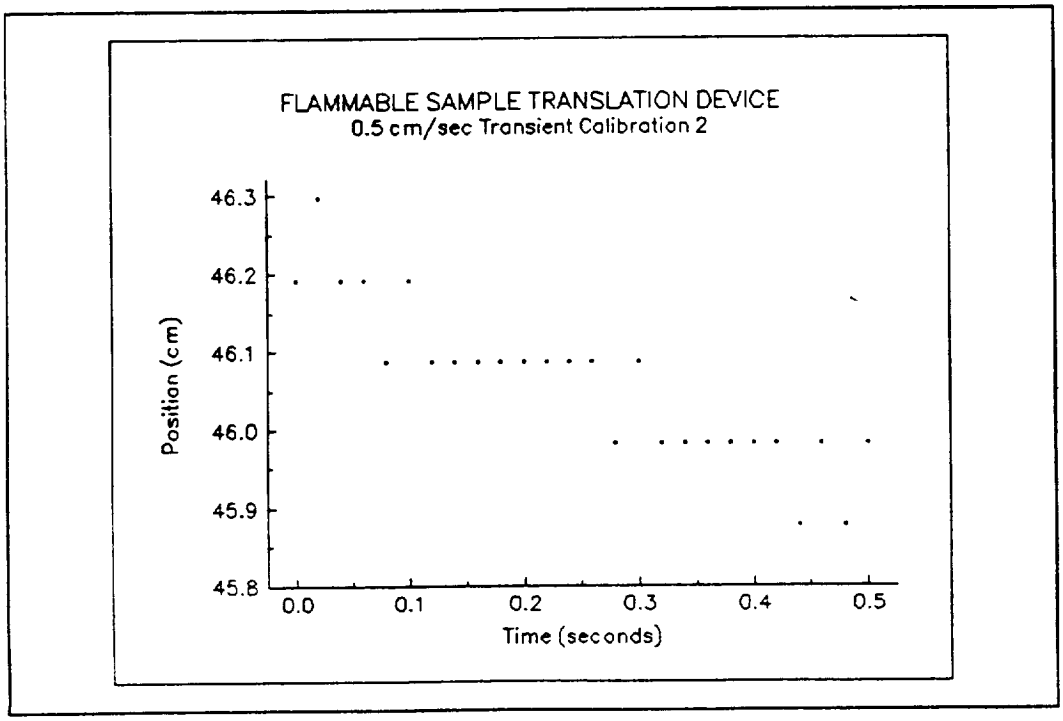

Figure 57 Steady-State and Transient Calibration, 0.5 cm/sec

REPORT DOCUMENTATION PAGE

Form Approved
OMB No. 0704-0188

1. AGENCY USE ONLY (*Leave blank*)	2. REPORT DATE	3. REPORT TYPE AND DATES COVERED
	October 1996	Final Contractor Report

4. TITLE AND SUBTITLE

An Experimental Study of Ignition Effects and Flame Growth Over a Thin Solid Fuel in Low-Speed Concurrent Flow Using Drop-Tower Facilities

5. FUNDING NUMBERS

WU-962-22-05-40
G-NAG3-1046

6. AUTHOR(S)

Richard Dale Pettegrew

7. PERFORMING ORGANIZATION NAME(S) AND ADDRESS(ES)

Case Western Reserve University
Cleveland, Ohio 44106

8. PERFORMING ORGANIZATION REPORT NUMBER

E-10471

9. SPONSORING/MONITORING AGENCY NAME(S) AND ADDRESS(ES)

National Aeronautics and Space Administration
Lewis Research Center
Cleveland, Ohio 44135-3191

10. SPONSORING/MONITORING AGENCY REPORT NUMBER

NASA CR-198537

11. SUPPLEMENTARY NOTES

This report was submitted as a thesis in partial fulfillment of the requirements for the degree Master of Science to Case Western Reserve University, Cleveland, Ohio, May 1995. Project Manager, Kurt R. Sacksteder, Space Experiments Division, NASA Lewis Research Center, organization code 6711, (216) 433-2857.

12a. DISTRIBUTION/AVAILABILITY STATEMENT

Unclassified - Unlimited
Subject Categories 34 and 31

This publication is available from the NASA Center for AeroSpace Information, (301) 621-0390.

12b. DISTRIBUTION CODE

13. ABSTRACT (*Maximum 200 words*)

An experimental study of ignition and flame growth over a thin solid fuel in oxidizer flow speeds from 0 to 10 cm/sec concurrent flow was performed. This study examined the differences between ignition using a resistively heated wire (woven in a sawtooth pattern over the leading edge of the fuel), and a straight, resistively heated wire augmented by a chemical ignitor doped onto the leading edge of the fuel. Results showed that the chemical system yielded non-uniform ignition bursts, while the system using only the hotwire gave more uniform ignition. At speeds up to 2.5 cm/sec, the chemical system yielded non-uniform pyrolysis fronts, while the hotwire system gave more uniform pyrolysis fronts. At speeds of 5 cm/sec or greater, both systems gave uniform pyrolysis fronts. The chemically-ignited flames tended to become too dim to see faster than the hotwire-ignited flames, and the flame lengths were observed to be shorter (after the initial ignition burst subsided) for the chemical system for all speeds. Flame and pyrolysis element velocities were measured. Temperature profiles for selected tests were measured using thermocouples at the fuel surface and in the gas phase. Comparisons between the flame element velocities and peak temperatures recorded in these tests with calculated spread rates and peak temperatures from a steady-state model are presented. Agreement was found to be within 20% for most flame elements for nominal velocities of 5 cm/sec and 7.5 cm/sec.

14. SUBJECT TERMS	15. NUMBER OF PAGES
Microgravity; Combustion; Flames; Diffusion flames; Flame spreading	137
	16. PRICE CODE: A07

17. SECURITY CLASSIFICATION OF REPORT	18. SECURITY CLASSIFICATION OF THIS PAGE	19. SECURITY CLASSIFICATION OF ABSTRACT	20. LIMITATION OF ABSTRACT
Unclassified	Unclassified	Unclassified	